CIVIL ENGINEERING STUDIES

STRUCTURAL RESEARCH SERIES NO. 463

RESISTANCE OF REINFORCED CONCRETE STRUCTURES UNDER HIGH INTENSITY LOADS

By
T. KRAUTHAMMER
W. J. HALL

UNIVERSITY OF ILLINOIS
at URBANA-CHAMPAIGN
URBANA, ILLINOIS
MAY 1979

RESISTANCE OF REINFORCED CONCRETE STRUCTURES
UNDER HIGH INTENSITY LOADS

by

T. Krauthammer

and

W. J. Hall

Department of Civil Engineering
University of Illinois
at Urbana-Champaign
Urbana, Illinois

May 1979

ACKNOWLEDGMENT

TABLE OF CONTENTS

LIST OF TABLES

LIST OF FIGURES

NOTATION

A_g - carcked surface area of concrete

A_s - cross section area of tensile reinforcement

A'_s - cross section area of compressive reinforcement

A_{sp} - cross section area of spiral reinforcement

A_v - cross section area of vertical reinforcement

A_{vh} - cross section area of horizontal reinforcement

a - shear span length

b'' - width of confined core, measured to outside of hoops

b_w - width of beam web

C - compressive force

D - nominal diameter of longitudinal reinforcing bars

D_c - diameter of confined core in spiral column

d - beam effective depth

d'' - nominal diameter of lateral reinforcing bars

E_s - elastic modulus for steel

E_c - elastic modulus for concrete, tangent modulus

F - force

f - stress

f_c - concrete stress

f'_c - concrete compressive strength, uniaxial

f_s - tensile reinforcement stress

f'_s - compressive reinforcement stress

f_r - concrete rupture stress

f_u - ultimate stress for steel bars

f_y - yield stress for main reinforcement

f''_y - yield stress for transverse reinforcement

h - beam total depth

h" - the average of the sides of the rectangular compressive zone, measured

    to the outside of the steel hoops.

jd - lever arm for moment calculation in beam

K - constant to define maximum concrete stress

K_1, K_2, K_3 - constants to define stress-strain curve for concrete

kd - depth of neutral axis

$k_u d$ - depth of neutral axis at ultimate loading stage

ℓ - clear span length

M – moment

M_u – ultimate moment

$M_{f\ell}$ – ultimate flexural moment

M_m – ultimate moment with axial load

N – axial load, or clamping force

N_u – axial force associated with ultimate moment capacity

P_1, P_2, P_3 – characteristic points that define the shape of the shear

        influence model

S – spacing of transverse reinforcement

S_h – spacing of hoops, or spacing of horizontal web reinforcement

T – tensile force

T_u – tensile force in truss mechanism

V – vertical reaction force, or total shear force

V_a – sum of vertical components of interlocking shear forces

V_c – shear force across the compressive zone

V_d – dowel force

V_u – shear force associated with ultimate moment

v_c – shear strength of plain concrete

v_s – shear strength of web reinforcement

v_u – ultimate shear strength of a structural member

v_{uf} – shear resistance across a crack

X – distance, or coordinate along the beam axis

Z – constant to define the stress-strain curve for confined concrete

Z' – lever arm for moment calculations in deep beams

α – crack inclination angle

β – inclination of web reinforcement

γ – constant, relates lateral confining pressure to axial strength of concrete

ϵ – strain

ϵ_0 – concrete strain associated with maximum concrete strength

ϵ_c – concrete strain

ϵ_{cu} – ultimate concrete strain

ϵ_s – steel strain

ϵ_{sh} – strain at which strain hardening begins

ϵ_{su} – ultimate steel strain

ϵ_u – strain at extreme concrete fiber in compression

$\epsilon_{0.3K}$ – concrete strain at which concrete strength is reduced to 0.3

　　　　　of maximum strength

λ – constant, defines the tensile strength of plain concrete

μ - coefficient of friction

ρ - percentage of longitudinal reinforcement in columns, or in compressive
   zone of beam

ρ_s - percentage of transverse reinforcement

ρ'' - percentage of confining reinforcement

ρ_w - percentage of web reinforcement

ρ_1^*, ρ_2^* - factored values of ρ''

σ - stress

ϕ - curvature

1. INTRODUCTION

1.1 Objectives of the Investigation

The design of protective structures to resist blast forces and ground shock arising from a nuclear detonation, must consider the large destructive capacity of modern nuclear weapons. The magnitude of the forces and ground shock resulting from a nuclear detonation can be evaluated both theoretically and experimentally. However, the force system that may act upon a protective structure is determined by various factors some of which are a matter of probability. A designer has only a limited amount of control on the expected force system, and therefore can only assure a certain level of survival probability for the structure under consideration. One has to consider the possibility that the acting forces may reach, or even exceed the upper limit of the expected force system for which the structure is designed.

The uncertainty involved in the design of protective structures, as a direct result of the nature of the expected force system, may require that the structure be designed to provide its full resistance if necessary. Any structural element failing to perform as expected under the given loading conditions may reduce the probability of survival of the entire structure. The designer is required to study various failure possibilities of the structure due to the expected loading conditions, and to propose a design which provides the desired degree of protection. It is also necessary to try to eliminate any possible brittle types of failure. The high intensity of the expected loads, and the necessity of maximum performance require the designer to employ accurate and reliable analytical methods by which the performance of the structure can be evaluated.

The design philosophies, and recommended analytical procedures employed to design protective structures are summarized and discussed in Appendix A. The general design procedure consists of three major design steps, as follows.

1. Preliminary design of the protective structure for equivalent static conditions. As a result preliminary dimensions and detailing of the structure are obtained.

2. Analysis of the structure and structural elements to determine if a dynamic analysis is necessary.

3. In the event that a dynamic analysis of the structure is necessary, to evaluate the resistance of the structural elements from the dynamic analysis and redesign the structure.

A dynamic analysis may not be necessary if the duration of the positive phase of the applied load is significantly longer than the natural period of the structural elements under consideration. In cases where dynamic analysis is not necessary the preliminary design can be employed to provide the detailing of the structure. A detonation of a nuclear weapon in the megaton range of yields usually results in a force system that may not require a dynamic analysis.

Dynamic loading conditions usually increase the strength of structural materials, as discussed in Appendix A. The improved material properties can be employed by the designer if justified by the expected rate of loading.

This study is limited to cases for which an equivalent static design is sufficient, and a dynamic analysis is not necessary. The objectives of the present study are the following.

1. To study and summarize the existing theories and design methods for simply supported reinforced concrete beams under static loading conditions. Evaluate the efficiency and accuracy of these methods when compared to experimental data, as reported in the literature.

2. To develop modified and improved design procedures that can be employed to analyze simply supported reinforced concrete beams, and which apply to the following cases.

   Slender and deep beams containing various amounts of longitudinal and transverse reinforcement under the influence of flexure, shear, axial loads, or any combination of these effects.

   The design procedures should be capable of determining the influence of shear reinforcement on the moment capacity and behavior of the beams under consideration, and

3. To evaluate the efficiency and accuracy of the proposed method compared to experimental data. Compare the analytical results with the behavior of protective structures and structural components, as reported in the literature.

1.2 Scope of the Investigation

The results of this study along with the procedures by which they were obtained are presented in the following chapters.

The concept of an "equivalent static design" for certain protective structures is presented in Appendix A. The present study is concerned only

with reinforced concrete protective structures subjected to blast loading from nuclear weapons in the megaton range of yields.

Chapter 2 contains a summary of the current theories and design procedures for reinforced concrete beams. The behavior of reinforced concrete beams under the influence of flexure, shear, axial loads, and a combination of these effects is presented. A modified analytical method is developed that can be applied to various types of reinforced concrete beams under the loading conditions previously mentioned. The results of parameter studies concerning the influence of shear reinforcement are presented in Appendix B.

In Chapter 3 the application of the proposed method to analyze reinforced concrete beams is demonstrated. The beams analyzed in this study were tested by other investigators, and the analytical results are compared to the experimental data. Three types of beams are analyzed in the present study and they are the following.

1. Simply supported reinforced concrete slender beams under the combined influence of flexure and shear.

2. Simply supported reinforced concrete slender beams under the effect of flexure, shear and axial loads.

3. Simply supported deep reinforced concrete beams under the combined effect of flexure and shear.

Experimental data from previous studies by other investigators on these beams; material and dimensions of the beams are presented in Appendix B. The numerical procedures are illustrated by flow-diagrams in Appendix C.

Chapter 4 contains a brief summary of existing theories and design recommendations for reinforced concrete structural joints. The behavior of certain

protective structures and structural elements is described, and some obser-

vations are made in the light of the results from this study.

In the last chapter, general conclusions resulting from the present

study are presented. Recommendations for future studies are also presented

in that chapter.

A detailed numerical example is provided in Appendix D to further

illustrate the proposed analytical procedures.

2. MODELS FOR CONCRETE, STEEL, AND REINFORCED CONCRETE

2.1 Introduction

Analytical methods to study the behavior of reinforced concrete structures rely on models that describe the behavior of the materials from which reinforced concrete is made. These models have to include the influence of material properties, geometrical shape, and the internal discontinuities on the behavior of structural members. The behavior of a loaded structure is determined by the interaction between the applied loads and the structural properties. Given a structure at equilibrium under a certain loading condition when the load is changed, the structure deforms until a new state of equilibrium is reached. The deformation of the structure induces strains in the structural members. From the assumed stress-strain relationships of the structural materials, one can calculate the stresses that result from the induced strains. The internal forces in the structural members are calculated by integrating the stresses over the corresponding cross sections. If the assumed stress-strain relationships for the structural materials closely simulate the actual stress-strain curves, it is possible to obtain approximately correct values for the stresses and forces in the member. Therefore, it is necessary to have accurate stress-strain relationships for the structural materials. Furthermore, it is necessary to have reliable numerical procedures to perform the analysis. Any improvement in the existing stress-strain relationships and the numerical procedures generally will result in a better approximation of the structural behavior.

Various empirical models for plain concrete, steel, and reinforced concrete have been proposed in the literature. The models are described

and discussed in this study. The influence of steel reinforcement on the behavior of structural members is also discussed. From the study of the previous models it was found that none of the models could describe the behavior of structural members in a wide range of loading conditions, between zero external load to ultimate load capacity. Furthermore, none of the previous models considered the direct influence of shear stresses on the structural behavior. The present study combines empirical results that were reported by other investigators with new assumptions about the behavior of structural members. As a result, an improved model for the analysis of reinforced concrete structures is proposed.

The experimental results reported in the literature clearly indicate that the behavior of plain concrete is different from the behavior of reinforced concrete. Indeed, the type and amount of reinforcement determine the shape of the stress-strain curve. The experimental data is carefully evaluated in the following sections. In addition models are developed to represent the influence of material properties and geometry of the cross section on beam behavior. The proposed stress-strain relationship for reinforced concrete takes into consideration internal changes in the cross sections of structural members. These changes result from the variations in both the location of the neutral axis and in the strain distribution over the cross section. The proposed model is continuously modified during the analysis to reflect the internal changes.

A low shear resistance of the structural members usually results in brittle modes of failure, reduction in rotational capacity, reduction in ductility, and reduction in ultimate load capacity. The introduction of

shear reinforcement into the member can significantly improve the behavior. The evaluation of the amount of shear reinforcement required by the ACI Code relies on the expected shear resistance of the concrete. However, experimental data discussed in the following sections indicate that the shear resistance of the concrete is unpredictable. Therefore, the amount of shear reinforcement evaluated by the ACI method may not be the necessary amount. Nevertheless, no procedure has been proposed in the literature that can accurately predict the ultimate moment capacity as a function of the amount of shear reinforcement.

The influence of shear reinforcement on the behavior of beams reported in the literature is studied and discussed. A model proposed by other investigators to describe the influence of shear on simply supported beams with only tensile reinforcement is adopted. This model is modified to describe the behavior of simply supported beams with tensile, compressive, and shear reinforcement. The proposed procedure can evaluate the reduction in the ultimate moment capacity and the inclination of the cracks in the beam as a function of material properties and the detailing of the beam. The application of this method to design makes it possible to check if the amount of shear reinforcement, as calculated by any recommended procedure, is sufficient to overcome the undesirable influence of shear.

This study also is concerned with the behavior of deep beams. The behavior of deep beams is discussed, and various methods to analyze deep beams as presented in the literature, are described. The experimental and theoretical studies by other investigators clearly show that the behavior of deep beams is different from the behavior of slender beams. The models

to evaluate the flexural capacity and shear influence for slender beams are considered for the analysis of deep beams. Only the procedure for the influence of shear is modified while the method to calculate the flexural capacity is found to be applicable for deep beams too.

The behavior of reinforced concrete beams with axial loads also is studied. The results of this study show that the proposed models for flexural moment capacity and for shear influence can be used to analyze such members. Furthermore, it is confirmed that axial loads improve the shear resistance of flexural members.

The analytical procedures proposed in this chapter have been developed in several stages as follows:

1. Determine the behavior of plain concrete and the influence of various types of transverse reinforcement on that behavior. Discuss the stress-strain relationships of concrete confined by rectangular hoops and determine the influence of various parameters on the relationships.

2. Discuss stress-strain relationships of reinforcing steel bars and determine a relationship to be used in the present study.

3. Develop a modified stress-strain relationship for concrete confined by rectangular hoops to be used in the present study.

4. Discuss and describe the numerical procedure to calculate the flexural moment capacity of slender beams. Describe the procedure to obtain a moment-curvature (M-ϕ) diagram for slender flexural members.

5. Discuss the influence of shear on the behavior of beams with or without shear reinforcement.

6. Develop a procedure to evaluate the influence of shear reinforcement on the flexural moment capacity, and the crack angles.

7. Discuss the behavior of flexural members under the combined effects of bending and axial loads. Decide on the numerical procedure to analyze these members.

8. Study the behavior of simply supported and continuous deep beams. Evaluate the efficiency of the proposed methods to analyze slender beams and their application for the analysis of deep beams.

9. Further develop the numerical procedure to account for the influence of shear on the behavior of beams so that it can be applied to deep beam analysis.

As a result of this study, a numerical procedure is proposed to analyze the behavior of beams. The procedure can be applied to slender or deep beams with or without axial loads. The proposed procedure makes it possible to describe the continuous behavior of such members under various loading conditions, as can be expected to act on structural members. The proposed procedure is both simple to use and reliable as will be demonstrated in Chapter 3.

This study introduces two significant improvements into existing analytical procedures to study the behavior of reinforced concrete structural members.

1. It determines the stress-strain relationship for reinforced and confined concrete in compression as a function of the part

of the cross section which is in compression. The result is a variable stress-strain relationship that depends on the location of the neutral axis, and the amount of confinement.

2. It evaluates the influence of shear reinforcement on the flexural moment capacity and crack inclination for beams.

2.2 Plain Concrete

Typical stress-strain curves for plain concrete can be found in the literature on reinforced concrete design. In general, plain concrete can resist a maximum stress f_c' and will crush at a strain ε_{cu}. The numerical value of f_c' defines the concrete strength, and is determined by standard laboratory tests on plain concrete specimens. From the same tests it was found that the values for ε_{cu} are usually in the strain range from 0.0028 to 0.004, when f_c' is in the range of 3000 psi to 5000 psi.

In reinforced concrete structures some confinement is almost always present. Therefore, the values of f_c' and ε_{cu} have to be considered only as basic properties of plain concrete, and reevaluated with the influence of confinement. The basic value ε_{cu} influences only the behavior of the concrete cover, which is the concrete that is not confined by the reinforcement. The behavior of the concrete cover is discussed in Section 2.5.1.

2.3 Confined Concrete

2.3.1 Introduction -- Richart et al. [1] found that concrete under a triaxial compression will exhibit a significant increase in strength and ductility. Based upon these results, it was proposed that the following relationship can be used to describe this behavior.

$$f_1 = f'_c + \gamma * f_2 \qquad\qquad (2.3.1)$$

where:

$\gamma = 4.1$

f_1 = axial compressive strength of the confined specimen

f_2 = lateral confining pressure

f'_c = uniaxial compressive strength of the unconfined specimen

The coefficient γ actually may vary between 4.5 to 7.0 with an average of 5.6 at low lateral pressures. This result was found by Balmer [74], after Eq. (2.3.1) had been proposed.

In a structural member, one cannot find an exact situation as in the experiments by Richart et al. However, a triaxial state of stress is present at advanced stages of loading when the concrete is compressed against the steel reinforcement. All types of reinforcement (longitudinal and transverse) provide confinement by the same general mechanism. At low levels of stress the concrete is able to resist the axial compression due to the deformation of the member under the loads. At higher stresses when the unconfined compressive strength (f'_c) of the concrete is reached, internal cracking and crushing of the concrete will reduce its stiffness, and the concrete will bulk and be "pushed" against the reinforcement. This interaction between the confined concrete and the reinforcement results in a confining pressure that improves the overall behavior of the member. The confining pressure is a function of the type and amount of reinforcement, the geometrical configuration of concrete and steel, and the material properties of the concrete and steel. It was shown, both theoretically and experimentally that better confinement will result in a better performance of the concrete.

2.3.2 <u>Concrete Confined by Circular Spirals</u> -- The effectiveness of spiral reinforcement was investigated by Iyengar <u>et</u> <u>al</u>. [2], and the general analysis of a specimen with spiral reinforcement can be found in books on reinforced concrete, as for example Park and Paulay [3]. From a free body diagram of a cross section of the specimen one can obtain the following equations, as illustrated in Fig. 2.1. (The Figures in this chapter are presented at the end of the chapter.)

$$2 * A_{sp} * f_s = D_c * S * f_r \tag{2.3.2}$$

If strain hardening is not considered for the reinforcement,

$$(f_r)_{max} = \frac{2 * A_{sp} * f_y}{D_c * S} \tag{2.3.3}$$

and when introduced into Eq. (2.3.1), where,

$$f_2 = (f_r)_{max} \tag{2.3.4}$$

one obtains the axial compressive strength of a spiral reinforced specimen as follows.

$$f_1 = f'_c + 8.2 * \frac{A_{sp} * f_y}{D_c * S} \tag{2.3.5}$$

where:

A_{sp} = cross section area of spiral reinforcement

f_s = average stress on the cross section A_{sp}

f_y = yield stress of spiral material

D_c = diameter of concrete core

S = spacing of spiral

f_r = lateral pressure on concrete core

2.3.3 <u>Concrete confined by rectangular hoops</u> -- Various models (i.e.,
stress-strain curves) for concrete confined by rectangular hoops are pre-
sented in the literature. Park and Paulay [3], describe some of these models,
and compare them. Based upon such models and further experimental evidence
Kent and Park [4] proposed a modified stress-strain curve for concrete con-
fined by rectangular hoops as illustrated in Fig. 2.2 and described
below.

The stress-strain curve is composed of three parts. The first is a
parabola, for the region of concrete strain smaller than 0.002. This is
based on the assumption that the maximum stress of the concrete is reached
at a strain of 0.002. In this region there is an increase in concrete
stress as the strain increases from zero to 0.002. The behavior in this
region is described by the following equation:

$$f_c = f'_c * [\frac{2 * \varepsilon_c}{0.002} - (\frac{\varepsilon_c}{0.002})^2] \qquad (2.3.6)$$

where:

f_c = concrete stress

ε_c = concrete strain

f'_c = concrete compressive strength (uniaxial)

The second part is a straight line, that shows a decrease in concrete
stress as the strain increases beyond 0.002. The lowest stress is assumed
to be 0.2 * f'_c. This line is described by Eq. (2.3.7).

$$f_c = f'_c * [1 - Z * (\varepsilon_c - 0.002)] \qquad (2.3.7)$$

where:

$$Z = \frac{0.5}{\varepsilon_{50u} + \varepsilon_{50h} - 0.002} \qquad (2.3.8)$$

$$\varepsilon_{50u} = \frac{3 + 0.002 * f'_c}{f'_c - 1000} \qquad (2.3.9)$$

$$\varepsilon_{50h} = \frac{3}{4} * \rho_s * \sqrt{\frac{b''}{S_h}} \qquad (2.3.10)$$

b" = width of confined core, measured to outside of hoops

S_h = spacing of hoops

$\rho_s = \dfrac{\text{volume of transverse reinforcement}}{\text{volume of concrete core, measured to outside of hoops}}$

The third part is for strains larger than ε_{20c}. (ε_{20c} is the strain at which the concrete stress has been reduced to $0.2 * f'_c$). Here, the assumption is that the concrete maintains its strength at:

$$f_c = 0.2 * f'_c \qquad (2.3.11)$$

Vallenas et al. [5] have also studied the stress-strain relationship for confined concrete, and compared their findings to models that had previously been proposed in the literature. They found that none of the methods approximated the experimental results obtained by them. Based upon the results obtained from columns tested under axial loads, Vallenas et al. proposed the following model: The parabolic part, for strains in the range from zero to ε_0 (ε_0 is the strain at which the concrete reaches the maximum stress) is described by Eq. (2.3.12).

$$f_c = f'_c * \frac{\frac{E_c\,\varepsilon_0}{f'_c} * (\frac{\varepsilon}{\varepsilon_0}) - K * (\frac{\varepsilon}{\varepsilon_0})^2}{1 + [\frac{E_c\,\varepsilon_0}{K\,f'_c} - 2] * (\frac{\varepsilon}{\varepsilon_0})} \qquad (2.3.12)$$

The straight line for strains larger then ε_0, but up to $\varepsilon_{0.3K}$ ($\varepsilon_{0.3K}$ is the strain at which the concrete stress has been reduced to $f_c = 0.3K * f'_c$), is described by Eq. (2.3.13).

$$f_c = f'_c * K * [1 - Z * \varepsilon_0 * (\frac{\varepsilon}{\varepsilon_0} - 1)] \qquad (2.3.13)$$

where:

$$\varepsilon_0 = 0.0024 + 0.005 * (1 - \frac{0.734 * S}{h''}) * \frac{\rho'' * f''_y}{\sqrt{f'_c}} \qquad (2.3.14)$$

$$K = 1 + 0.0091 * (1 - 0.245 * \frac{S}{h''}) * \frac{(\rho'' + \frac{d''}{D} * \rho) * f''_y}{\sqrt{f'_c}} \qquad (2.3.15)$$

$$Z = \frac{0.5}{\frac{3}{4} * \rho'' * \sqrt{\frac{h''}{s}} + (\frac{3 + 0.002 * f'_c}{f'_c - 1000}) - 0.002} \qquad (2.3.16)$$

The third part of the curve, for strains larger than $\varepsilon_{0.3K}$:

$$f_c = 0.3 * K * f'_c \qquad (2.3.17)$$

The stress-strain curve that was proposed in Ref. [5], is illustrated in Fig. 2.3.

E_c = "Elastic" modulus of concrete (tangent modulus), [psi]

h'' = core dimensions of square tied column, [in]

ρ'' = $\dfrac{\text{volume of confining steel}}{\text{volume of confined core}}$

ρ = percentage of longitudinal reinforcement

f''_y = yield stress of hoops, [psi].

S = spacing of hoops, [in].

d" = nominal diameter of lateral reinforcing bars, [in].

D = nominal diameter of longitudinal reinforcing bars, [in].

The values for maximum stress of the concrete and the influence of the longitudinal reinforcement on the stress-strain curve were investigated by Sargin [6,7]. Sargin found that the change in maximum stress in the concrete is a function of the following parameters,

a. spacing of the transverse reinforcement.

b. amount and strength (i.e., yield stress) of the transverse reinforcement.

c. loading duration, and load type.

d. strain gradient.

e. size of the specimen.

Sargin also noticed that the tangent modulus E_c, of the concrete, was not the same for the confined and unconfined specimens. The value of E_c decreased as more steel was present in the specimen, and caused more discontinuities in the concrete mass. These findings were confirmed by Vallenas et al. [5].

The results reported by Vallenas et al. [5], clearly show that the proposed model represents the behavior quite accurately, but some modifications are necessary to obtain a better representation of the experimental data. The modification is required for the region defined by strains larger than ε_0 (i.e., the straight line range, after maximum stress has been reached).

2.3.4 <u>Confinement Effectiveness</u> -- The mechanism of confinement, and the influence on the behavior of columns and flexural members has been studied quite extensively. Nevertheless, the exact effectiveness, and the resulting stresses induced in the confined zones of a member are still not completely understood. Vallenas <u>et al</u>. [5] stated that they could not find a consistent method with which to compute the lateral pressure on the confined concrete, and the effectiveness of various confinement geometries.

Base and Read [8], and McDonald [9] also studied the influence of confinement on the behavior of reinforced concrete members. The results of these studies show clearly that when confinement is increased, the behavior of beams becomes more ductile. There is a significant increase in rotation capacity even close to the ultimate moment. All types of transverse reinforcement cause improved behavior. They include spirals, rectangular hoops, ties, stirrups, and wire meshes. The spirals and wire meshes have been found to be most effective [9].

Sheikh [73] performed experiments similar to those reported in Ref. [5]. He also proposed a method to describe the confined core of a column, in such a way that the confinement effectiveness can be calculated. The stress-strain curve that is proposed in that analysis has many elements that have been described previously. Despite the good results reported by Sheikh, his model does not improve the understanding of the behavior in the strain range beyond ε_0, where the concrete stress decreases with an increase in strain.

The influence of the concrete cover on the behavior was studied by Vallenas <u>et al</u>. [5], and Sheikh [74]. They also describe previous studies

on this subject and their results. From these studies it is clear that the concrete cover reduces the effectiveness of the confinement, as a result of the reduction in core area when the cover spalls off, and removes chunks of the core between hoops. This spalling results in the increase in arching action between lateral reinforcing bars.

The results of all investigations that have been discussed in this chapter, clearly show that the longitudinal reinforcement provides support for the transverse reinforcement. When the longitudinal bars buckle or rupture that support is lost, and usually a significant decrease in the performance of the members is noticed, which may ultimately cause a complete loss of resistance to the applied load.

2.3.5 <u>Modulus of Elasticity of Concrete</u> -- The modulus of elasticity for concrete, which is the initial slope of the stress-strain curve, has been studied by several investigators. Some of the proposed equations to calculate E_c, are given below. E_c and f'_c are in psi units.

$$\text{ACl:} \qquad E_c = 57000 * \sqrt{f'_c} \qquad (2.3.18.a)$$

$$\text{Blume } \underline{et} \ \underline{al}. \ [11]: \quad E_c = 41574 * \sqrt{f'_c} \qquad (2.3.18.b)$$

$$\text{Kent and Park } [4]: \quad E_c = 66030 * \sqrt{f'_c} \qquad (2.3.18.c)$$

$$\text{Sargin } [6,7]: \qquad E_c = 72000 * \sqrt{f'_c} \qquad (2.3.18.d)$$

$$\text{experiments } [5]: \qquad E_c = 45963 * \sqrt{f'}_c \qquad (2.3.18.e)$$

The ACl method, Eq. (2.3.18.a), is very close to the average of the other methods.

2.4 Reinforcing Steel Bars

The stress-strain curves for steel reinforcing bars frequently used in the analysis of reinforced concrete members are of three types, in general. In the first, the elasto-plastic model, elastic behavior is assumed up to the yield point and from there on the behavior is perfectly plastic, as illustrated in Fig. 2.4. In the second, the same elastic part exists as before, with a plastic part after yield, but from a certain strain ε_{sh} (strain at which strain hardening in the material is noticed to begin) any increase in strain will result in a linear increase in stress. This model is composed of two inclined lines connected by a horizontal line. The slopes of the inclined lines represent the elastic modulus E, and the strain hardening constant. In the third model, the behavior is modelled the same as in the second, up to the strain ε_{sh}; from there on the increase in stress due to hardening is not linear but a polynomial of the second degree.

In order to obtain a realistic analytical method for reinforced concrete members, one has to consider the influence of strain hardening. The assumption of a linear strain hardening coefficient will not be considered because it represents only a special case. Two general methods are commonly employed to describe the strain hardening part of the stress-strain curve. The first was proposed by Burns and Siess [12] and is as follows.

$$f_s = f_y * [\frac{112 * (\varepsilon_s - \varepsilon_{sh}) + 2}{60 * (\varepsilon_s - \varepsilon_{sh}) + 2} + \frac{(\varepsilon_s - \varepsilon_{sh})}{(\varepsilon_{su} - \varepsilon_{sh})} * (\frac{f_u}{f_y} - 1.7)] \qquad (2.4.1)$$

where:

ε_s = strain at which the stress f_s is to be evaluated

ε_{sh} = strain at which strain hardening begins

ε_{su} = ultimate strain

f_y = yield stress

f_u = ultimate stress

The second model was proposed by Park and Paulay [3] as follows.

$$f_s = f_y * [\frac{m * (\varepsilon_s - \varepsilon_{sh}) + 2}{60 * (\varepsilon_s - \varepsilon_{sh}) + 2} + \frac{(\varepsilon_s - \varepsilon_{sh}) * (60 - m)}{2 * (30 * r + 1)^2}] \qquad (2.4.2)$$

where:

$$m = \frac{(\frac{f_u}{f_y}) * (30 * r + 1)^2 - 60 * r - 1}{15 * r^2} \qquad (2.4.2a)$$

$$r = \varepsilon_{su} - \varepsilon_{sh} \qquad (2.4.2b)$$

The stress-strain relationship described by Eqs. (2.4.2) is of a more general form than the relationship described by Eq. (2.4.1). Eqs. (2.4.1) and (2.4.2) may be compared as follows. The same strain parameters obtained experimentally (see Ref. [12]) and presented in Table B2 of Appendix B, are introduced into these equations. The following relationships are found for tensile bars in beam J-2.

at 1 percent strain: $(f_s)_{Eq. (2.4.2)} = 1.025 * (f_s)_{Eq. (2.4.1)}$

at 10 percent strain: $(f_s)_{Eq. (2.4.2)} = 1.05 * (f_s)_{Eq. (2.4.1)}$

Similar results are obtained for strains from other bars.

These results and preliminary evaluations of the numerical procedure described in the following sections indicate that Eq. (2.4.2) should be

preferred for the analysis of reinforced concrete beams. However, the accuracy of the numerical procedure does not depend only upon the stress-strain relationship for the steel bars, as will be discussed in the following sections.

2.5 Modified Model for Confined Concrete

In section 2.3 various stress-strain curves for confined concrete have been described, and discussed. After these methods for describing the behavior of confined concrete were compared especially to experimental data as presented in the literature, the model proposed by Vallenas et al. [5] was chosen as a basic method, in which some modifications would have to be made in order to apply it to the present research.

The first modification, that has later been justified by the numerical results, was to rotate the stress-strain curve upward in the region defined by $\varepsilon_0 \leq \varepsilon \leq \varepsilon_{0.3K}$. The axis of rotation was the point of maximum stress on the stress-strain curve, as illustrated in Fig. 2.5. This change caused the stress-strain curve to approach the experimental results, even at strains larger than ε_0. The equations that describe the stress-strain curve are the following.

Part 1: for the strain range defined by $0 \leq \varepsilon \leq \varepsilon_0$.

The behavior in this region is described by Eq. (2.3.12) as follows.

$$f_c = f'_c * \frac{\dfrac{E_c * \varepsilon_0}{f'_c} * (\dfrac{\varepsilon}{\varepsilon_0}) - K * (\dfrac{\varepsilon}{\varepsilon_0})^2}{1 + [\dfrac{E_c \varepsilon_0}{K f'_c} - 2] * (\dfrac{\varepsilon}{\varepsilon_0})} \tag{2.5.1}$$

Part 2: for the strain range defined by $\varepsilon_0 < \varepsilon < \varepsilon_{0.3K}$.

The behavior in this region is as follows.

$$f_c = f'_c * K * [1 - 0.8 * Z * \varepsilon_0 * (\frac{\varepsilon}{\varepsilon_0} - 1)] \qquad (2.5.2)$$

The rotation, as explained earlier, is obtained by the introduction of the coefficient 0.8 into Eq. (2.3.13).

Part 3: for the strain range defined by $\varepsilon > \varepsilon_{0.3K}$.

The behavior in this region is described by Eq. (2.3.17) as follows.

$$f_c = 0.3 * K * f'_c \qquad (2.5.3)$$

The equations to calculate the parameters ε_0, K, Z are the same as Eqs. (2.3.14), (2.3.15), (2.3.16), respectively.

$$\varepsilon_0 = 0.0024 + 0.005 * (1 - \frac{0.734 * S}{h''}) * \frac{\rho'' * f''_y}{\sqrt{f'_c}} \qquad (2.5.4)$$

$$K = 1 + 0.0091 * (1 - 0.245 * \frac{S}{h''}) * \frac{(\rho'' + \frac{d''}{D} * \rho) * f''_y}{\sqrt{f'_c}} \qquad (2.5.5)$$

$$Z = \frac{0.5}{\frac{3}{4} * \rho'' * \sqrt{\frac{h''}{s}} + (\frac{3 + 0.002 * f'_c}{f'_c - 1000}) - 0.002} \qquad (2.5.6)$$

The model that was proposed by Vallenas et al. [5], and described in Section 2.3.3, is based upon the behavior of axially loaded columns. The various variables in the equations, as defined in Section 2.3, are related to column geometry and behavior. Before this model can be applied to the analysis of beams the variables have to be redefined in terms of beam geometry and behavior.

The stress-strain relationship that has been described here, is for confined concrete under compression. Therefore, in the case of flexural members, only the concrete in the compressive zone (i.e., in general a cross section of a flexural member is divided into two zones by the neutral axis, one zone is in compression while the other is in tension) should be considered when this stress-strain relationship is to be applied. The state of stress in the tensile zone will be discussed later in this section.

Based upon this assumption, the following changes in the definition of the variables have been made (see Section 2.3.3, for definitions).

ρ'' = only part of the transverse reinforcement that acts to confine the compressive zone. Therefore, only this volume of steel, and the volume of concrete, defined by the compressive zone and the spacing of the transverse reinforcement, should be considered to calculate this variable.

ρ = only the steel bars in the compressive zone (i.e., compressive reinforcement) should be considered.

h'' = beams usually do not have a square compressive zone. Therefore, h'' has to represent the average dimension of this zone, as follows.

$$h'' = \frac{1}{2} * (h''_1 + h''_2) \tag{2.5.7}$$

where h''_1 and h''_2 are the two sides of the rectangle that describes the compressive zone, measured to the outside of the steel hoops.

All variables and parameters are also described and defined in the Notation section. Also, see application of the procedure in Appendix D.

All the other variables in the equations that describe the stress-strain curve for confined concrete in compression have the same definition as in Section 2.3.

It is clear that for flexural members the stress-strain curve for concrete will not have a fixed shape. Any shift in the location of the neutral axis will cause changes in the values of ε_0, K, Z (due to changing the values of the variables in the expressions that define these parameters), and therefore, the values of the concrete stress calculated from any of the Eqs. (2.5.1), (2.5.2), (2.5.3) will also change. That means that one does not have a stress-strain curve for the concrete, but a family of curves. The curve to be used for each stage of the analysis depends on the location of the neutral axis at that particular stage, as illustrated in Fig. 2.6.

The changes in the definitions of the variables ρ'', ρ, h" are such that when a column is considered, they resume their original definition as presented in Ref. [5]. Therefore, it is possible to analyze beams and columns by the same general model for reinforced concrete.

2.5.1 The Concrete Cover -- Some observations about the behavior of the concrete cover have been made in the previous section. Several assumptions are made here to provide a base for a consistent description of the behavior of the concrete cover, and the contribution of the concrete cover to the behavior of a flexural member, as follows.

a. The concrete cover crushes at a strain of 0.004 $\frac{in}{in}$.

b. The concrete cover may continue to resist compressive stresses even after crushing, as long as the cover has not spalled off. But, spalling is assumed to occur when the compressive bars reach a strain of 0.004.

c. At strains smaller than 0.004 $\frac{in}{in}$ the concrete cover behaves as
    the confined concrete, and the same stress-strain relationships
    describe the behavior. At strains larger than 0.004 $\frac{in}{in}$ the
    concrete cover exhibits a behavior different from that of the
    confined concrete. This assumption was proposed by Blume et
    al. [11], and by Baker and Amarakone [10].

d. Concrete cover located at an elevation higher than the bottom
    of the compressive reinforcement, spalls off at strains which
    exceeds 0.004 $\frac{in}{in}$. However, concrete cover located between the
    bottom of the compressive reinforcement and the neutral axis
    may remain on the member even at strains larger than 0.004 $\frac{in}{in}$.

e. The concrete cover remaining on the member at strains which
    exceed 0.004 $\frac{in}{in}$ resists compressive stresses in the range
    between 0.5 f'_c to 0.85 f'_c. This assumption is justified by
    the numerical results presented in Chapter 3.

2.5.2 Concrete in Tension -- The behavior of concrete in tension is

assumed to be linear up to a stress f_r, at which tensile cracks will cause a

complete loss of resistance. The slope of the line that describes this

behavior is E_c, the same as for early stages in compression. Park and

Paulay [3] recommend the following expression for the ultimate tensile

stress f_r, as illustrated in Fig. 2.7.

$$f_r = \lambda * \sqrt{f'_c} \qquad\qquad (2.5.8)$$

where λ is in the range of 7 to 13.

$\lambda = 7.5$ is assumed to define a lower bound for f_r.

The contribution of the concrete in tension is not considered in the analysis because the present study concentrates on the behavior beyond the yield stage of the tensile reinforcement, and up to ultimate loading conditions. At such advanced stages of loading the concrete in the tensile zone is cracked and the contribution of this zone to the in-plane force system is negligible. The only parameter from the tensile zone which is considered in a later section is the inclination of cracks and their influence on the behavior of a member.

2.5.3 The Stress-Strain Curve -- Based upon the discussion in this chapter the general shape of the stress-strain curve for confined concrete is illustrated in Fig. 2.7. This study will consider only the contribution of concrete in compression to the behavior of reinforced concrete members. The shape of the stress-strain curve in compression is influenced by the parameters K, and ε_0. These parameters depend upon the location of the neutral axis at each loading stage. Therefore, each loading stage requires the use of a different stress-strain curve, as will be demonstrated later.

2.6 The Numerical Procedure for the Analysis of Flexural Members

The method used to analyze reinforced concrete flexural members in this study is similar to the procedure developed by Kent and Park [4], and described by Park and Paulay [3]. However, some changes are introduced into the general procedure in order to make the analysis conform with the real geometry of the members under consideration, and with the stress-strain relationships for steel and concrete that have been discussed earlier.

Before the method is described in detail, it should be clear that the influence of shear is not considered at this stage. The influence of shear is discussed in a later section of this study, where a method to account for this influence is developed.

The basic procedure used to analyze reinforced concrete flexural members, as presented in the literature, is quite straight forward. First a strain distribution is assumed for the cross section under consideration. Then, from stress-strain relationships for concrete and steel, the stresses are calculated. Next, one calculates the forces due to these stresses, and sums all tensile forces, and separately the compressive forces. If the sum of the compressive forces equals the sum of the tensile forces, the cross section is in equilibrium and the moments and curvatures corresponding to this situation are calculated. In this type of analysis usually a linear strain distribution is assumed. This assumption of "plane sections before bending remain plane after bending" is a basic assumption in reinforced concrete analysis and design. However, this assumption may not be correct locally near cracks in the tensile zone, which indicates local bond failure. Furthermore, when deep beams are considered, or regions of high shear stresses are present in the member, this assumption is not valid. If these cases are excluded, the assumption is known to hold reasonably well for all stages of loading, up to flexural failure.

In order to obtain a numerical procedure which is simple for application, the cross section under consideration is divided into layers, parallel to the neutral axis. As mentioned earlier only the compressive zone needs

to be considered because the contribution, of the concrete in the tensile zone at advanced stages of loading is neglected.

The first stage of the analysis is to assume a depth (i.e., location) of the neutral axis. Then a linear strain distribution is imposed on the cross section. Usually this can be done either by assuming a strain at the tensile steel level, or at the extreme concrete fiber that is in compression. The strains of each layer of concrete, or steel bars, is found by simple geometrical consideration. The results are values of ε_{ci}, and ε_{sj}. where:

ε_{ci} = strain at layer i of the concrete

ε_{sj} = strain of steel bar j (or of steel bars at elevation j from the neutral axis)

From the corresponding stress-strain relationships for steel and concrete one can calculate the stresses at each layer and in each bar. The stress-strain curve for the concrete has to be evaluated for each shift of the neutral axis, as explained in Section 2.5.

The forces acting on the cross section are calculated as follows.

$$F_{sj} = f_{sj} * A_{sj} \qquad\qquad (2.6.1)$$

$$F_{ci} = f_{ci} * A_{ci} \qquad\qquad (2.6.2)$$

where:

F_{sj} = force in steel bar(s) j (tensile or compressive)

A_{sj} = area of steel bar(s) j

f_{sj} = stress in steel bar(s) j

F_{ci} = force in concrete layer i

f_{ci} = stress in concrete layer i

A_{ci} = area of concrete layer i

When the cross section is in equilibrium the sum of all forces is zero. The forces are summed as follows.

$$P = \sum_j F_{sj} + \sum_i F_{ci} \qquad (2.6.3)$$

If $P \neq 0$ a new assumption for the neutral axis location (kd) has to be made, and all the previous stages have to be repeated until a kd value is found for which $P = 0$. (kd is the distance of the neutral axis from the extreme concrete fiber.)

When $P = 0$, moments of all forces are summed with respect to a specific point (usually all moment are summed with respect to the tensile steel level).

$$M = \sum_i (F_{ci} * Y_i) + \sum_j (C'_{sj} * Y_j) \qquad (2.6.4)$$

where:

Y_i = distance from concrete layer i to tensile steel level

Y_j = distance from compression bar j to tensile steel level

C'_{sj} = compressive force in steel bar j

The curvature is defined by:

$$\phi = \frac{\varepsilon_{cm}}{kd} \qquad (2.6.5)$$

where:

ε_{cm} = strain at top compressive fiber

kd = depth of neutral axis from top of the member

Variation of the linear strain distribution over the cross section, and repetition of all these calculations, will result in a set of M-ϕ values.

These values when plotted comprise a moment-curvature diagram that describes
the behavior of the member under consideration at various stages of loading
(from yield to ultimate in this study).

In this study, three types of forces on the cross section are considered.

a. Forces in the longitudinal reinforcement bars. These steel
   bars are considered in their exact location on the cross
   section.

b. Forces in the concrete that is confined by the reinforcement.

c. Forces in the concrete cover.

An illustration of the method is presented in Appendix C.

Norton [13], and Park and Sampson [14], employed the same general pro-
cedure in their studies. The difference between their approach and the
present procedure is the following. Here, the longitudinal reinforcing bars
are considered at the exact location in the cross section, while the same
bars have been "distributed" into an equivalent steel tube in Refs. [13]
and [14]. This approach of distributing discrete bars into a continuous
tube could be justified for columns and, even then, only when the entire
cross section is in compression. When a flexural member is analyzed,
usually not the entire cross section is in compression, and the location
of the tensile and compressive forces is important, especially when these
forces are actually acting on a small area, relative to the cross section.

2.7 The Influence of Shear on the Behavior of Slender Beams

2.7.1 Introduction -- The influence of shear stresses on the behavior
of reinforced concrete beams has been studied quite extensively in the last

twenty years. Despite the large amount of information about the influence of shear and the better understanding of the shear mechanisms, there exists no rational theory yet that can describe mathematically the influence of shear on the behavior of reinforced concrete members. The nature of failures influenced by shear is brittle and therefore it is of great importance to avoid such results by minimizing the influence of shear. The evaluation of the shear strength of a member is based upon elastic theory and empirical formulations. In order to understand the problems concerning shear in reinforced concrete members one should first try to evaluate the behavior when no shear reinforcement is present. Theoretical and experimental results concerning the shear influence on reinforced concrete members are found in the report of ACI-ASCE Joint Committee 426 [15], and other sources, as discussed later.

2.7.2 <u>Slender Beams Without Web Reinforcement</u> -- In the general case of an elastic isotropic homogeneous beam, the combination of flexure and shear results in a biaxial state of stress. The necessity for the presence of shear stresses in a beam when the applied loading conditions cause the beam to bend is discussed in books on strength of materials. This biaxial state of stress can be illustrated by drawing the trajectories of the principal stresses (tensile and compressive) on a vertical plane parallel to the longitudinal axis of the beam (Fig. 2.8). In the case of a concrete member, flexural cracks are formed at the bottom of the beam, when the tensile stresses exceed the tensile strength of the concrete. However, because the orientation of the principal tensile stresses varies at points higher up towards the top of the beam, the cracks that are initiated as vertical

near the bottom of the beam follow the general orientation of the principal tensile stress lines; hence inclined cracks are formed. In certain cases inclined cracks will form in the webs of T or I beams, without being extensions of flexural cracks at the bottom of the members, as a result of high shear stresses in the web.

In the case of reinforced concrete beams without web reinforcement, the load to cause flexural and shear influenced cracks could be lower than for the theoretical case previously described. Lower loads to cause shear cracking are a result of the discontinuities in the members, and the associated stress concentrations. (Some of these include the concrete aggregate, the interface between steel and concrete, cracks due to shrinkage of the concrete, and flexural cracks at the bottom of the beam.)

If one examines the equilibrium force system of a free body diagram for a part of a beam, as illustrated in Fig. 2.9, the following equation is obtained.

$$V = V_c + V_a + V_d \qquad (2.7.1)$$

where:

V = vertical reaction over the support

V_c = shear force across the compressive zone

V_a = sum of vertical component of interlocking shear forces

V_d = dowel force across the crack transmitted by the main reinforcement

The moment for this case is given by

$$M = x * V = jd * (T + V_d * \cot \alpha) \qquad (2.7.2)$$

where:

jd = vertical distance between the tension T and the resultant com-
pression C

T = tensile force in the main (tensile) reinforcement

α = inclination of the crack to horizontal

x = horizontal distance between V and V_c

In design, the force V_d is usually ignored and Eq. (2.7.2) becomes a
simpler expression.

$$M = jd * T \qquad (2.7.3)$$

At present, it is assumed that two types of mechanisms are involved in
the resistance to the shear stresses. It is necessary to identify these
mechanisms and describe their action in order to understand the behavior of
a member under various loading conditions. An extensive discussion of the
subject can be found in the book by Park and Paulay [3]. Here, only a
brief review is given.

From basic principles of mechanics the following relationship is assumed.

$$V = \frac{dM}{dX} \qquad (2.7.4)$$

where:

V = shear force

M = moment

X = coordinate along the beam axis

When Eq. (2.7.3) is introduced into Eq. (2.7.4) the following result is obtained.

$$V = \frac{dM}{dX} = jd * \frac{dT}{dX} + T * \frac{d(jd)}{dX} \tag{2.7.5}$$

Noting that

$$\frac{d}{dX}(jd) = 0 \tag{2.7.6}$$

Therefore:

$$V = jd * \frac{dT}{dX} \tag{2.7.7}$$

This mechanism is only justified if the shear flow, or bond force $\frac{dT}{dX}$, can be efficiently transferred between the longitudinal reinforcement and the surrounding concrete. This mechanism is referred to in the literature as the "beam action" mechanism, and is largely affected by the presence of bond between steel and concrete.

If the bond between steel and concrete along the tensile reinforcement is destroyed over a finite length of the shear span then $\frac{dT}{dX} = 0$, and the "beam mechanism" is no longer valid. In such case the resistance to shear is obtained by inclined compression. While the contributions made by aggregate interlock and dowel forces may assist in general they are ignored at present. This mechanism is known as "arch action", and is described by Eq. (2.7.8).

$$V = T * \frac{d}{dX} (jd) = C * \frac{d}{dX} (jd) \tag{2.7.8}$$

C = sum of compressive forces, that is equal to T, in the cross section of the beam, without axial load.

In general, it is assumed that both mechanisms resist the shear stresses simultaneously. The contribution of each mechanism depends upon the amount of cracking and bond in the member.

In the case of "beam action", the cracks in the tensile zone of the member create concrete blocks that are separated from each other by the cracks. These blocks are acting like concrete cantilevers, where one end is "built in" into the compressive zone of the beam, and the other is acted upon by the tensile reinforcement. There are several forces that should also be considered in this case:

1. Variation in tensile forces between cracks, ΔT

2. Shear from aggregate interlock, along cracks

3. Dowel forces across the longitudinal reinforcement

4. "Built in reactions" at the base of the cantilever

Fenwick and Paulay [16], and Leonhardt and Walther [17] have found experimentally that up to 20% of the bond force could be resisted by flexure at the "built in" end of the concrete blocks. The dowel action is governed by the tensile strength of the concrete, and is reduced when splitting of the concrete, near the tensile reinforcement, takes place. However, dowel action has been found to contribute only about 25% to the cantilever resistance, [16,18]. Dowel action can be increased by the use of web reinforcement that supports the longitudinal bars. The contribution of dowel forces to resist shear, has been studied by Taylor [18], Bauman and Rüsch [19], and O'Leary [20]. This behavior of the dowel forces is most applicable near a plastic hinge, after the main reinforcement bars have yielded or along joints where shear-sliding occurs.

Aggregate interlock in beams without web reinforcement has been found

to resist 50% to 70% of the bond force acting on a "concrete cantilever" [16,

21], and up to 1000 psi of shear stress [27].

Leonhardt and Walther [17], found that only 25% to 40% of the shear

resistance is contributed by the portion of the beam above the neutral axis.

Therefore, most of the resistance to shear   takes place below the neutral

axis.

The "arch action" mechanism is illustrated in Fig. 2.10. The forces

acting on the inclined compressive zone are a vertical reaction at the sup-

ports, a horizontal tensile force from the tensile reinforcement, and a

horizontal compressive force in the upper part of the beam. Tensile cracks

can form only outside the area in compression, and compatibility in dis-

placements of steel and concrete is obtained by slipping of concrete over

the steel bars of the tensile reinforcement. For arch action the following

conditions are necessary, as presented in Ref. [3].

1. Arch action is present only if no bond, between tensile reinforce-

    ment and concrete influence the slip mechanism.

2. Near load points the neutral axis is higher than elsewhere in the

    beam, and the location of the neutral axis cannot be calculated

    by the same methods employed for other areas of the member.

3. Relative displacements between steel bars and concrete is

    largest under the load points.

The use of deformed bars reduces the amount of arch action, and only after

the bond between steel and concrete is destroyed does arch action become ef-

fective. Another variable that controls the amount of arch action is the

resistance to compressive stresses in the inclined compressive zone and in the compressive zone above the neutral axis. It was found that the compressive stresses are a function of the shear span to depth ratio $(\frac{a}{d})$. This ratio may be described by following variables.

$$\frac{a}{d} = \frac{V}{V} * \frac{a}{d} = \frac{M}{V * d} \qquad (2.7.9)$$

There are three types of failures associated with arch action:

1. Shear compression failure - when shear cracks reduce the size of the compressive zone, and the compressive stresses exceed the compressive strength of the concrete. The result is crushing of the concrete in the compressive zone.

2. Flexural tension - when the thurst of the arch is eccentric, crushing may occur along that line.

3. Diagonal compression - this is for beams that have a shear span to depth ratio $\frac{a}{d} < 2$ (i.e., deep beams). The result is a reduction of flexural capacity.

Leonhardt and Walther [17] also found that the beams could be classified by the $\frac{a}{d}$ ratio that influences the behavior as follows.

1. $3 < \frac{a}{d} < 7$: the arch mechanism cannot resist the load.

2. $2 < \frac{a}{d} < 3$: shear compression or flexural tension failure.

3. $\frac{a}{d} < 2.5$: failure by crushing or splitting of concrete

Another type of failure is due to beam action. When the inclined cracks propagate towards the compressive zone, they reduce the area of the "built in" end of the concrete cantilevers. This causes an increased rotation at

the other end of the cantilever. The result, a decrease of dowel forces due to increased cracking near the tensile reinforcement, and decrease of aggregate interlock. The increased deformation increases the tensile stresses at the base of the cantilever, which in return causes further cracking. This type of failure is referred to as "diagonal tension".

Based upon the results obtained by Leonhardt and Walther [17], it is clear that the influence of shear on the behavior of a beam is in the following $\frac{a}{d}$ range: $1.5 < \frac{a}{d} < 7$. Actually the flexural moment capacity of a beam has been found to be a function of the ratio $\frac{a}{d}$ and the amount of longitudinal tensile reinforcement, as illustrated in Figs. 2.11 through 2.17. These results have been confirmed by Kani [22].

For design purposes the following procedure is recommended by the ACl 318-77 code to evaluate the shear strength of concrete in a beam without shear reinforcement.

$$v_c = \frac{V_c}{b_w d} = 1.9 * \sqrt{f'_c} + 2500 * \rho_w * \frac{V_u * d}{M_u} \leq 3.5 * \sqrt{f'_c} \qquad (2.7.10)$$

where:

$$\rho_w = \frac{A_s}{b_w * d} \qquad (2.7.10.a)$$

$$\frac{V_u * d}{M_u} \leq 1 \qquad (2.7.10.b)$$

A_s = area of tensile reinforcement, $[in^2]$

b_w = width of beam, $[in]$

d = effective depth of beam, $[in]$

The accuracy of these equations is illustrated in Fig. 2.18. Based upon dimensional analysis and statistical methods, Zsutty [23] proposed the use of the following expression.

$$v_c = 59 * (\frac{f'_c * \rho_w * d}{a})^{1/3} \tag{2.7.11}$$

and for beams where $\frac{a}{d} \leq 2.5$ he proposed the following change.

$$v_c = 59 * (\frac{f'_c * \rho_w * d}{a})^{1/3} * (2.5 * \frac{d}{a}) \tag{2.7.12}$$

2.7.3 <u>Beams With Web Reinforcement</u> -- When web reinforcement is introduced into the beam construction the behavior of the member may improve as a result of the following contributions.

1. Support of the longitudinal bars, and therefore increased dowel action.

2. Support of the concrete cantilevers which resist tensile stresses across cracks.

3. Improvement of the compressive strength of the confined concrete.

4. Restraint of crack opening and support of aggregate interlock.

5. Support of bond forces between tensile reinforcement and concrete, and delay in the splitting of concrete along these bars.

It has been shown previously, when the flexural properties of beams were discussed, that web reinforcement confines the concrete in the compressive zone, and improves the flexural moment capacity and rotational capacity of the members.

One of the analytical methods for calculating the amount of shear re-
inforcement is the "truss mechanism" analogy. In that method it is assumed
that a beam acts like a truss, composed of concrete compressive members and
steel tensile members. The static analysis of the equivalent truss yields
the forces in the truss members, from which the amount of shear reinforcement
can be evaluated. That method is discussed in books on reinforced concrete
design, for example see Park and Paulay [3].

There are two major design philosophies concerning the amount of web
reinforcement to resist shear. In the first, as recommended by the ACl Code,
it is assumed that both the concrete and web reinforcement resist the shear
stresses. Therefore, the amount of shear reinforcement can be calculated
from the following expression.

$$v_u = v_s + v_c \qquad\qquad (2.7.13)$$

where:

v_u = ultimate shear strength of a member.

v_s = shear strength contribution by web reinforcement

v_c = shear strength contribution by concrete, from Eq. (2.7.10) or

    equivalent

Because of the relatively large possible error in evaluating the magni-
tude of v_c there are safety requirements that may cause the design to become
conservative.

The second philosophy of evaluating the required amount of shear rein-
forcement is used in Europe [24], where the web reinforcement is required to

resist the total shear stress, and the contribution of the concrete is neglected. Here too, in some cases the design may become conservative. One major advantage of the second method is that one does not have to try to evaluate the shear resistance of the concrete.

One of the results from the "truss mechanism" analysis is that when cracks are formed in a beam, the tensile forces increase. This result is presented in Ref. [3], and is illustrated by the following equation.

$$T_u = \frac{M_u}{jd} + \frac{e_v}{d} V_u \qquad\qquad (2.7.14)$$

where:

$$\frac{e_v}{d} = \cot \alpha - \frac{\eta}{2} * (\cot \alpha + \cot \beta) \qquad\qquad (2.7.14.a)$$

when no cracks form:
$$\frac{e_v}{d} = - \frac{\eta}{2} * \cot \beta \qquad\qquad (2.7.14.b)$$

$$\eta = \frac{V_s}{V_u} = \frac{v_s}{v_u} \qquad\qquad (2.7.14.c)$$

α = inclination of the cracks to the horizontal

β = inclination of the stirrups to the horizontal (opposed to α)

This increase requires better anchorage of the web reinforcement to prevent premature failure.

The influence of axial loads on the behavior is discussed in a later section.

The deformations of slender members are not affected significantly by shear; however, such is not the case for deep beams. The effect of shear on the behavior of deep beams is discussed in a separate section.

2.7.4 <u>Aggregate Interlock and Dowel Action</u> -- The mechanisms of aggregate interlock and dowel action have been mentioned before, in this chapter. Nevertheless, it is important to describe these mechanisms before the model for shear resistance is presented.

Basically these two mechanisms transfer shear stresses, from one part of the member to another. Dowel action transfers shear stresses across a crack in the member. Aggregate interlock is present before cracking, and even after cracking as long as aggregate particles are in contact.

Mattock and Hawkins [25] studied these mechanisms. When the specimen was uncracked the principal stresses could be evaluated by the use of a failure envelope of the type proposed by Bresler and Pister [26], from which one can find the stage at which a crack will form and its orientation. After the formation of the crack the transverse reinforcement had to develop a clamping force that prevented sliding along the shear plane parallel to the shear crack. When the shear reinforcement yielded the clamping force was greatly reduced, and the cracks propagated.

When precracked specimens were used an initial displacement was required in order to bring aggregate from both sides of the crack into full contact, at which the shear resistance was activated. This displacement was larger than the displacement in the uncracked specimen for the same amount of shear resistance. As the initial width of the cracks for the precracked specimens was increased the initial displacement also increased, and the ultimate shear resistance decreased (aggregate size was kept constant).

Paulay and Loeber [27] also studied this problem but used external clamping mechanisms to replace the shear reinforcement by which a constant

crack width was maintained. They found an increase in shear stress, as the shear displacement increased, and in general this relationship was bilinear, for stresses up to 1000 psi. Aggregate size in the range of $\frac{3''}{8}$ to $\frac{3''}{4}$ (9 mm to 19 mm) had no influence on the results.

Dowel action is obtained when steel bars resist the relative displacements across a crack. This resistance could develop due to three types of imposed deformations on the bars: flexure, shear, and kinking. Paulay et al. [28] found that kinking is probably the major mechanism in dowel action, particularly when small diameter bars are concerned. The mechanisms of flexure and shear should be considered as upper case results. In these studies [28] aggregate interlock was minimized by smooth and waxed surfaces in the cracks. However, when results were compared to those from aggregate interlock experiments it was found that the dowel stresses are smaller, and less important.

The calculation of shear resistance across a crack is based upon a simple frictional model, as follows.

$$v_{uf} = \mu * \frac{A_{vf} * f_y}{A_g} = \mu * \rho_{vf} * f_y \tag{2.7.15}$$

where:

v_{uf} = shear stress transferred across a crack

μ = coefficient of friction; from ACI code 318-77:

μ = 1.4 if member monolithically cast

μ = 1.0 if concrete placed against hardened concrete

A_{fv} = area of reinforcing bars that clamp the concrete

f_y = yield stress of bars

A_g = cracked surface area of concrete

Mattock and Hawkins [25] proposed the following expression.

$$v_{uf} = 200 + 0.8 * (\rho_{vf} * f_y + \frac{N}{A_g}) < 0.3 * f'_c \quad [psi] \quad (2.7.16)$$

N = externally applied clamping force, normal to the boundary. If

N is tension, consider as a negative number.

Based upon the experimental results that have been discussed, it is quite clear that web reinforcement constitutes an important component in a reinforced concrete member. The increase in the concrete compressive strength due to confinement, and the increase in shear resistance due to aggregate interlock and dowel action, are a direct result of the introduction of shear reinforcement into the member.

2.8 A Modified Method to Evaluate the Influence of Shear on Slender Beams

2.8.1 Introduction -- At present the design procedures that are employed in the U.S. and Europe require one to evaluate the amount of shear reinforcement that is necessary to minimize the influence of shear on the performance of a member. These methods have been discussed in the previous sections. However, none of these methods state that a certain level of moment capacity is associated with a certain amount of shear reinforcement. The artificial separation between shear resistance and moment capacity of a member could result in a design that may have the minimum amount of shear reinforcement, but will not be able to reach the desired moment capacity. Therefore, it is

reasonable to expect that if a method could be developed to predict the moment capacity as a function of the shear influence one could evaluate the optimum amount of shear reinforcement that will assure full moment capacity of the member. Furthermore, the incorporation of that method into the numerical procedure to evaluate the moment capacity, and rotation of a beam (see Section 2.6) will result in an improved method to evaluate the performance of reinforced concrete beams.

2.8.2 <u>Beams Without Web Reinforcement</u> -- Based upon results obtained by Leonhardt and Walther [17,29], and Kani [22], the moment capacity of a beam is a function of two variables. In the case of beams without web reinforcement, only the ratio $\frac{a}{d}$ (shear span to effective depth ratio), and ρ (percentage of tensile reinforcement) have been found to influence the moment capacity. This relationship is described by Figs. 2.11 through 2.17. From these results the following observations are made.

a. The minimum moment capacity is found to fall in the range:

$$2 \leq \frac{a}{d} \leq 3$$

b. For slender beams (i.e., $\frac{a}{d} > 3$) no moment reduction is observed for $\frac{a}{d}$ values larger than 7.

c. For deep beams (i.e., $\frac{a}{d} < 3$) no moment reduction is observed for $\frac{a}{d}$ values smaller than 1.

d. The behavior of the moment capacity is almost linear with respect to $\frac{a}{d}$ on both sides of the minimum moment capacity.

e. The value of the minimum (see observation a) is a function of ρ only. There is no indication that the ratio $\frac{a}{d}$ has any significant influence on this minimum, except to define its location with respect to the $\frac{a}{d}$ axis.

Based upon these observations one can formulate the dependence of the ultimate moment as a function of $\frac{a}{d}$ and ρ. This function is expected to have the following form.

$$\frac{M_u}{M_{f\ell}} = f(\frac{a}{d}, \rho) \qquad\qquad (2.8.1)$$

M_u = ultimate moment with shear influence

$M_{f\ell}$ = ultimate flexural moment without shear influence

2.8.3 <u>Minimum Moment Capacity as a Function of ρ</u> -- The first stage is to define the line that describes the deepest location in the moment reduction valley (Fig. 2.17). This line is constructed of three straight line segments, for three ranges of ρ. These segments are illustrated in Fig. 2.19, and defined as follows.

$$\rho \leq 0.65\% \qquad\qquad (\frac{M_u}{M_{f\ell}})_m = 1.0 \qquad\qquad (2.8.2.a)$$

$$0.65\% < \rho \leq 1.88\% \qquad (\frac{M_u}{M_{f\ell}})_m = 1 - 0.366 * (\rho - 0.65\%) \qquad (2.8.2.b)$$

$$1.88\% < \rho \leq 2.8\% \qquad (\frac{M_u}{M_{f\ell}})_m = 0.6 \qquad\qquad (2.8.2.c)$$

These equations have been obtained from Fig. 2.13 by numerical evaluation and are not given in the literature.

2.8.4 <u>The Relationship Between Moment Capacity and a/d - Slender Beams</u> -- The minimum moment capacity of slender beams with respect to the $\frac{a}{d}$ ratio is found in the following range.

$$2 \leq \frac{a}{d} \leq 3$$

This observation was made in Section 2.8.2. Furthermore, assume that the $\frac{a}{d}$ value at minimum is P_2, and the ratio of moment capacity with respect to full moment capacity is defined by $(\frac{M_u}{M_{fl}})_m$. At $\frac{a}{d} = 7$ the ratio of the moment capacity with respect to the full moment capacity is $\frac{M_u}{M_{fl}} = 1$.

Two points have been defined on the curve that describes the relationship between the ratio $\frac{M_u}{M_{fl}}$ and the ratio $\frac{a}{d}$. The first point represents minimum moment capacity at $\frac{a}{d} = P_2$, and the second point represents full moment capacity at $\frac{a}{d} = 7$ (or $\frac{a}{d} = P_3$).

Assume a straight line relationship between the two points that have been defined. This line is described by the following equation.

$$\frac{M_u}{M_{fl}} = 1.0 + [(\frac{M_u}{M_{fl}})_m - 1.0] * (\frac{\frac{a}{d} - 7.0}{P_2 - 7.0}) \tag{2.8.3}$$

Eq. (2.8.3) describes the moment capacity of a slender beam without web reinforcement. The parameter $\frac{a}{d}$ has direct influence on the moment capacity, while the parameter ρ has an indirect influence through the parameter $(\frac{M_u}{M_{fl}})_m$, as described by Eq. (2.8.2).

As a next stage, Eq. (2.8.3) has to be modified to include the influence of the shear reinforcement.

2.8.5 <u>The Influence of Shear Reinforcement on Slender Beams</u> -- The influence of the shear reinforcement on the moment capacity of a slender beam has been found to be indirect, as far as the mathematical formulation is concerned. The shear reinforcement has an influence on the inclination of cracks in the member. When the inclination is incorporated into the empirical formulation that was obtained previously, as described by Eq. (2.8.3), a modified equation that takes into account the contribution of the shear reinforcement is obtained.

Based upon the "truss mechanism" from which the shear reinforcement is usually calculated, the highest shear resistance that the shear reinforcement can contribute is given by Eq. (2.8.4).

$$(v_s)_{max} = \frac{A_v * \sin \beta * (\cot \alpha + \cot \beta) * f''_y}{S * b_w} \qquad (2.8.4)$$

where:

A_v = area of shear reinforcing bars in the cross section

β = inclination of shear reinforcement to the horizontal

α = angle of compression struts (cracks), measured from horizontal

S = spacing of shear reinforcement

b_w = web width of beam

for vertical shear reinforcement (i.e., $\beta = 90°$), Eq. (2.8.4) becomes

$$(v_s)_{max} = \frac{A_v * f''_y * \cot \alpha}{S * b_w} \qquad (2.8.5)$$

Eq. (2.8.5) indicates that both the amount of shear reinforcement and the angle α determine the shear resistance of a beam. Furthermore, it could

be possible that the amount of shear reinforcement influences the angle α. In design it is assumed that the crack inclination angle is 45 degrees. However, experimental data indicate that a wide range of crack inclinations is possible. Therefore, a nominal parameter is defined with $\cot \alpha = 1$, as follows.

$$(v_s)_{45°} = \frac{A_v * f''_y}{S * b_w} \qquad (2.8.6)$$

The percentage of shear reinforcement is defined as follows.

$$\rho'' = \frac{A_v}{b_w * S} \qquad (2.8.7)$$

When Eq. (2.8.7) is compared to Eq. (2.8.6), the following is found.

$$\rho'' = \frac{(v_s)_{45}}{f''_y} \qquad (2.8.8)$$

f''_y = yield stress of shear reinforcement.

The following parameters are defined.

$$\rho^*_1 = \rho'' * \frac{f''_y}{f'_c} \qquad (2.8.9.a)$$

$$\rho^*_2 = \rho'' * \frac{f''_y}{\sqrt{f'_c}} \qquad (2.8.9.b)$$

From experimental results by Burns and Siess [12], it is possible to calculate values of ρ''_1, and ρ''_2, and plot them as a function of the inclination of cracks, that have been measured. Four types of relationships are studied.

1. $\rho_1^* * \frac{a}{d}$ vs. α (Fig. B3 in Appendix B)

2. $\rho_2^* * \frac{a}{d}$ vs. α (Fig. B4 in Appendix B)

3. $\rho_1^* * \frac{a}{d}$ vs. $\tan \alpha$ (Fig. B5 in Appendix B)

4. $\rho_2^* * \frac{a}{d}$ vs. $\tan \alpha$ (Fig. B6 in Appendix B)

From these relationships it is obvious that the inclination of the cracks is a function of the amount of shear reinforcement. Only the linear relationships are considered in this study.

The first corresponds to item 1, as follows.

$$\alpha = -261.3 * (\rho_1^* * \frac{a}{d}) + 109.0 \qquad\qquad (2.8.10)$$

The second corresponds to item 2, as follows.

$$\alpha = -3.68 * (\rho_2^* * \frac{a}{d}) + 107.46 \qquad\qquad (2.8.11)$$

From each of these equations, one can evaluate the expected crack inclination α for the beam under consideration at ultimate moment conditions.

The influence of the shear reinforcement is illustrated in Fig. 2.20, and evaluated as follows.

1. Locate points 2 and 3 as defined in Section 2.8.4. Point 2 represents the minimum moment capacity for a beam without shear reinforcement at $\frac{a}{d} = P_2$. Point 3 represents full moment capacity at $\frac{a}{d} = P_3$.

2. Draw a straight line between points 2 and 3, as defined by Eq. (2.8.3).

3. Calculate a new minimum moment capacity that includes the in-
    fluence of the shear reinforcement. The shear reinforcement
    is represented by the crack angle α, and the new value $(\frac{M_u}{M_{f\ell}})'_m$
    as given by Eq. (2.8.12). This value is illustrated as point
    4 in Fig. 2.20. The angle α is found from Eq. (2.8.10), or
    Eq. (2.8.11).

$$(\frac{M_u}{M_{f\ell}})'_m = (\frac{M_u}{M_{f\ell}})_m + [1 - (\frac{M_u}{M_{f\ell}})_m] * \cot \alpha \leq 1.0 \qquad (2.8.12)$$

4. Define a new linear relationship illustrated by a straight line
    between point 4 and point 3 in Fig. 2.20 and described by the
    following equation.

$$\frac{M_u}{M_{f\ell}} = 1.0 + [(\frac{M_u}{M_{f\ell}})'_m - 1.0] * \frac{\frac{a}{d} - 7.0}{P_2 - 7.0} \qquad (2.8.13)$$

Eq. (2.8.13) is obtained by substituting $(\frac{M_u}{M_{f\ell}})'_m$ for $(\frac{M_u}{M_{f\ell}})_m$

in Eq. (2.8.3).

An increase in the amount of shear reinforcement results in a

point 5 which is closer to $\frac{M_u}{M_{f\ell}} = 1$ than point 4, and the beam

has a higher moment capacity than before.

5. When the $\frac{a}{d}$ ratio of the beam under consideration is introduced

    into Eq. (2.8.13), one can evaluate the expected moment capacity

    as a function of the following parameters.

    a. Amount of tensile reinforcement.

    b. Amount of shear reinforcement.

    c. The $\frac{a}{d}$ ratio.

    d. Material properties of the beam.

The relationship between shear reinforcement and ultimate moment capacity for slender beams as presented herein, is characterized as follows.

a. The ultimate moment capacity of slender beams without shear
    reinforcement is a function of the longitudinal steel content
    ρ, and the shear span to depth ratio $\frac{a}{d}$. This relationship is
    described by the straight line passing through points 2 and
    3 in Fig. 2.20.

b. The influence of the shear reinforcement is represented by the
    parameter cot α. The crack inclination angle α is related to
    the shear reinforcement as discussed in Section B2 of Appendix
    B. The properties of the shear reinforcement represented by
    the parameters $\rho_1^* * \frac{a}{d}$ and $\rho_2^* * \frac{a}{d}$, as defined by Eqs. (2.8.9.a),
    (2.8.9.b) determine the magnitude of the crack inclination
    angle α.

c. As the magnitude of the parameters $\rho_1^* * \frac{a}{d}$ and $\rho_2^* * \frac{a}{d}$ increase,
    the angle α decreases. Large amounts of shear reinforcement
    (assuming that the material properties of steel and concrete
    remain unchanged) result in low angled cracks, and high values
    of cot α.

d. When the crack inclination angle is in the following range,

    $$45° \leq \alpha \leq 90°$$

    an increase in the amount of shear reinforcement results in
    a decrease of crack inclination angles α. Therefore, higher
    values of cot α, which increase the magnitude of $\left(\frac{M_u}{M_{f\ell}}\right)'$ in Eq.
    (2.8.12), result in higher ultimate moment capacity, as
    defined by Eq. (2.8.13).

e. For crack angles smaller than 45 degrees, it is assumed that no

further increase in ultimate moment capacity can be obtained,

and the slender beam can reach its full flexural moment capacity.

f. There is no indication that excessive amounts of shear reinforce-

ment may cause a reduction in the ultimate moment capacity of

slender beams.

2.9 Flexure and Axial Loads

2.9.1 Introduction -- The combined behavior of a beam when flexure and

axial loads are considered to act simultaneously is reflected in the "inter-

action diagram" for a member. The interaction diagram is the graphical repre-

sentation of points (M, P) for various combinations of ultimate moment and

axial load. Each combination represents a failure situation. There are

several methods to construct such diagrams, and one can find the theoretical

and practical explanations for such methods in books on reinforced concrete

design, for example Park and Paulay [3]. However, these methods are dis-

cussed briefly before the proposed procedure is explained.

The conventional method, as recommended in the literature, calls for

the calculation of three representative points that show the behavior at three

special stages of loading, and several more points in between. The three

points that actually define the shape of the diagram are the following:

ultimate axial force without bending, balanced failure, and ultimate flex-

ural moment without axial load. The first point is calculated by assuming

that the cross section of the member is under compression, with the concrete

and steel having reached the highest possible stress (for design purposes,

the concrete stress is $0.85 * f_c'$, and the steel stress is f_y). The balance

point is calculated by assuming a linear strain distribution, where the tensile reinforcement is at the yield stress while the top concrete fiber in compression is at a strain of 0.003. The third point is calculated as for a beam in flexure at ultimate moment capacity. The points that are needed to complete the diagram are obtained by assuming various linear strain distributions, where the strain at the top concrete compression fiber is not greater than 0.003. For each stage, the strains imposed on the cross section result in stresses, from which the forces are evaluated. The difference between tensile and compressive forces is the axial load, and from moment considerations the moment on the cross section is calculated. The moment can be calculated as for a beam, or around the plastic centroid of the cross section. The plastic centroid is the location of the resultant force on the cross section, if the concrete is compressed to a stress $0.85 * f_c'$ and the steel is compressed to f_y. For design purposes the ACI rectangular stress block can be used, or any other equivalent method. The strain hardening of the steel bars is usually not considered.

2.9.2 The Proposed Method -- The method that has been adopted in this study is based upon the results from the analysis of beams in flexure without axial loads, and proceeds generally as follows. A linear strain distribution is assumed over the cross section of the member. The procedure to calculate stresses, as proposed for beams without axial loads, is employed, and the distribution of the stresses over the cross section is evaluated. The tensile or compressive forces are calculated by integrating the stresses over the corresponding areas. The difference between the sum of compressive

forces and the sum of tensile forces defines the axial load. The moment is calculated with respect to the plastic centroid. The numerical values of the axial load P, and the moment M, define a point on the interaction diagram. When a sufficient number of points have been calculated, the diagram can be plotted by a curved line passing through the given points.

In this study it is assumed that the crushing strain of plain concrete is 0.004. The members that are analyzed in Chapter 3 have been tested by Yamashiro and Siess [38]. Here, as in the case of beams without axial loads, the concrete strain may exceed the crushing strain and still provide some resistance, as will be demonstrated.

2.10   The Effect of Axial Loads on Members with Flexure and Shear

When axial loads are acting on a member some modifications are needed in order to consider the changes in the behavior. Based upon the report by ACI-ASCE Committee 326 [37], the following equation describes the modified ultimate moment to be considered:

$$M_m = M_u - \frac{(4h - d)}{8} * N_u \qquad (2.10.1)$$

where:

M_u = factored moment at section (may not be section capacity)

h = total depth of member

d = effective depth of member

N_u = axial force (+ for compression, - for tension)

Introducing Eq. (2.10.1) into Eq. (2.7.10), the new value for concrete shear resistance becomes:

$$v_c = 1.9 * \sqrt{f'_c} + 2500 * \rho_w * \frac{V_u * d}{M_m} \quad \text{[psi]} \quad (2.10.2)$$

The ACl 318-71 code allows the use of the following equation instead of Eq. (2.10.2).

$$v_c = 2 * (1 + 0.0005 * \frac{N_u}{A_g}) * f'_c \quad \text{[psi]} \quad (2.10.3)$$

but the following restriction is required

$$v_c \leq 3.5 * \sqrt{f'_c} * \sqrt{1 + 0.002 * \frac{N_u}{A_g}} \quad \text{[psi]} \quad (2.10.4)$$

A_g = gross concrete area of cross section.

(These equations do not apply to prestressed members.)

It was found experimentally that axial compression reduces the angle between the diagonal cracks and the horizontal (i.e., cracks are closer to horizontal). These angles are usually smaller than 45°. Therefore, the design assumption of cracks at 45° may result in a solution which is con-sidered as conservative.

Based upon the theoretical results that have been discussed in Section 2.8, where it was found that an increase in the amount of shear reinforcement will result in flatter cracks, it is clear that axial loads and shear rein-forcement have the same type of influence on the behavior of a member, and represented by the crack angle α.

2.11 Deep Beams

2.11.1 Introduction -- Beams are defined as "deep" when the ratio of shear span to effective depth $\frac{a}{d}$ is below a certain value. Simply supported beams

are classified as deep when $\frac{a}{d}$ is smaller than 2, while continuous beams have

to reach $\frac{a}{d}$ values smaller than 2.5 in order to be classified as deep. There

is one major factor that separates deep beams from slender beams. The tra-

ditional assumptions for the strain distributions over the cross section of

the beam are no longer valid in the case of deep beams. Linear strain dis-

tributions could be justified only at initial stages of loading, but as the

loading increases considerable deviations from the Bernoulli-Navier theory

are found. These deviations from the slender beam behavior increase even

more as the $\frac{a}{d}$ ratio decreases. This behavior has been verified by Leonhardt

and Walther [29], and discussed by Park and Paulay [3].

Deep beams are sensitive to boundary conditions such as, type of loading,

area of loading, type and geometry of supports, and the relative geometry of

the member with respect to the adjoining members. Despite numerous experi-

mental results, the ACI 318-77 code has only some provisions concerning deep

beams. However, one can obtain more information from the European Concrete

Committee [30].

2.11.2 Simply Supported Deep Beams -- Simply supported deep beams have

been studied quite extensively, and there is more information about this

type of deep beam than about the continuous deep beam. The study by

de Paiva and Siess [31] showed that deep beams without web reinforcement

could sustain loads larger than required for inclined cracking. Vertical

and inclined stirrups had no major influence on crack formation and ultimate

strength, for beams failing in flexure on shear. However, vertical rein-

forcement reduced the deflection at ultimate load. Based upon these findings

the authors proposed the following equations to evaluate the behavior:

$$v_s = \frac{V}{bD} = 200 + 0.188 * f'_c + 21300\ p_t \qquad (2.11.1)$$

$$p_t = \frac{A_s * (1 + \sin \alpha)}{bD} \qquad (2.11.1.a)$$

$$P'_s = 2 * v_s * b * D \qquad (2.11.2)$$

$$\frac{P''_s}{P'_s} = 0.80 * (1 - 0.6 * \frac{x}{D}) \qquad (2.11.3)$$

$$0 \leq x \leq 1.0$$

where:

V = shear force, [lbs]

v_s = nominal shear stress, [psi]

b = beam width, [in]

D = beam total depth, [in]

$A_s * (1 + \sin \alpha)$ = total steel area crossing a vertical section, [in^2]

α = inclination of reinforcement to beam axis, [deg.]

P'_s = load at failure due to shear, [lbs]

P''_s = computed shear strength, [lbs]

x = clear shear span between load blocks, [in]

Kani [32], investigated the safety of large reinforced concrete beams, and proposed a method to evaluate the relative strength of such beams when failure is governed by shear. The relative strength is a function of beam parameters and is given by:

$$r_u = \frac{0.215}{100 * \rho * \frac{d}{(in)}} * \frac{a}{d} \leq 1.0 \qquad (2.11.4)$$

where:

$$\rho = \frac{A_s}{bd}$$

$\frac{a}{d}$ = shear span to effective depth ratio

The error of Eq. (2.11.4) compared to experimental data is ±10%. The relative strength is defined by:

$$r_u = \frac{M_u}{M_{f\ell}} \tag{2.11.5}$$

M_u = actual ultimate moment

$M_{f\ell}$ = ultimate flexural moment = T * jd = ρ * b * d * f_y * jd

Another study by Ramakrishnan and Ananthanarayana [33], proposed the following equation for the ultimate load P_c.

$$P_c = \beta * K * f_t * b * H \tag{2.11.6}$$

where:

β = shear span coefficient

K = concrete strength coefficient

$$K = \begin{cases} 1.57 \text{ for cylinder split test} \\ 1.363 \text{ for diagonal cube split test} \\ 1.112 \text{ lower bound value} \end{cases} \tag{2.11.7}$$

$$f_t = \frac{\text{Maximum splitting force}}{K * \text{Area to resist the splitting force}} \tag{2.11.8}$$

b = beam thickness

H = beam total depth

Several cases of single point load, two point load, and uniformly distributed load have been studied.

Kong et al. [34] studied the behavior of deep beams made of regular concrete. Their findings were as follows.

1. For low $\frac{L}{D}$ ratios (span to depth ratio), only horizontal web reinforcement near the bottom of the beam is needed. Vertical web reinforcement is useful only for $\frac{L}{D} > 1.5$, and for $\frac{L}{D} = 3$ vertical reinforcement is better than horizontal reinforcement.

2. The primary cause of failure was diagonal cracking, while bearing failure was secondary.

3. Formulation to calculate ultimate loads could be either Eqs. (2.11.1) through (2.11.3), or Eq. (2.11.6). However, the first set of equations was recommended for very low $\frac{L}{D}$ ratios, at areas close to the longitudinal reinforcement.

A second study by Kong et al. [35], for lightweight concrete deep beams resulted in the following conclusions.

1. Inclined web reinforcement was most effective for all ranges of $\frac{L}{D}$. However, for low $\frac{L}{D}$ values, horizontal bars near the bottom of the members, gave also good results.

2. The primary cause of failure was diagonal cracking. However, inclined web reinforcement prevented this mode of failure, and the failure was caused by either beam splitting above the supports, or concrete crushing at the bearing blocks.

3. The methods proposed in Refs. [31,33] and described by Eq. (2.11.1) through Eq. (2.11.3), or by Eq. (2.11.6) are not valid for these cases.

4. The provisions for deep beams in the ACI 318-71 code, are quite

conservative.

Crist [36,39] investigated the static and dynamic behaviors of deep beams. He found that web reinforcement could prevent shear failures, and influence the crack patterns. Closely spaced light web reinforcement caused the cracks to form uniformly over the entire beam.

At a critical section located at $x_c = 0.2 * L$ the following analysis is proposed; $(x_c \sim d)$.

the total shear capacity:

$$V_u = V_{uc} + V_v \tag{2.11.9}$$

V_{uc} is the ultimate shear resistance contributed by the concrete, and is evaluated from Eq. (2.11.10).

$$\frac{V_{uc}}{bd} = [3.5 - \frac{4}{3} * (\frac{M}{V}) * \frac{1}{d}] * [1.9 * \sqrt{f'_c} + 2500 * \rho * (\frac{V}{M})_c * d] \tag{2.11.10}$$

V_v is the shear resistance of the vertical reinforcement evaluated as follows.

$$V_v = 1.5 + f_y * d * [\frac{A_v}{s} * \frac{1}{12} * (1 + \frac{L}{d}) + \frac{A_{vh}}{s_h} * \frac{1}{12} * (11 - \frac{L}{d})] \tag{2.11.11}$$

where:

A_v = area of vertical web reinforcement, [in^2]

A_{vh} = area of horizontal web reinforcement, [in^2]

S = spacing of web reinforcement along the beam axis, [in]

S_h = spacing of horizontal web reinforcement, [in]

The moment capacity of deep beams is given by the following equation when only the tensile reinforcement is allowed to be in the strain hardening region but all other reinforcing bars cannot exceed the yield stress f_y.

$$M_u = A_s * f_s * d * [1 - \frac{K_2}{K_1 * K_3} * (\frac{\rho * f_s}{f'_c})] \qquad (2.11.13)$$

The stress of the tensile reinforcement f_s evaluated from the strain distribution over the beam depth, and the stress strain curve for the steel bars is described by the following equations.

$$f_s = f(\varepsilon_s) \qquad (2.11.12.a)$$

$$f_s = K_1 * K_3 * \frac{f'_c}{\rho} * \frac{\varepsilon_c}{\varepsilon_c + \varepsilon_s} \qquad (2.11.12.b)$$

it was assumed that $\varepsilon_{cu} = 0.003 \frac{in}{in}$

The error of this method has been evaluated with respect to experimental data, and found to be in the range of ± 10 percent.

Based upon studies by Leonhardt and Walther [29], it is concluded that the internal lever arm of the forces acting on the cross section of a deep beam, can be calculated by the following equations.

$$Z' = 0.2 * (\ell + 2h) \qquad 1 < \frac{\ell}{h} < 2 \qquad (2.11.13.a)$$

$$Z' = 0.6 * \ell \qquad \frac{\ell}{h} < 1 \qquad (2.11.13.b)$$

where:

ℓ = span length

h = beam depth

Z' = lever arm

Furthermore, the same studies show that for deep beams the depth of the tensile zone is only about 0.25 * h from the bottom of the beam. Therefore, the tensile reinforcement should be placed in that region. However, the amount of tensile reinforcement, based upon this type of analysis should not be smaller than the amount of tensile reinforcement from slender beam type analysis.

The span length ℓ should be the smaller value of the following.

ℓ = center to center distance between supports

or ℓ = 1.15 * clear span

The European Code [30], also recommends that the flexural reinforcement should be placed in a region located not higher than 0.25H to 0.05ℓ, from the bottom of the beam (h < ℓ).

It is assumed that in the case of deep beams loads are transferred to the supports by arch action. Therefore, it is recommended in Ref. [30] that at the inner face of the supports the anchorage should be able to develop not less than 80% of the calculated steel force. Furthermore, only small diameter bars should be used, or mechanical anchorage should be provided.

2.11.3 <u>Continuous Deep Beams</u> -- The discussion on continuous deep beams is based on results that have been obtained in Europe [29,30]. Here, the deviation from linear strain distribution is even larger than for simply supported deep beams. As the span to depth ratio decreases towards 1.0, the internal lever arm Z also decreases. However, after cracking the lever arm will increase in both the negative ane positive moment zones, and this behavior is magnified after the yielding of the flexural reinforcement. It is recommended in Ref. [30] that the internal lever arm be calculated in the following way.

$$Z^{\cdot\cdot} = 0.2 * (\ell + 1.5 * h) \qquad 1.0 \leq \frac{\ell}{h} \leq 2.5 \qquad (2.11.14.a)$$

$$Z^{\cdot} = 0.5 * \ell \qquad \frac{\ell}{h} < 1.0 \qquad (2.11.14.b)$$

The combination of shear stresses and the vertical compression over the supports results in steeply inclined principal compression stresses. This state of stress indicates that arch action is a major mechanism to transfer forces to the supports.

The bending moment can be evaluated as for a slender continuous beam, $\frac{w\ell^2}{12}$ over the supports, and $\frac{w\ell^2}{24}$ at midspan (this is for a case of a uniformly distributed load w, and span ℓ). However, in the case of a cracked beam the lever arm becomes smaller at the supports and larger at midspan; the moment will also change correspondingly. This behavior was verified by Leonhardt and Walther [29].

The placing of the longitudinal reinforcement for continuous deep beams should be as follows.

At positive moment zones, just as for simply supported deep beams. Special attention to anchoring of the reinforcement is required.

At negative moment zones the reinforcement should be divided into two equal parts. One part should extend over the full length of the adjacent spans, while the other part can be cut off at a distance of 0.4 * ℓ or 0.4 * h (whichever smaller) from the edge of the supports. Furthermore, the negative moment reinforcement should be placed in two uniform bands, as illustrated in Fig. 2.21.

The upper band should be 0.2 * h deep, from the top of the member, and have the following reinforcement area.

$$A_{s1} = 0.5 * (\frac{\ell}{h} - 1) * A_s \qquad (2.11.15a)$$

The lower band should be just under the first band, 0.6 * h deep, and have the following reinforcement area.

$$A_{s2} = A_s - A_{s1} \qquad (2.11.15.b)$$

In all cases, only beam depths that are not larger than the span should be considered. Furthermore, in order to assure satisfactory behavior the maximum shear should be limited as follows.

$$V_{max} \leq 0.08 * \phi * b_w * h * f'_c \qquad (2.11.16)$$

where:

$\phi = 0.85$

h = beam depth ($h \leq \ell$), [in]

b_w = beam width, [in]

f'_c = compressive strength of concrete, [psi]

2.11.4 <u>Web Reinforcement in Deep Beams</u> -- In general, deep beams require less web reinforcement than slender beams, as a result of the higher stiffness associated with concrete mass. Furthermore, the main force transfer mechanism in deep beams is arch action, and larger parts of the beam are in compression.

The ACI 318-77 code has some provisions for simply supported deep beams, based upon an ASCE-AC report [15].

The shear resistance of the concrete is given by the following equation.

$$v_c = (3.5 - 2.5 * \frac{M_u}{V_u * d}) * (1.9 * \sqrt{f'_c} + 2500 * \rho_w * \frac{V_u * d}{M_u}) \leq 6 * \sqrt{f'_c}$$

$$\text{(psi units)} \qquad (2.11.17)$$

The first term in Eq. (2.11.17), represents the deep beam contribution, and should comply with the following restriction.

$$3.5 - 2.5 * \frac{M_u}{V_u * d} \leq 2.5 \qquad (2.11.17.a)$$

The resistance to shear due to the web reinforcement is as follows.

$$v_s = v_u - v_c = [\frac{A_v}{12 * s} * (1 + \frac{\ell}{d}) + \frac{A_{vh}}{12 * S_h} * (11 - \frac{\ell}{d})] * \frac{f_y}{b_w}$$

$$(2.11.18)$$

where:

$$v_u = \frac{V_u}{b_w * d}$$

Eq. (2.11.18) is similar to Eq. (2.11.11). Furthermore, this procedure is restricted by several conditions that are described in the ACI 318-77 code.

When this procedure is compared to the European method [30], as presented in Eq. (2.11.16), it is found that the ACI restrictions are about twice as high as the European restrictions for maximum allowable shear stresses, as discussed in Ref. [3].

2.12 A Modified Method to Evaluate the Influence of Shear on Deep Beams

2.12.1 Introduction -- The general behavior, as reported in the literature, and some design considerations for deep beams have been discussed in Section 2.11. It was noted in Section 2.11 that shear reinforcement in deep beams should be placed in a different way than for slender beams. However,

the basic assumption that if the amount of shear reinforcement is adequate

the beam can reach the desired ultimate performance should also be valid

for deep beams. Therefore, it is necessary to develop a method to evaluate

the expected ultimate moment capacity as a function of the beam parameters,

including the shear reinforcement. This method should not consider explicitly

the shear resistance of the concrete because this property of the concrete is

quite unpredictable, as discussed in Section 2.7. The procedure of developing

a method that can consider the influence of shear reinforcement on the be-

havior of deep beams is similar to the one employed for slender beams,

described in Section 2.8, and follows next.

2.12.2 Deep Beams Without Web Reinforcement -- The experimental results

that were reported by Leonhardt and Walther [17,39], and Kani [22,32], clearly

demonstrate that the reduction in the ultimate flexural moment due to shear,

in beams that contain only tensile reinforcement, is a function of the fol-

lowing parameters, as discussed in Sections 2.7 and 2.8.

a. The amount of tensile reinforcement, ρ.

b. The shear span to depth ratio, $\frac{a}{d}$.

The minimum moment capacity $(\frac{M_u}{M_{f\ell}})_m$ is a function of ρ and is located in

the range $2 \leq \frac{a}{d} \leq 3$, as discussed in Section 2.8. The numerical value of

$(\frac{M_u}{M_{f\ell}})_m$ can be obtained from Eqs. (2.8.2), as illustrated in Fig. 2.19. In

Section 2.8 it was observed that the reduction in moment capacity due to

shear is negligible when $\frac{a}{d} < 1$. Assume a linear variation of $\frac{M_u}{M_{f\ell}}$, as

a function of $\frac{a}{d}$. This assumption can be justified by the experimental data, as illustrated in Figs. 2.11, and 2.13 through 2.17.

Two points have been identified, as follows.

1. At $\frac{a}{d} = P_1$, where $P_1 = 1.0$, $\frac{M_u}{M_{f\ell}} = 1.0$

2. At $\frac{a}{d} = P_2$, where $2 \leq P_2 \leq 3$, $\frac{M_u}{M_{f\ell}} = (\frac{M_u}{M_{f\ell}})_m$

The general relationship can be defined by these points, and formulated as follows.

$$\frac{M_u}{M_{f\ell}} = [(\frac{M_u}{M_{f\ell}})_m - 1.0] * (\frac{\frac{a}{d} - P_1}{P_2 - P_1}) \qquad (2.12.1)$$

This relationship is illustrated in Fig. 2.22, and is considered as a lower bound for the model that described the behavior of deep beams with shear reinforcement.

2.12.3 <u>Deep Beams With Shear Reinforcement</u> -- The influence of the shear reinforcement on the moment capacity of deep beams is evaluated by the same procedure as employed for slender beams. The shear reinforcement influences the inclination of the cracks that develop in the beams resulting from the loading conditions as will be discussed later. The crack inclination α is a variable in the "truss mechanism" that influences the total shear resistance of the beam. Therefore, it is necessary to obtain a model that describes the relationship between the amount of shear reinforcement and the crack inclination.

The general procedure and definitions of the various parameters are described in Section 2.8.5. Experimental data reported by Crist [36,39] is used to obtain the necessary relationships. The experimental data and the possible relationships are presented in Appendix B. Two linear relationships are proposed, as follows.

1. $\log (\rho_1^* * \frac{a}{d})$ vs. $\log \alpha$ (see Fig. B7 in Appendix B) (2.12.2a)

2. $\log (\rho_2^* * \frac{a}{d})$ vs. $\log \alpha$ (see Fig. B8 in Appendix B) (2.12.2.b)

The equations for the proposed models obtained from geometrical considerations are as follows.

From Fig. B7 the following equation is obtained.

$$\log \alpha = 0.039396 * \log (\rho_1^* * \frac{a}{d}) + 1.97558 \qquad (2.12.3)$$

From Fig. B8 the following equation is obtained.

$$\log \alpha = 0.042 * \log (\rho_2^* * \frac{a}{d}) + 1.903 \qquad (2.12.4)$$

The crack inclination α can be evaluated from either one of these expressions.

When the crack angle α is known, one can modify Eq. (2.12.1) to include the influence of shear reinforcement. The procedure employed to modify Eq. (2.12.1) is identical to that used for slender beams, as described in Section 2.8.5. The following steps are performed, as illustrated in Fig. 2.22.

1. Points 1 and 2 have been defined in Section 2.12.2, and the straight line through these points, as defined by Eq. (2.12.1), describes the moment capacity of deep beams without shear reinforcement.

2. If shear reinforcement is included in the member, evaluate the crack inclination α, from Eq. (2.12.3) or Eq. (2.12.4).

3. Calculate a new minimum moment capacity $\left(\dfrac{M_u}{M_{f\ell}}\right)_m'$ for the value $\dfrac{a}{d} = P_2$.

    Employ Eq. (2.8.12) to perform this step, as follows.

$$\left(\frac{M_u}{M_{f\ell}}\right)_m = \left(\frac{M_u}{M_{f\ell}}\right)_m + \left[1 - \left(\frac{M_u}{M_{f\ell}}\right)_m\right] * \cot \alpha \leq 1.0 \qquad (2.8.12)$$

The values $\left(\dfrac{M_u}{M_{f\ell}}\right)_m'$ and P_2 define a point 4 in Fig. 2.22.

4. Obtain the equation for the straight line that connects points 4 and 1 by substituting in Eq. (2.12.1) $\left(\dfrac{M_u}{M_{f\ell}}\right)_m'$ for $\left(\dfrac{M_u}{M_{f\ell}}\right)_m$, as follows.

$$\frac{M_u}{M_{f\ell}} = \left[\left(\frac{M_u}{M_{f\ell}}\right)_m' - 1.0\right] * \left(\frac{\frac{a}{d} - P_2}{P_2 - P_1}\right) \qquad (2.12.5)$$

5. The expected moment capacity of a deep beam can be evaluated when the $\dfrac{a}{d}$ ratio of the beam under consideration is introduced into Eq. (2.12.5). The following parameters are considered in the present model.

    a. Amount of tensile reinforcement.

    b. Amount of shear reinforcement

    c. The $\dfrac{a}{d}$ ratio.

    d. Material properties of the beam.

The relationship between the amount of shear reinforcement and the ultimate moment capacity for deep beams as presented herein is characterized as follows.

a. The ultimate moment capacity of deep beams without shear rein-
    forcement is a function of the longitudinal steel content, ρ,
    and the shear span to depth ratio, $\frac{a}{d}$. This relationship is
    described by the straight line passing through points 1 and 2
    in Fig. 2.22.

b. The influence of the shear reinforcement is represented by the
    parameter cot α. The crack inclination α is related to the
    shear reinforcement as defined by Eqs. (2.12.3), (2.12.4) and
    discussed in Section B3 of Appendix B.

c. An increase in the magnitude of the parameters $\rho_1^* * \frac{a}{d}$ and
    $\rho_2^* * \frac{a}{d}$ results in the increase of the crack inclination angle
    α. Larger amounts of shear reinforcement (assuming that the
    material properties of steel and concrete remain unchanged)
    result in steeper crack angles, and lower values of cot α.

d. When the crack angle α is in the following range:

    $45° \leq \alpha \leq 90°$

    an increase in the amount of shear reinforcement decreases
    the value of cot α which results in a reduction of the ratio
    $(\frac{M_u}{M_{f\ell}})_m'$. This influence of the shear reinforcement is illustrated
    in Fig. 2.22 as follows. Point 4 represents the minimum flexural
    moment capacity corresponding to a certain amount of shear rein-
    forcement. When the amount of shear reinforcement is increased
    the minimum moment capacity decreases, as illustrated by point
    6 in Fig. 2.22. The ultimate moment capacity of the beam under
    consideration is defined by the straight line passing through

points 6 and 1 and the $\frac{a}{d}$ ratio for the beam, or described alge-
braically by Eq. (2.12.5). The downward rotation of the straight
line around point 1 indicates that an increase in the amount of
shear reinforcement results in a reduced ultimate moment capacity
of deep beams. This behavior of the model implies that deep beams
are sensitive to excessive amounts of shear reinforcement. There-
fore, it is desirable to avoid any unnecessary web reinforcement.

e. The optimum amount of shear reinforcement evaluated from the pro-
posed model corresponds to expected crack inclination angles of
45 degrees. The corresponding amount of shear reinforcement is
calculated from Eqs. (2.12.3) or (2.12.4). When the optimum
amount of shear reinforcement is provided the deep beam is
expected to develop the full ultimate flexural moment as il-
lustrated by the horizontal line through point 1 in Fig. 2.22
(i.e., $\frac{M_u}{M_{f\ell}} = 1.0$).

At present the proposed model accounting for the influence of shear
reinforcement cannot describe the behavior of deep beams with low amounts
of shear reinforcement. When the amount of shear reinforcement corresponds
to crack inclination angles smaller than 45 degrees the present model im-
plies that the moment capacity increases beyond the full ultimate moment
capacity, which is not physically possible. Therefore, the present model
should not be employed to analyze deep beams having light shear reinforcement.
Furthermore, the apparent discontinuity in the model at 45 degrees implies
that the behavior of deep beams is not fully understood. However, the ex-
perimental data reported in Refs. [36,39] clearly demonstrate that all crack

angles measured on seventeen deep beams were in the following range $50° < \alpha < 90°$. (These beams are analyzed in Chapter 3 and the results are compared to experimental data.) Therefore, the present model is employed to analyze these beams despite the discontinuous behavior at 45 degrees.

The basic mechanism associated with deep beam behavior may provide some explanation about the observed difficulties to describe the influence of low amounts of shear reinforcement on these members. Arching action is the major mechanism responsible for the load resisting capacity of deep beams. As a result large zones in the deep beams sustain compressive stresses which also contribute to improve the shear resistance of the concrete. Furthermore, it is possible that the shear reinforcement in deep beams has a different type of influence on the behavior than the influence associated with slender beams. This problem should be investigated further in the future.

The procedure to consider the influence of shear reinforcement on the ultimate moment capacity of deep beams is combined with the corresponding procedure for slender beams, as presented in Section 2.8.5. The resulting generalized method can be employed to evaluate the influence of shear rein-forcement on the ultimate moment capacity of slender or deep beams. A com-puter program TKSH4 is developed to perform the analysis, as described by the flow diagram in Fig. C2 of Appendix C and illustrated in Fig. 2.23.

2.13 Summary of the Proposed Analytical Method

2.13.1 Introduction -- The analytical method to analyze the behavior of reinforced concrete beams that is developed in this study, is composed of two major parts. In the first part only the flexural moment capacity is evaluated without the influence of shear. This step is described in Section

2.6. In the second part the influence of shear is introduced into the solution. This step separates the behavior of slender beams from the behavior of deep beams, as discussed in Sections 2.8 and 2.12. The method that is proposed as a result of this study can be applied to analyze slender or deep beams, with or without shear reinforcement. Furthermore, the method can be applied to analyze such beams even when axial loads act on the members.

2.13.2 <u>Flexural Analysis</u> -- The method to evaluate the flexural moment capacity, and the rotational capacity of beams is described in Section 2.6. In general terms, the method employs the concept of a variable stress-strain curve for reinforced and confined concrete, as discussed in Section 2.5, and the experimental stress-strain curves for steel bars. The variable stress-strain curve for reinforced and confined concrete is developed in this study from a model for reinforced concrete columns that was reported in the literature by other investigators. The numerical procedure is described in Section 2.6, and illustrated by a flow-diagram in Appendix C. Examples that demonstrate the application of the method to analyze flexural members are presented in Chapter 3.

The behavior of beams with axial loads is discussed in Sections 2.9 and 2.10. The method to analyze beams without axial loads is proposed for the analysis of flexural members under the combined effect of bending and axial load. The numerical procedure is demonstrated in Chapter 3.

2.13.3 <u>The Influences of Shear and Shear Reinforcement</u> -- The influence of shear on the behavior of slender beams is discussed in Section 2.7, and the behavior of deep beams is described in Section 2.11. The method employed for

evaluating the influence of shear reinforcement on the behavior of slender and

deep beams developed in this study is based on experimental and analytical

results reported by other investigators. The procedure for slender beams is

developed in Section 2.8, and for deep beams in Section 2.12. These separate

procedures are combined in this study into a generalized method by which one

can evaluate the influence of shear reinforcement on the behavior of both

slender and deep beams. The analysis is performed by a computer program

that has been developed in this study. The program TKSH4 is described by

the flow diagram in Appendix C, and illustrated in Fig. 2.23.

The proposed procedure to account for the influence of shear reinforce-

ment is based on a small amount of data. It is clear the influence of shear

is not fully understood, and further study is necessary to complete the model.

2.13.4 <u>The Combined Procedure</u> -- The analytical procedures for flexure

and shear are combined in this study to analyze various types of beams.

The beams under consideration were studied before, both experimentally and

theoretically by other investigators. The numerical results presented in

Chapter 3 are compared to the experimental results in order to evaluate the

nature and quality of the proposed method.

The procedure developed in this study does not consider the effects of

bond failure between the concrete and tensile reinforcement.
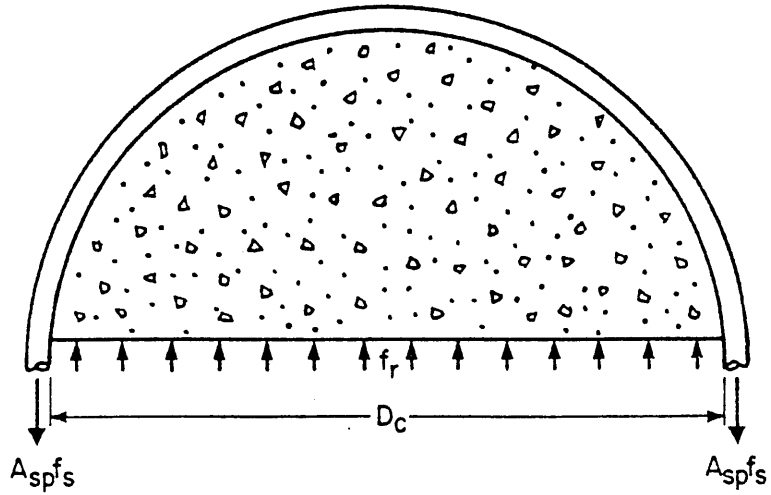
FIG. 2.1 Free-body diagram of concrete confined
with spiral reinforcement. Source Ref. [5]
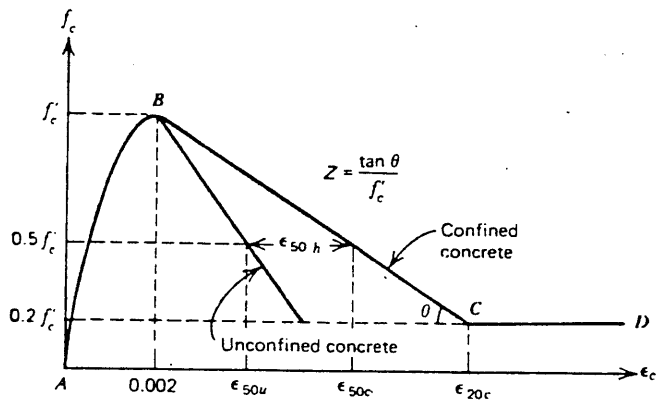
FIG. 2.2 Stress-strain curve for concrete confined by rectangular
hoops, Kent and Park. Source Ref. [3]
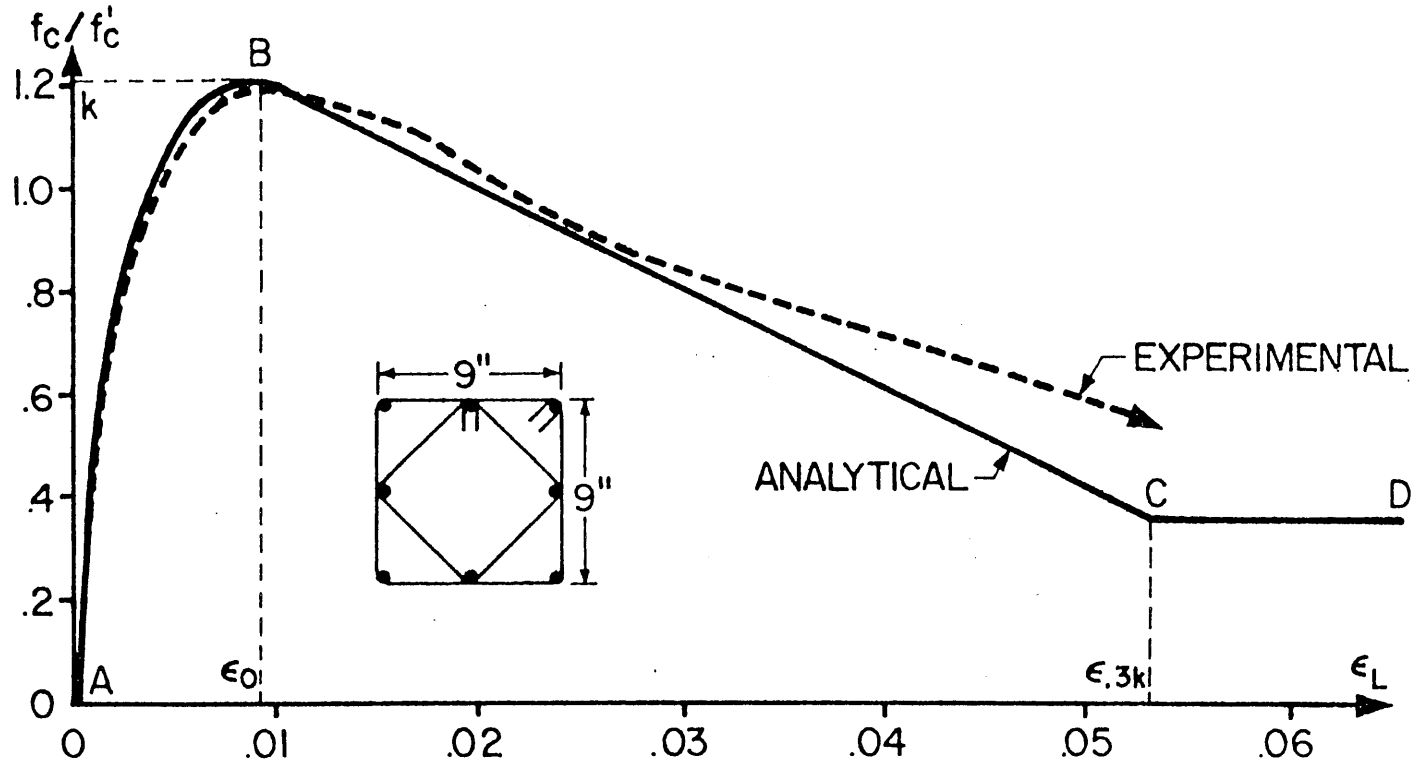
FIG. 2.3 New analytical curve and experimental results for confined concrete with longitudinal reinforcement. Source Ref. [5]

78
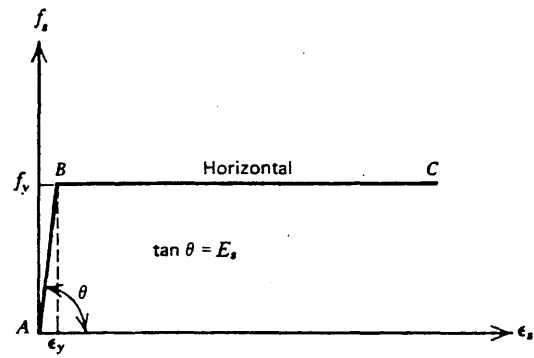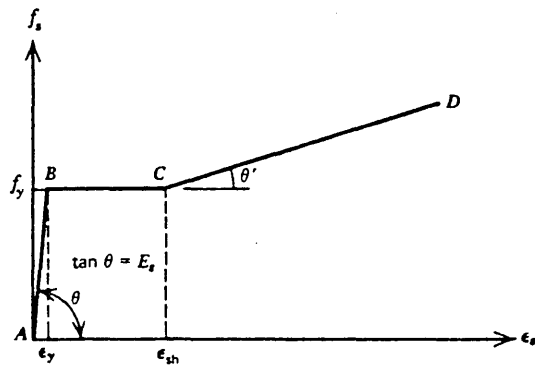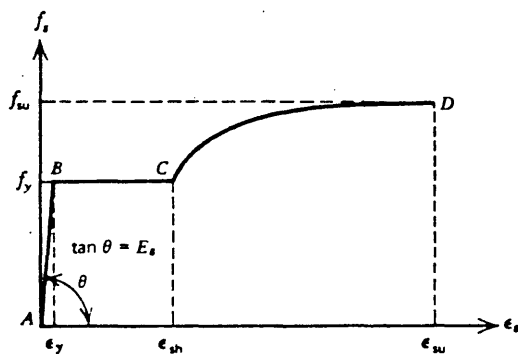
FIG. 2.4 Idealizations for the stress-strain curve for steel in tension or compression. (a) Elastic perfectly plastic approximation, (b) Trilinear approximate, (c) complete curve. Source Ref. [3]
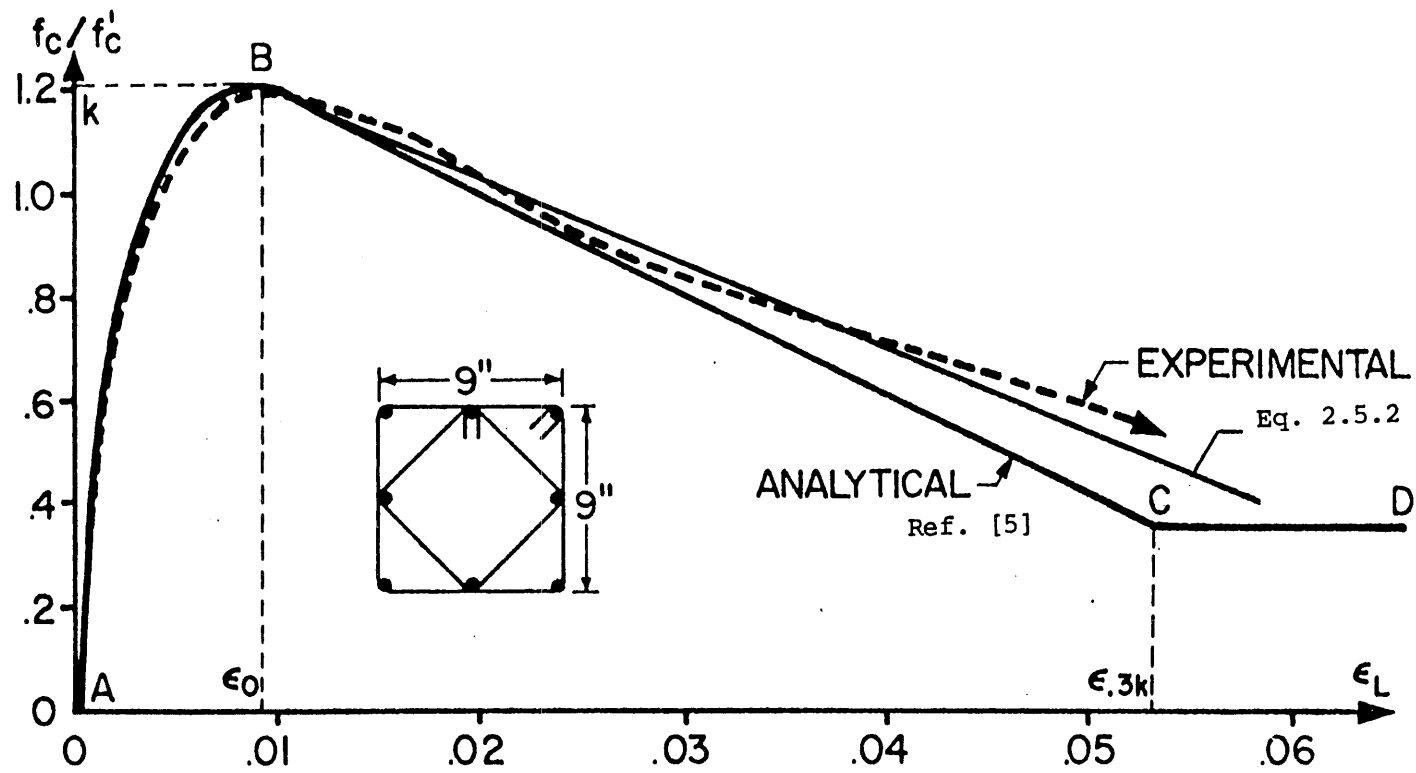
FIG. 2.5 Modified stress strain curve for confined concrete compared to model from Ref. [5].
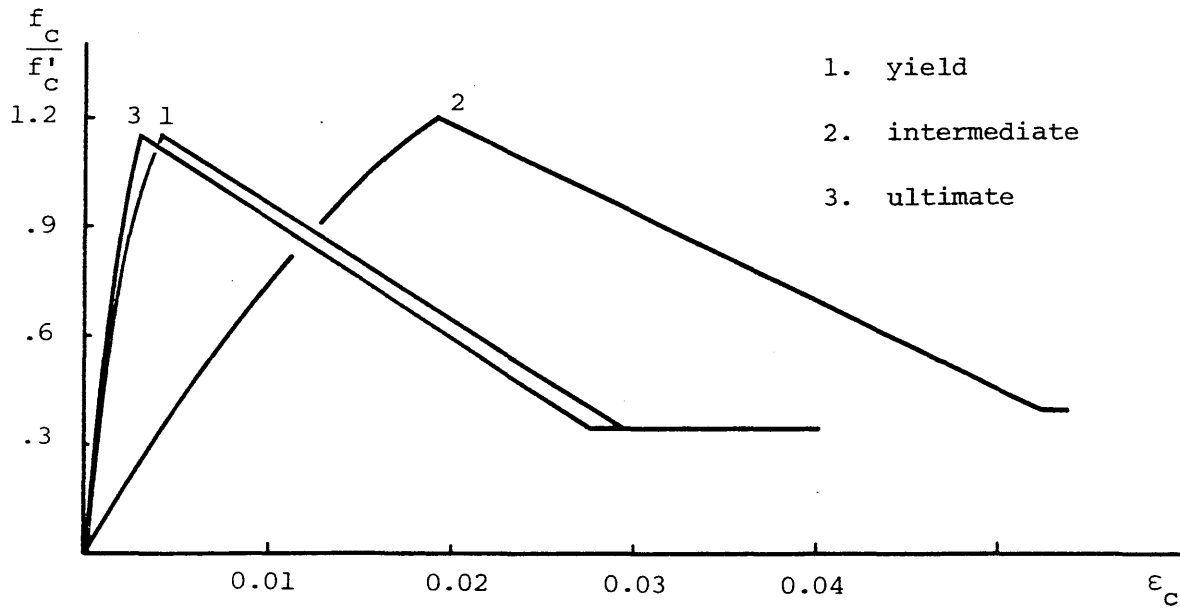
FIG. 2.6   Illustration of stress-strain curves as a function
of neutral axis. Location in Beam J-2.
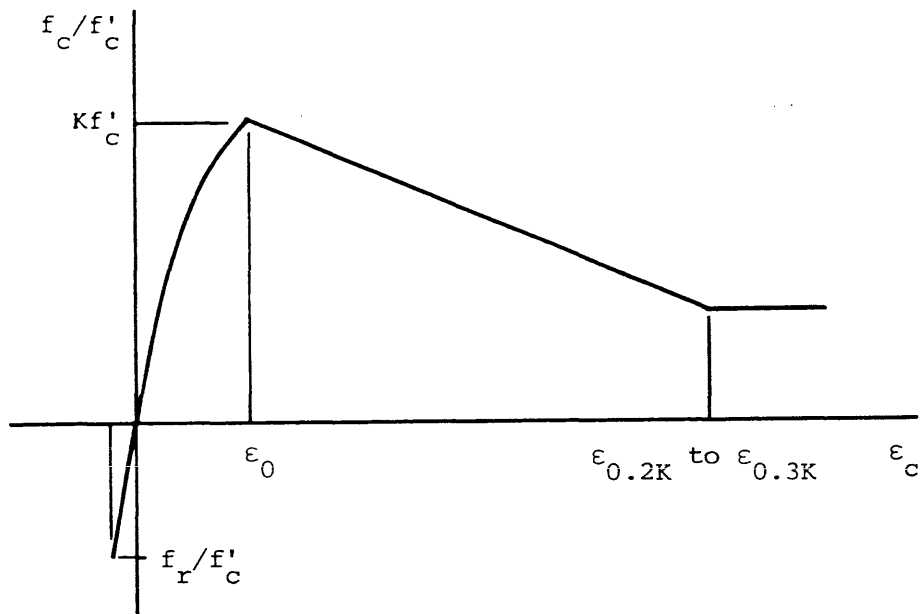
FIG. 2.7   Proposed stress-strain curve for reinforced and
confined concrete
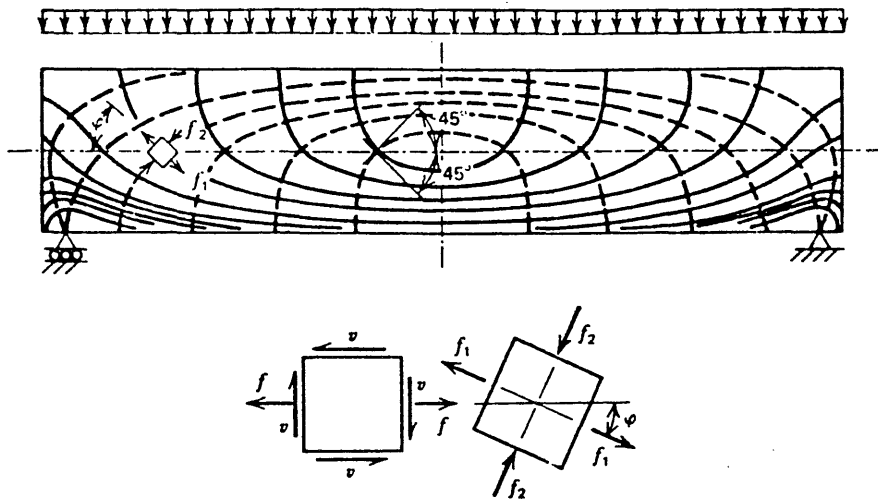
FIG. 2.8   Trajectories of principal stresses in a homogeneous
isotropic beam.   Source Ref. [3]
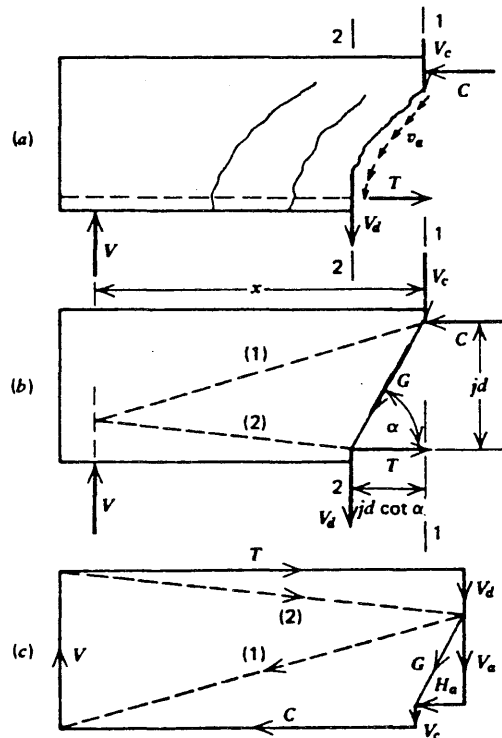
FIG. 2.9   Equilibrium requirements in the shear span of a beam
Source Ref. [3]
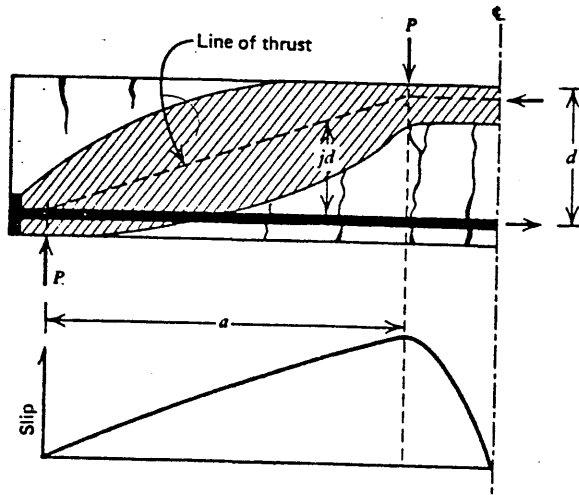
FIG. 2.10 Slip associated with arch action in an
idealized beam. Source Ref. [3]
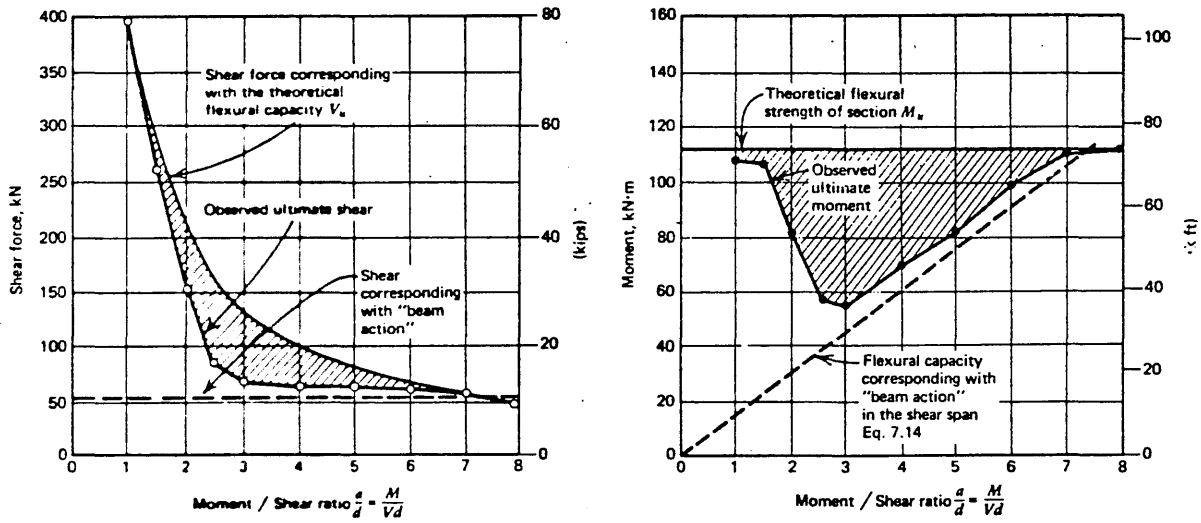
FIG. 2.11 Moments and shears at failure plotted against
shear span to depth ratio. Source Ref. [3]
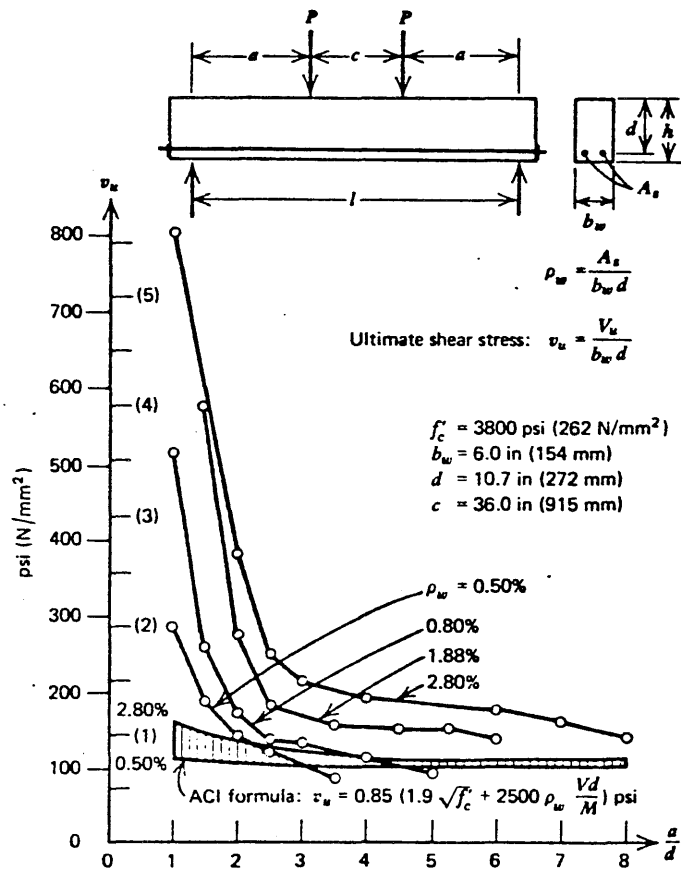
FIG. 2.12 Shear stress at failure as a function of the shear
span to depth ratio. Source Ref. [22]
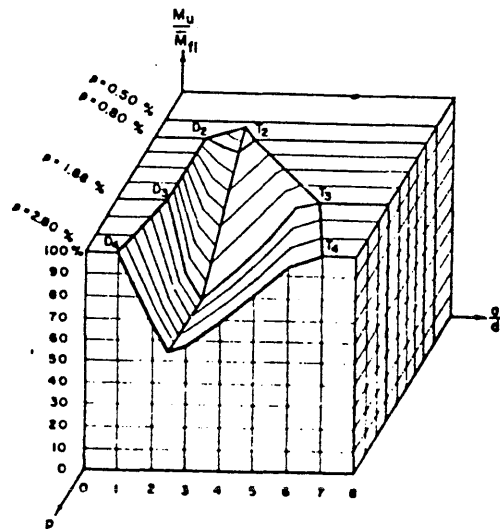
FIG. 2.13 Relative beam strength $M_u/M_{f\ell}$ versus a/d and ρ.
Source Ref. [22]
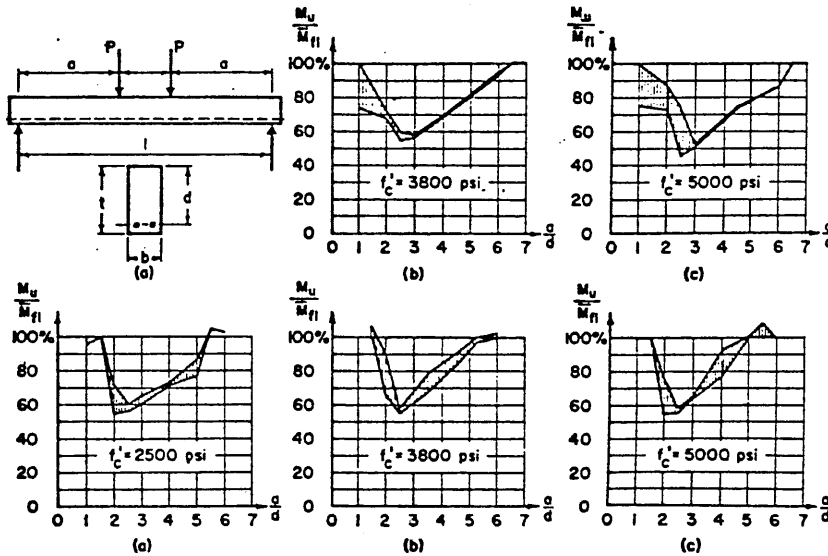
FIG. 2.14 (top) - Influence of the basic parameters, f_c' and a/d, on the relative beam strength for ρ = 2.80 percent. Source Ref. [22]

FIG. 2.15 (bottom) - Influence of the basic parameters, f_c' and a/d, on the relative beam strength for ρ = 1.88 percent. Source Ref. [22]
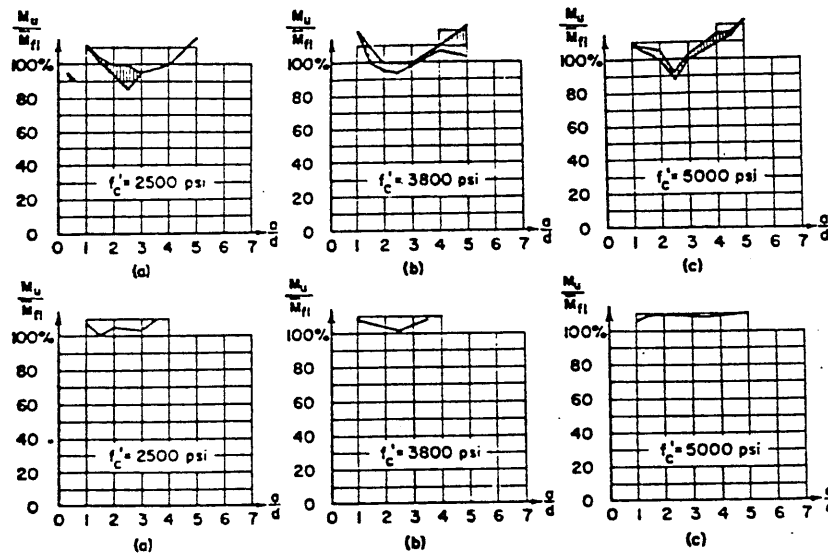
FIG. 2.16 (top) - Influence of the basic parameters, f_c' and a/d, on the relative beam strength for ρ = 0.80 percent. Source Ref. [22]

FIG. 2.17 (bottom) - Influence of the beam strength, f_c' and a/d, on the relative beam strength for ρ = 0.50 percent. Source Ref. [22]
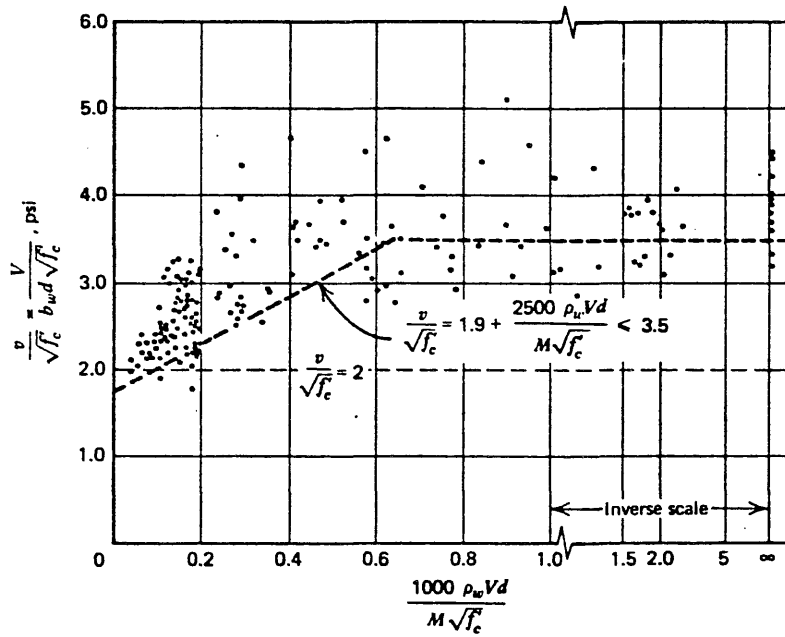
FIG. 2.18 Comparison of Eq. 2.7.10 with experimental results. Source Ref. [3]
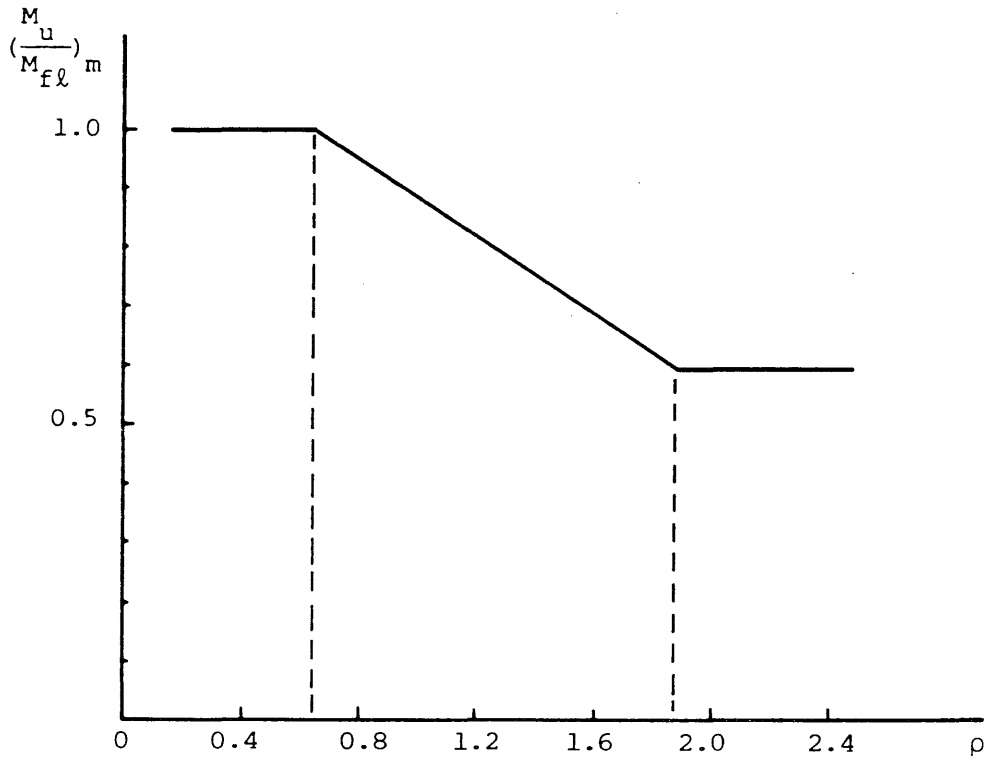
FIG. 2.19 Variation of $(\dfrac{M_u}{M_{f\ell}})_m$ with respect to tensile reinforcement content.
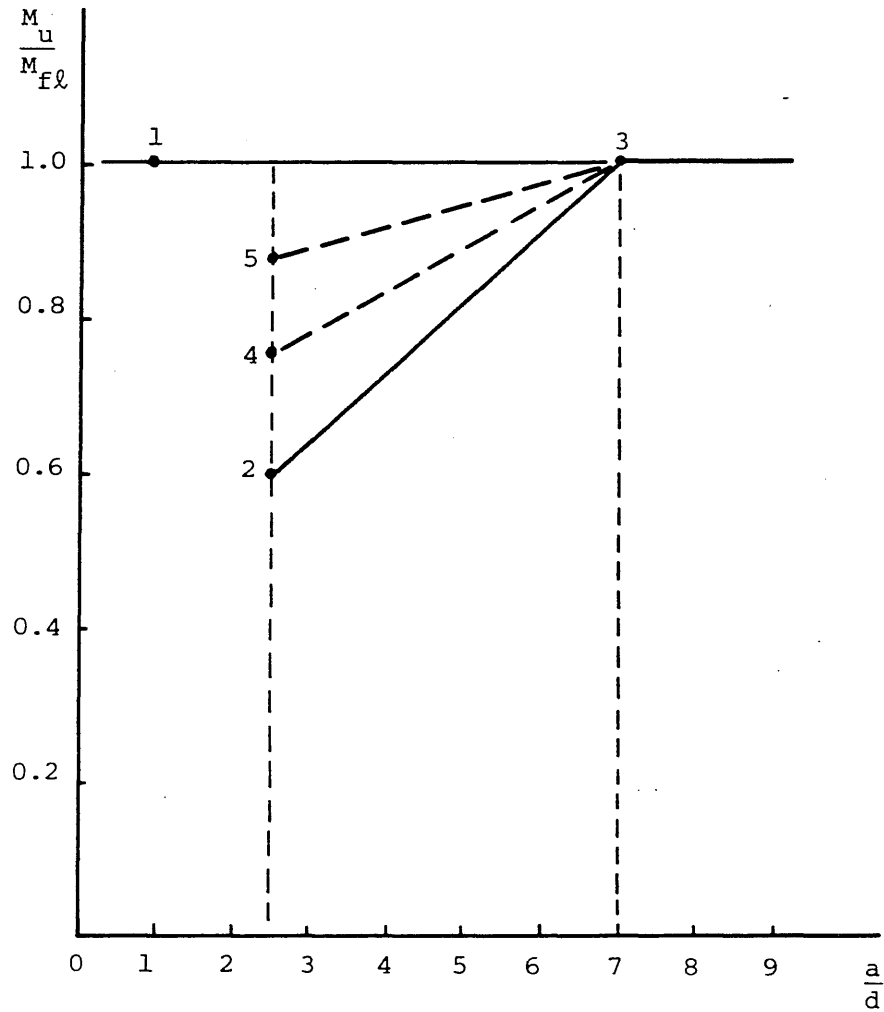
FIG. 2.20 The influence of shear reinforcement on the flexural
moment capacity of slender beams.
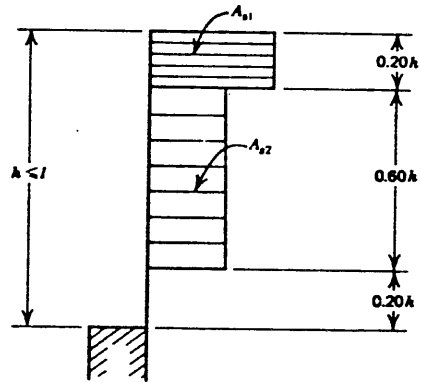
FIG. 2.21 Suggested distribution of negative flexural reinforcement at support of continuous deep beams. Source Ref. [3]
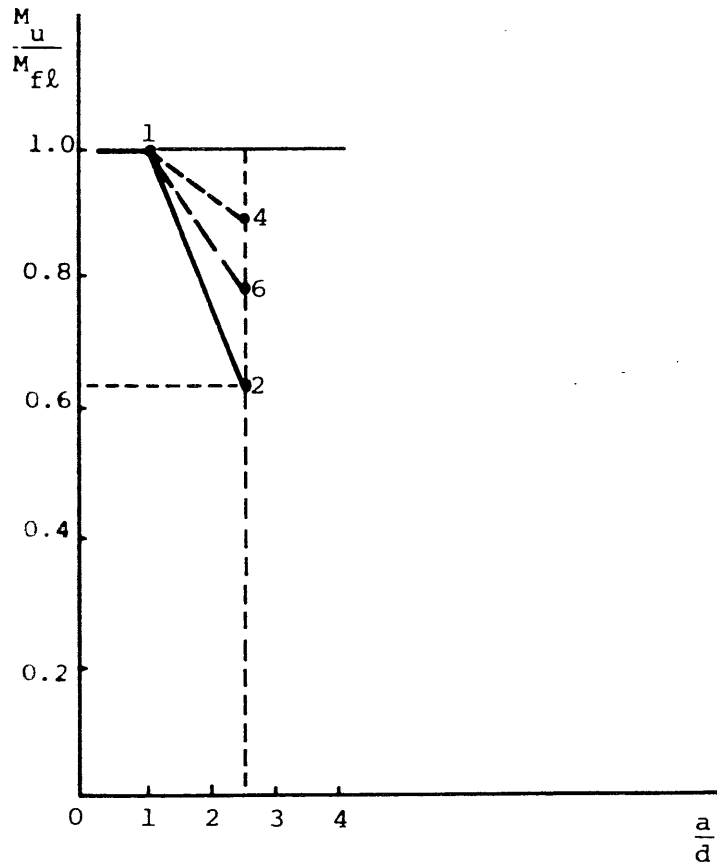
FIG. 2.22 The influence of shear reinforcement on the flexural moment capacity of deep beams.
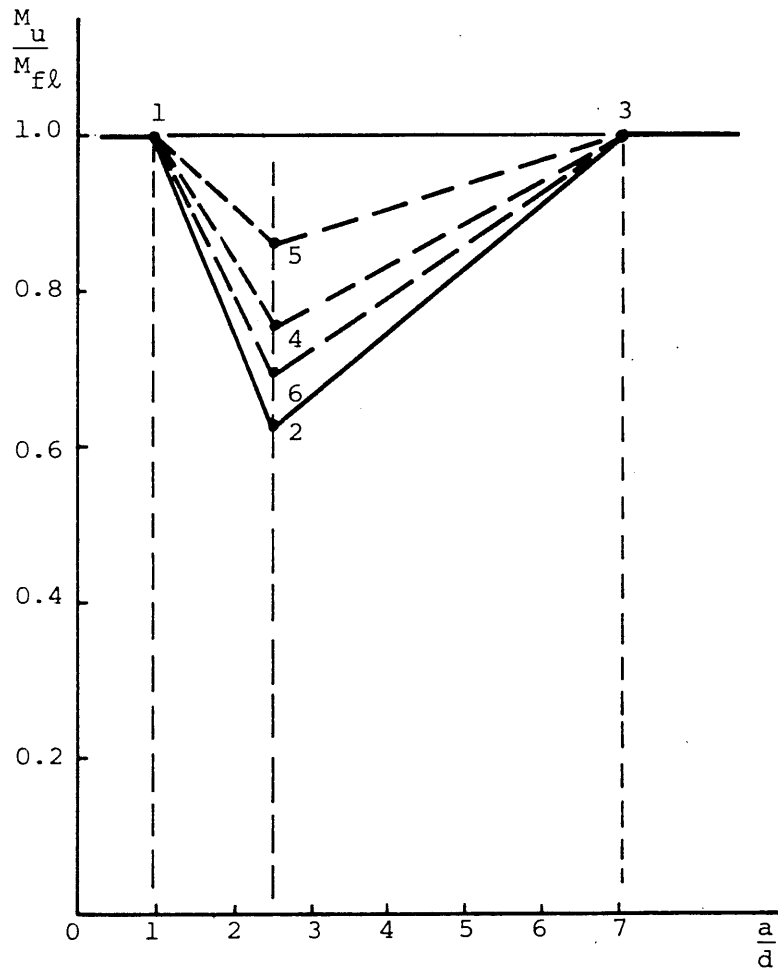
FIG. 2.23 The influence of shear reinforcement on the flexural
          moment capacity of slender and deep beams.

3. ANALYSIS

3.1 Introduction

The theoretical models developed in Chapter 2 for the analysis of rein-
forced concrete beams are employed in Chapter 3 to analyze several cases.
The beams analyzed herein had been studied both experimentally and analytically
by other investigators. The results obtained from the present analysis are
compared to the previous experimental and analytical data, as presented in
the literature.

Three groups of members are considered in this study. In the first are
beams in flexure without axial loads that had been studied previously by Burns
and Siess [12]. In the second are beams under flexural and axial loads that
had been studied previously by Yamashiro and Siess [38]. In the third are
deep beams that had been studied by Crist [36,39]. All the members are ana-
lyzed by the methods presented in Chapter 2. The analysis is performed in
two steps. In the first step only the flexural behavior is considered, while
in the second step the influence of shear is incorporated into the analysis.
The numerical results are illustrated by moment-curvature diagrams (M-ϕ), for
slender beams without axial loads, and by interaction diagrams (P-M), for
flexural members with axial loads. The results are compared to the experi-
mental data reported by other investigators, and to analytical results based
upon other recommended methods, as described in the literature. The deep
beams are analyzed only for ultimate moment conditions. The results obtained
for deep beams are compared to the experimental and analytical data, as
reported by Crist [36,39], and to data obtained by employing the ACI recom-
mended procedure for the analysis.

3.2 Flexural Members Without Axial Loads

3.2.1 Introduction -- The members that are analyzed in this section, had been studied by Burns and Siess [12]. The geometrical and material properties of the members are presented in Appendix B, Section B1.

In order to demonstrate the application of the proposed method, and the accuracy of the numerical results, three beams have been chosen for which a detailed analysis is presented. A fourth beam is analyzed only for ultimate moment conditions. These beams represent each of the three groups (classified by the $\frac{a}{d}$ ratio) that had been studied in Ref. [12]. Furthermore, the beams that are analyzed herein are those for which the largest differences between the experimental and the analytical results had been reported in Ref. [12]. The accuracy of the proposed method is demonstrated by the significant decrease in the differences between experimental and analytical results.

The analysis of each of the three beams (J-2, J-14, J-22) is for loading conditions between the yielding of the tensile reinforcement and ultimate moment. Beam J-20 is analyzed for ultimate moment only.

3.2.2 The Numerical Procedure -- The numerical procedure has been presented and discussed in Section 2.6, and illustrated by a flow diagram in Appendix C. Each loading stage is represented by the numerical values of strains, stresses, and forces at each layer. A scaled drawing of the cross section on which the locations of the neutral axis, and the layers is also presented for the last iteration (i.e., equilibrium) of each loading stage. The moment and curvature are calculated, and the point representing the moment (M), and the curvature (ϕ) is plotted on the M-ϕ diagram that is enclosed at the end of the analysis for each member.

The numerical procedure is explained in detail for the first case, the beginning of the analysis. The same procedure is employed for all other cases discussed in this chapter.

Beam J-2

Fig. 3.2.1 illustrates the cross section of beam J-2 at the ultimate moment condition. The following steps are performed during the analysis, as illustrated in Fig. 3.2.1.

1. Assume a location for the neutral axis, and a numerical value of the strain at a certain location on the cross section. For ultimate moment condition of beam J-2 it is assumed that the strain at the tensile reinforcement level is $0.044 \frac{in}{in}$, and the neutral axis is located at a distance of 4.5 in. from the top of the beam. Several attempts are made until the "right" combination is found, as explained in the following steps.

2. Find the location at which the concrete in compression reaches a strain $0.004 \frac{in}{in}$ by assuming a linear strain distribution over the cross section. If this location is below the bottom of the compressive reinforcement assume that the unconfined concrete cover located above the bottom of the compressive reinforcement has spalled off. However, if the strain $0.004 \frac{in}{in}$ is located between the bottom of the compressive reinforcement and the top of the cross section, all the concrete cover which is subjected to strains larger than $0.004 \frac{in}{in}$ may spall off. These assumptions increase the accuracy of the proposed method.

3. Divide the compression zone of the cross section into horizontal layers. For the present case the following layers are obtained.

a.   The concrete at the compressive reinforcement level. This
layer is as thick as the diameter of the reinforcing bars,
and its length is defined by the distance between the in-
ternal vertical lines of the rectangular hoop.

b.   The concrete between the neutral axis and the line that
corresponds to the strain $0.004 \frac{in}{in}$. The length of this
layer is defined by the beam width.

c.   The confined concrete located between the bottom of the
steel bars and the location of the strain $0.004 \frac{in}{in}$ is
divided into three equal layers. The length of each layer
is defined by the distance between the external vertical
lines of the rectangular hoop. The number of layers may
vary for each case.

d.   The concrete cover located between the bottom of the steel
bars, and the line at which the concrete strain is $0.004 \frac{in}{in}$
is considered as a single and separate layer. The width of
this layer is defined by the distance between the external
vertical line of the rectangular hoop and the external
vertical line of the beam cross section.

4.   For each layer, except the concrete cover defined in step 2.d.,
calculate the strain at the mid-height horizontal plane. The strains are
calculated corresponding to the linear strain distribution assumed previously
in step 2.

5.   Employ Eqs. (2.5.4), (2.5.5), (2.5.6) to calculate the parameters
of the stress strain curve for the confined concrete.

6. Employ Eq. (2.5.1) to calculate the stress at a layer if the strain is smaller than ε_0, as defined by Eq. (2.5.4). If the strain at a layer is in the range defined by $\varepsilon_0 < \varepsilon \leq \varepsilon_{0.3K}$, calculate the stress from Eq. (2.5.2). If the strain is larger than $\varepsilon_{0.3K}$ employ Eq. (2.5.3) to calculate the stress.

7. Assume that the stress on the concrete cover defined in step 2.d. is between $0.5 * f'_c$ and $0.85 * f'_c$. This assumption increases the accuracy of the results, as demonstrated in the following cases.

8. Calculate the area of each layer from the layer dimensions, as defined in step 2.

9. Calculate the stress in the steel bars by introducing the steel strains into Eq. (2.4.2). The parameters of the stress strain curves for the steel bars are presented in Table B2 of Appendix B.

10. Calculate the force at each layer; multiply the stress of the layer by the area of the layer. Calculate the force in the steel bars; multiply the stress in the bars by the area of the bars. The concrete layer defined in step 2.b. is considered as a uniform layer. The concrete cover is at a strain smaller than $0.004 \frac{in}{in}$ and is assumed to behave as confined concrete. This assumption is discussed in Section 2.5.1.

11. Sum all compressive forces and compare to the sum of all tensile forces. Here it is assumed that if the difference between tensile and compressive forces is less than 1%, the cross section is in equilibrium. However, if that difference is larger than 1% one has to assume a new location for the neutral axis and return to step 1.

12. When the cross section is in equilibrium calculate the moment as follows. Multiply the force in each compressive layer, or bar by the vertical distance from the center of the layer to the center of the tensile reinforcement.

Sum all moments corresponding to the compressive forces with respect to the tensile reinforcement.

13. Calculate the curvature of the member in equilibrium as follows. Divide the strain at any point on the cross section by the vertical distance from that point to the neutral axis. Usually the strain and location of the tensile reinforcement, or the top concrete fiber in compression are used to calculate the curvature.

14. For ultimate loading conditions, apply the procedure to correct the moment due to the influence of shear and shear reinforcement. Use program TKSH4 to calculate the shear reduction factor (SRF). Multiply the ultimate moment (step 12) by the SRF to obtain the modified ultimate moment.

15. The numerical values of the moment M, and the curvature ϕ define a point on the moment-curvature diagram.

16. Locate the following points on the moment-curvature diagram.

   a. Ultimate moment condition, as discussed in the preceding steps.

   b. Yielding of tensile reinforcement. Assume the tensile reinforcement yielded (the strains are presented in Appendix B, Table B2), and perform the procedure as described in steps 1 through 13.

   c. Calculate several points by assuming strain values for the tensile reinforcement which are between the ultimate moment strain and the yield strain.

17. Plot the moment-curvature diagram by passing a curved line through all points.

The number of layers as defined in Item 3 may change for other cases under consideration. A detailed numerical example is provided in Appendix D.
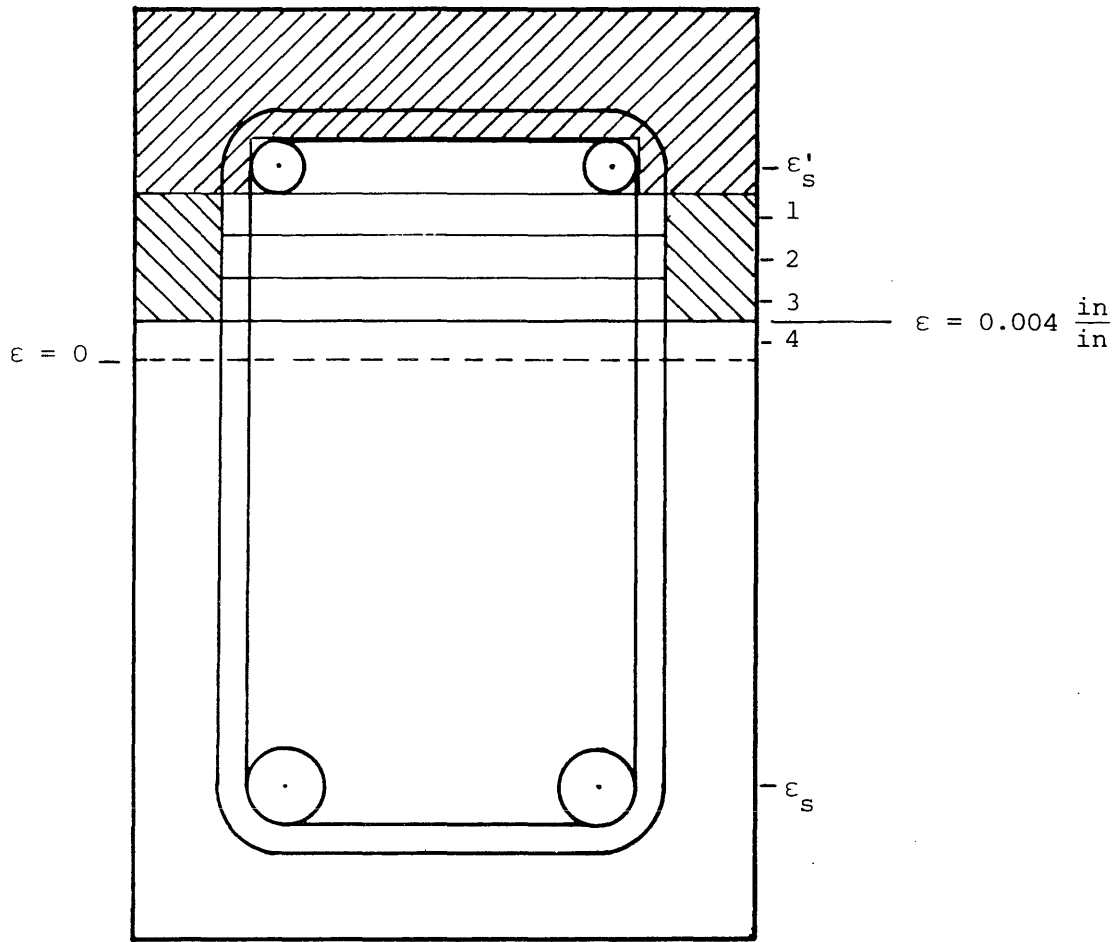
FIG. 3.2.1 Beam J-2 cross section at ultimate stage (Case 1)

Case 1:

Ultimate Moment Capacity

The geometrical representation of the cross section, for this loading stage is shown in Fig. 3.2.1. The numerical values for equilibrium are presented in the following tabulation. Equilibrium is obtained when the neutral axis shifted to $k_u d = 4.5$ in, and the strain of the tensile reinforcement is $0.044 \frac{in}{in}$.

layer	step 4 ε	steps 5,6,7,9 f [psi]	step 8 Area [in^2]	step 10 F [lbs]	
1	0.015	3014.5	3.19	9616.25	
2	0.0106	3619.5	3.19	11546.2	
3	0.0062	4224.5	3.19	13476.15	
4	0.002	4241.5	4.0	16966.0	
concrete at comp. rein. level	0.02	2327.1	2.89	6722.4	
cover	>0.004	2468.0	3.795	13161.0	step 11
comp. rein.	0.02	56235.0	0.88	49486.8	ΣC = 120974.8 lbs
ten. rein.	0.044	76268.2	1.58	120503.7	

$\frac{\Sigma C}{T}$ = 1.004   difference = 0.4%   (step 11)

step 12: The moment with respect to the tensile reinforcement

$\qquad$ M = 877.0   in. - K.

step 13: The curvature

$\qquad \phi = \dfrac{0.02}{2.5} = 0.008 \frac{rad.}{in.}$

The measured moment: M_m = 919 in. - K. From the analysis for shear; no significant reduction due to shear because $\frac{a}{d}$ > 7.0.

$$\frac{M_{cal}}{M_m} = 0.9543 \qquad \text{difference} = 1 - \frac{M_{cal}}{M_m} = 4.57\%$$

Case 2:

Yielding of Tensile Reinforcement

The same procedure is applied to this case. Here, the strain at the tensile reinforcement level is known from Table B1. The cross section is illustrated in Fig. 3.2.2, and the results are presented in the following tabulation. The procedure follows the steps described previously for ultimate moment conditions.

The solution converges to equilibrium for kd = 4.1 in. In this case all compressive strains are smaller than 0.004 $\frac{in}{in}$, and there is no spalling of concrete cover. Therefore the compression zone is divided into layers of the type defined in step 2.b. For layers that contain steel bars the area of the steel is subtracted from the area of concrete when forces are calculated.

layer	step 4 ε	steps 5,6,7,9 f [psi]	step 8 Area [in^2]	step 10 F [lbs]	
1	0.00108	3645.87	4.0	14583.5	
2	0.000939	3140.42	4.0	12561.7	
3	0.000799	2967.69	4.0	10565.0	
4	0.000659	2149.74	3.56	7653.1	
5	0.000519	1570.5	3.56	5590.9	
6	0.000379	1283.0	4.0	5132.2	
7	0.000238	739.35	4.0	2957.4	
8	0.000084	255.33	4.8	1225.6	
comp. rein.	0.000589	17082.95	0.88	15033.0	step 11 $\Sigma C = 75302.4$ lbs
ten. rein.	0.001655	48000.0	1.58	75840.0	

$\dfrac{\Sigma C}{T} = 0.9929$ difference = 0.7%   (step 11)

The moment, with respect to the tensile reinforcement: (step 12)

$\qquad$ M = 643.0 in. - K

measured [12]: M_m = 685.0 in. - K

$\dfrac{M_{cal}}{M_m}$ = 0.939   difference = 6.1%

It is assumed that the measured moment is not exactly for the yield condition, because the loading had to be higher than to cause yielding of the tensile reinforcement in order to detect this situation.

The curvature for this stage: (step 13)

$$\phi = \frac{0.001655}{5.9} = 0.00028 \ \frac{rad.}{in.}$$
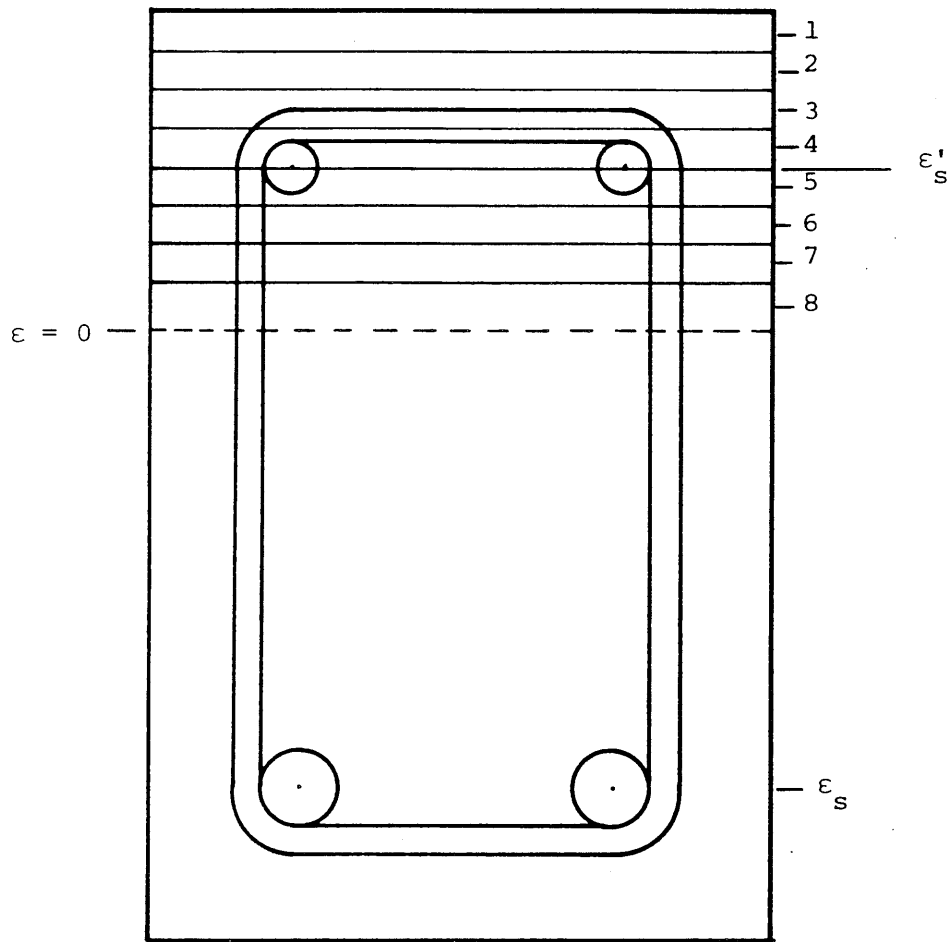
FIG. 3.2.2 Beam J-2 cross section at yielding stage (Case 2).

Case 3:

This case describes the following state of equilibrium as illustrated in Fig. 3.2.3.

$$\varepsilon_s = 0.002 \qquad (\varepsilon_y < \varepsilon_s < \varepsilon_{sh})$$

$$kd = 4.15 \text{ in.}$$

The numerical results are presented in the following tabulation.

layer	ε	f [psi]	Area [in^2]	F [lbs]	
1	0.00133	3074.3	4.0	12297.2	
2	0.00116	2778.1	4.0	11112.4	
3	0.00099	2454.9	4.0	9819.6	
4	0.00082	2103.8	3.56	7489.5	
5	0.00065	1724.5	3.56	6139.2	
6	0.00048	1316.0	4.0	5264.0	
7	0.000307	869.9	4.0	3479.6	
8	0.000136	397.9	4.0	1591.6	
9	0.000026	77.6	1.2	93.12	
comp. rein.	0.000735	21315.0	0.88	18757.2	$\Sigma C = 76043.5$ lbs
tent. rein.	0.002	48000.0	1.58	75840.0	

$$\frac{\Sigma C}{T} = 1.0027 \qquad \text{difference} = 0.27\%$$

Moment with respect to the tensile reinforcement:

$$M = 640.1 \text{ in.} - K$$

Curvature:

$$\phi = \frac{0.002}{5.85} = 0.000342 \ \frac{\text{rad.}}{\text{in.}}$$
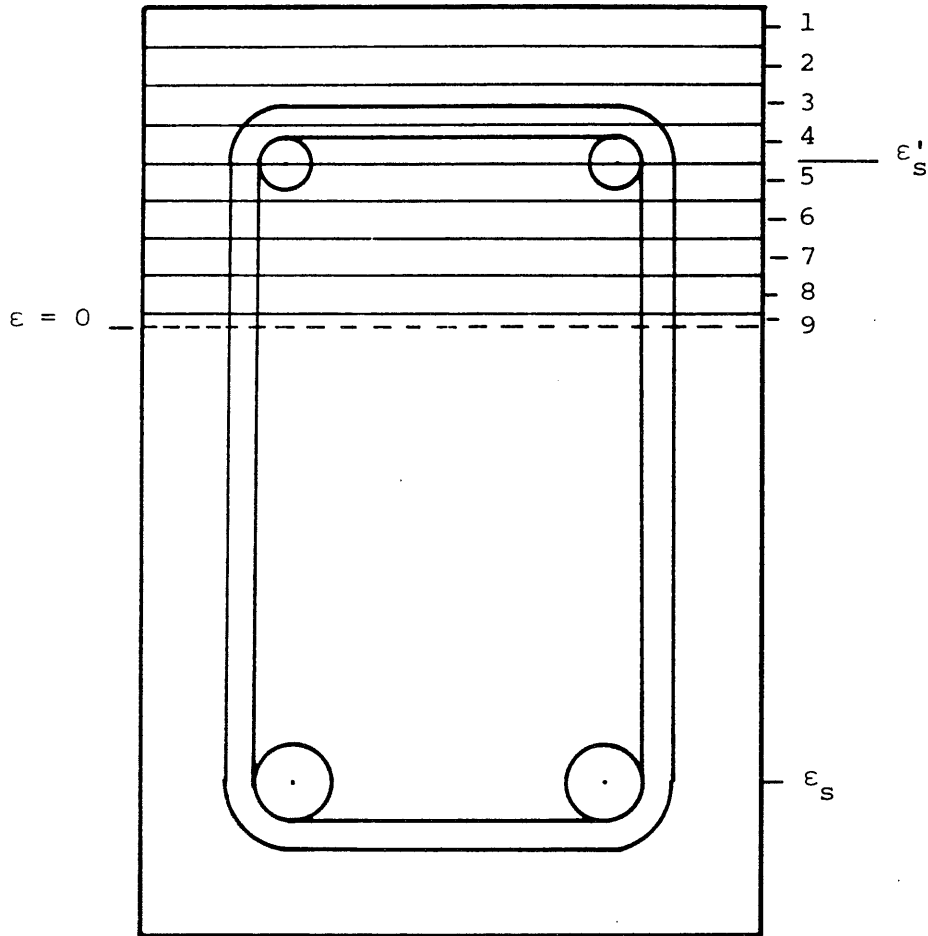
FIG. 3.2.3 Beam J-2 cross section for Case 3.

Case 4:

This case represents the following strain distribution, as illustrated in Fig. 3.2.4.

$\varepsilon_s = 0.0096 = \varepsilon_{sh}$, from Table B2

$kd = 2.7$ in.

The numerical results are presented in the following tabulation.

layer	ε	f [psi]	Area [in^2]	F [lbs]	
1	0.00322	3539.4	4.0	14157.6	
2	0.00256	3235.9	4.0	12943.6	
3	0.0019	2824.3	4.0	11297.2	
4	0.00125	2246.7	3.56	7998.2	
5	0.00059	1345.5	3.56	4790.0	
6	0.00013	364.7	1.6	583.5	
comp. rein.	0.00092	26680.0	0.88	23478.4	$\Sigma C = 75248.5$ lbs
ten. rein.	0.0096	48000.0	1.58	75840.0	

$\dfrac{\Sigma C}{T} = 0.9922$ difference = 0.77%

Moment with respect to the tensile reinforcement:

$M = 651.9$ in. $- K$.

Curvature:

$$\phi = \frac{0.0096}{7.3} = 0.001315 \ \frac{\text{rad.}}{\text{in.}}$$
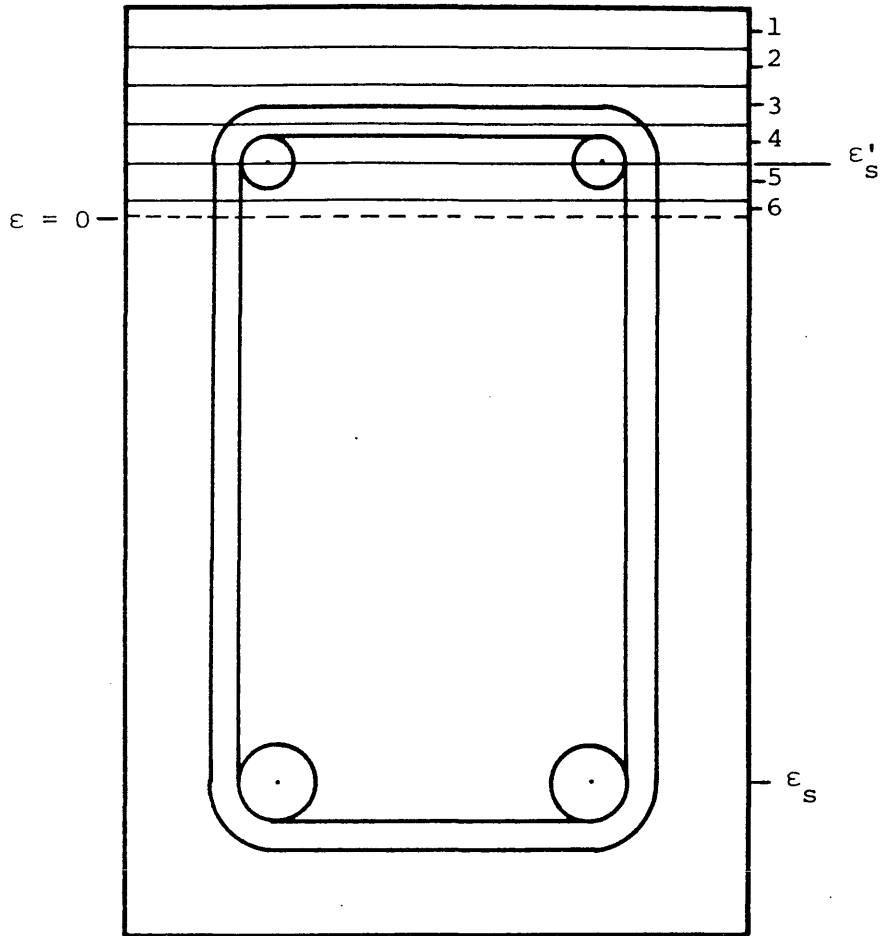
FIG. 3.2.4 Beam J-2 cross section for Case 4.

Case 5:

This case represents the following strain distribution, as illustrated in Fig. 3.2.5.

$$\varepsilon_s = 0.02 \qquad (\varepsilon_s > \varepsilon_{sh})$$

Equilibrium was obtained for kd = 3.1 in.

The numerical results are presented in the following tabulation.

layer	ε	f [psi]	Area [in^2]	F [lbs]	
1	0.00652	2040.0	13.0	26520.0	
2	0.00101	1979.2	5.6	11083.5	
concrete at comp. steel level	0.003188	3595.2	2.87	10318.2	
cover$_1$	0.00304	3514.2	2.1	7379.8	
cover$_2$	0.00413	2040.0	0.285	581.4	
comp. rein.	0.003188	48600.0	0.88	42768.0	ΣC = 98651.0 lbs
ten. rein.	0.02	62500.9	1.58	98751.4	

$$\frac{\Sigma C}{T} = 0.9989 \qquad \text{Difference} = 0.1\%$$

Moment with respect to the tensile reinforcement:

$$M = 811.8 \text{ in.} - K.$$

Curvature:

$$\phi = \frac{0.02}{6.9} = 0.002898 \frac{\text{rad.}}{\text{in.}}$$
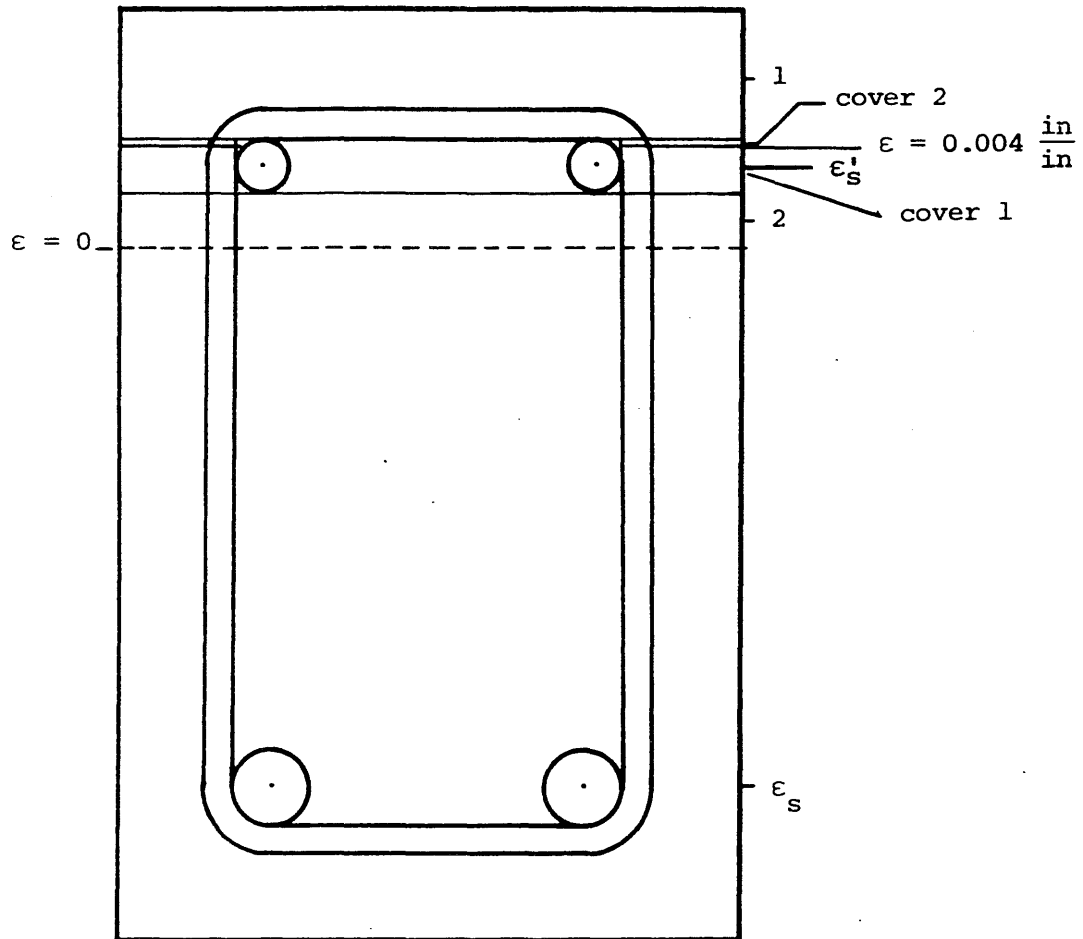
FIG. 3.2.5 Beam J-2 cross section for Case 5.

Case 6:

This case represents the following strain distribution, as illustrated in Fig. 3.2.6.

$$\varepsilon_s = 0.03 \; > \; \varepsilon_{sh}$$

Equilibrium is obtained for kd = 4.3 in, and the numerical results are presented in the following tabulation.

layer	ε	f [psi]	Area [in^2]	F [lbs]	
1	0.008684	3915.2	3.42	13397.8	
2	0.005394	4355.5	3.42	14904.5	
3	0.002368	4566.0	3.42	15624.8	
4	0.002	4249.5	1.4	5949.3	
concrete at comp. steel level	0.0121	3458.1	2.87	9924.7	
cover	>0.004	2284.0	4.028	9200.0	
comp. rein.	0.0121	48600.0	0.88	42768.0	$\Sigma C = 111769.1$ lbs
ten. rein.	0.03	70777.0	1.58	111827.0	

$$\frac{\Sigma C}{T} = 0.999 \qquad \text{difference} = 0.05\%$$

Moment with respect to the tensile reinforcement:

$$M = 831.7 \text{ in.} - K.$$

The curvature:

$$\phi = \frac{0.03}{5.7} = 0.005263 \frac{\text{rad.}}{\text{in.}}$$
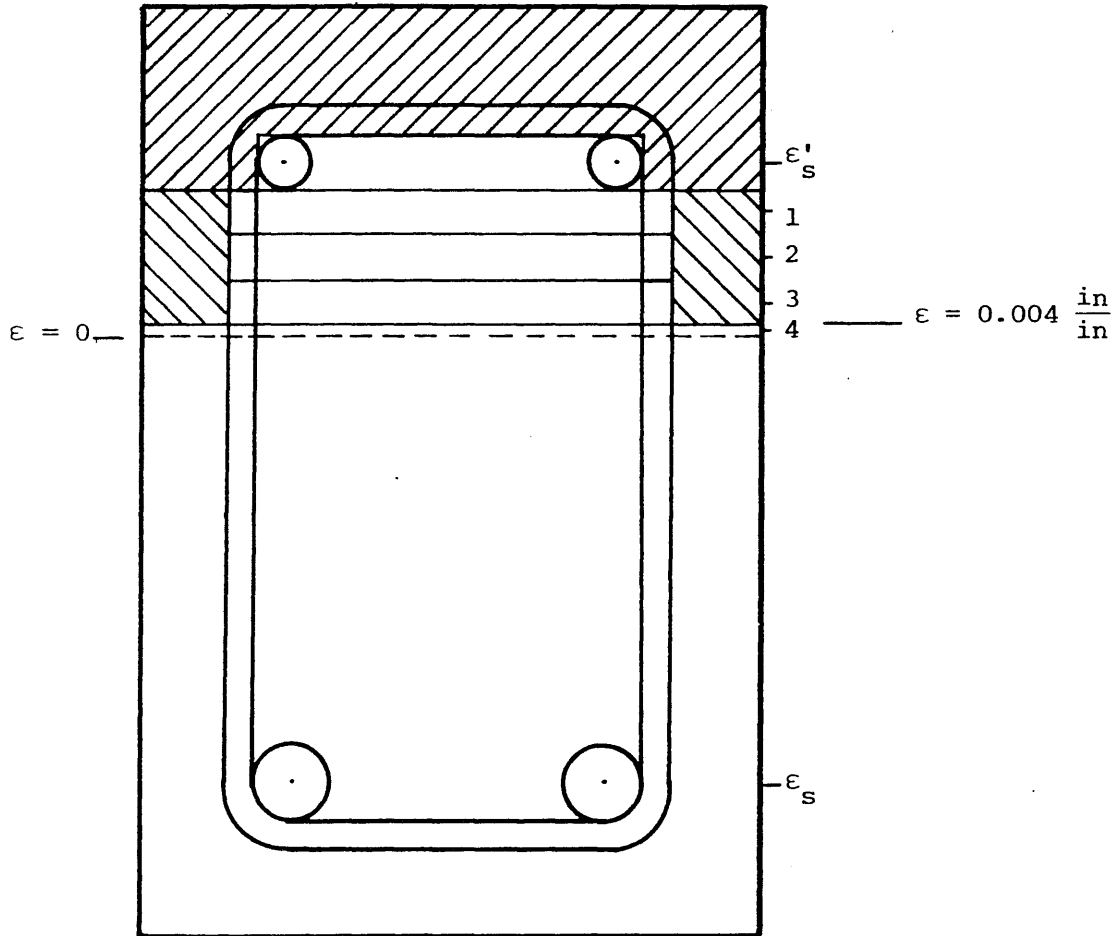
FIG. 3.2.6 Beam J-2 cross section for Case 6.

Case 7:

This case represents the following strain distribution, as illustrated in Fig. 3.2.7.

$$\varepsilon_s = 0.006 \qquad (\varepsilon_y < \varepsilon_s < \varepsilon_{sh})$$

Equilibrium is obtained for kd = 3.1 in, and the numerical results are presented in the following tabulation.

layer	ε	f [psi]	Area [in^2]	F [lbs]	
1	0.002478	3252.5	4.0	13010.0	
2	0.00204	2946.8	4.0	11787.2	
3	0.001609	2626.7	4.0	10506.8	
4	0.001174	2188.4	3.56	7790.7	
5	0.00074	1607.2	3.56	5721.6	
6	0.00026	688.0	4.8	3302.4	
comp. rein.	0.0009565	27738.5	0.88	24409.9	$\Sigma C = 76528.6$ lbs
ten. rein.	0.006	48000.0	1.58	75840.0	

$$\frac{\Sigma C}{T} = 1.009 \qquad \text{difference} = 0.9\%$$

Moment with respect to the tensile reinforcement:

$$M = 655.5 \text{ in. } - \text{ K.}$$

The curvature:

$$\phi = \frac{0.006}{6.9} = 0.0008695 \frac{\text{rad.}}{\text{in.}}$$
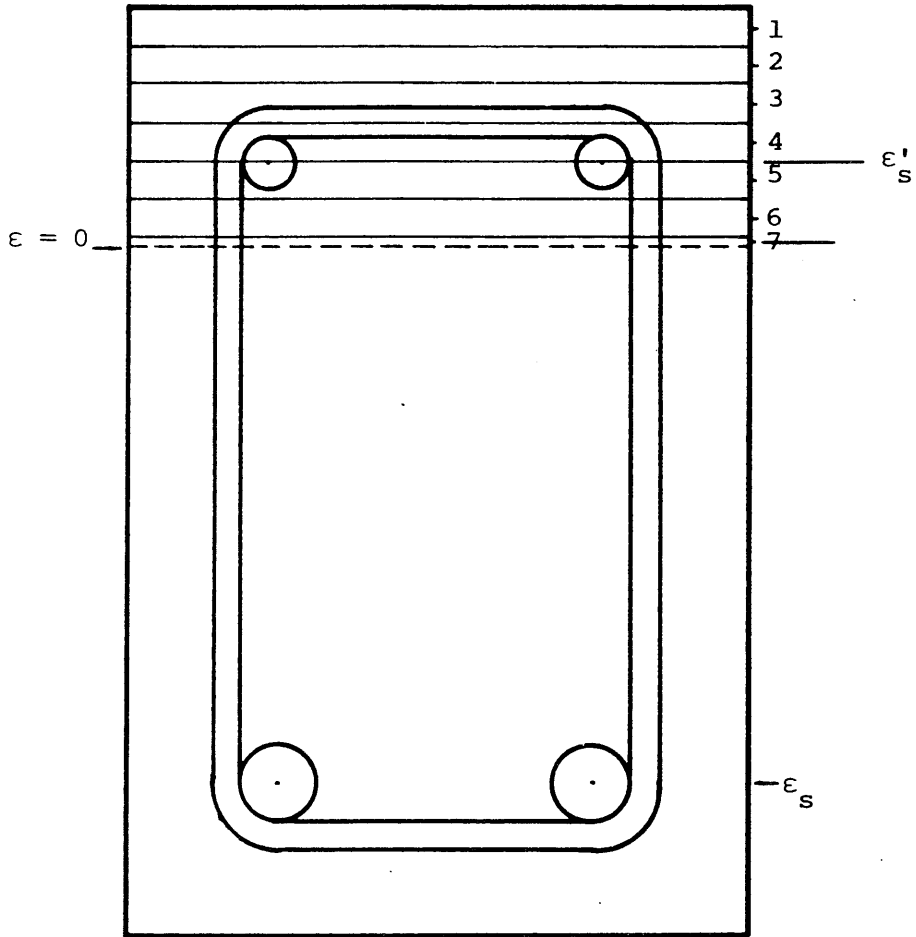
FIG. 3.2.7 Beam J-2 cross section for Case 7.

The results that have been obtained for beam J-2, are used to plot the M-ϕ curve. The numerical values of the points for this curve are presented in the following tabulation

case	M [in. - K.]	ϕ [$\frac{rad.}{in.}$]
yield	643.0	0.00028
3	640.1	0.000342
7	655.5	0.0008695
4	651.9	0.001315
5	811.8	0.002898
6	831.7	0.005263
ultimate	877.0	0.008

The M-ϕ curve is illustrated in Fig. 3.2.8.

The analysis of the following cases does not include illustrations of the cross sections under consideration. The procedure to obtain such illustrations is identical to the method described previously and applied for the analysis of beam J-2. The parameters and dimensions of the beams under consideration are presented in Appendix B.
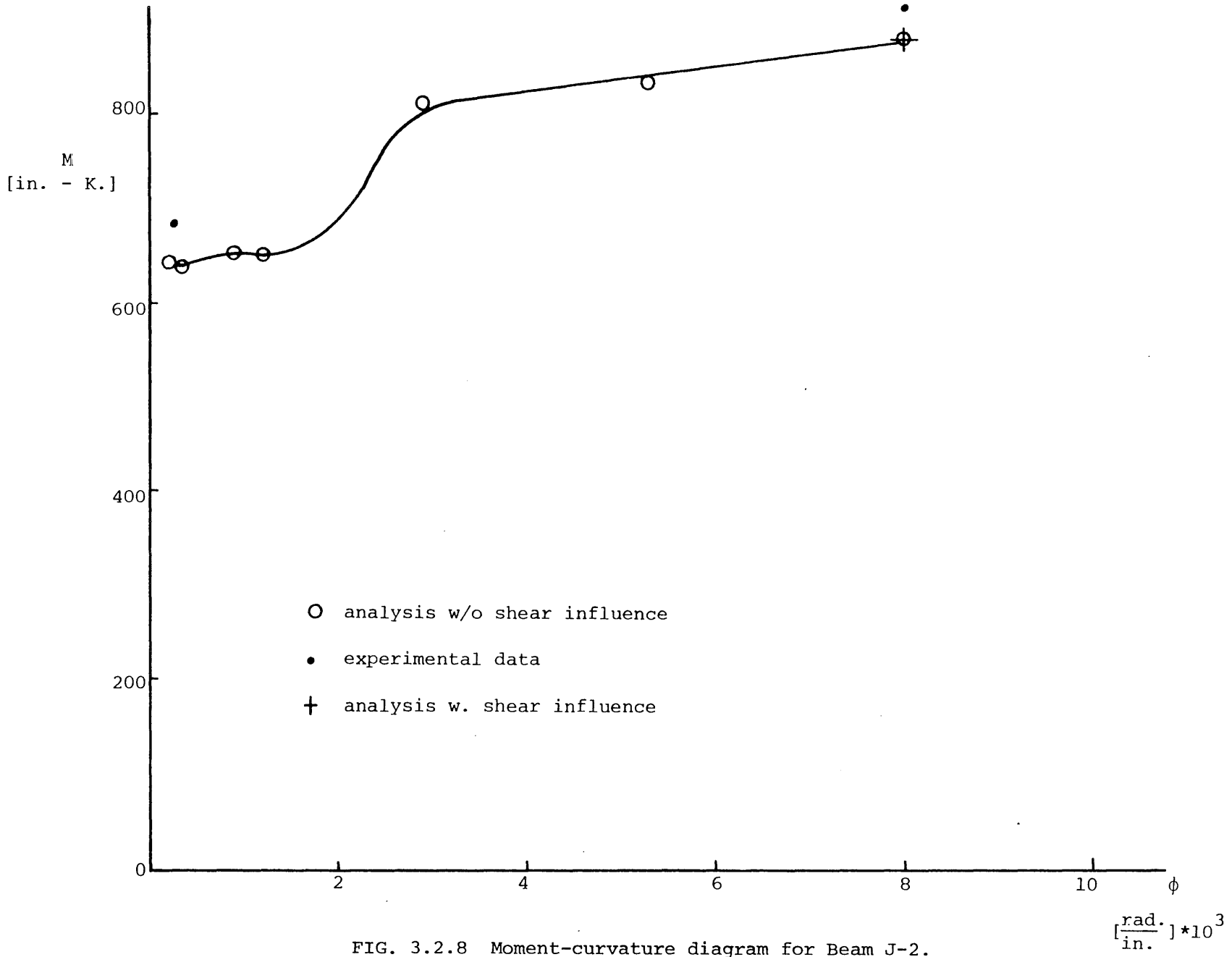
FIG. 3.2.8 Moment-curvature diagram for Beam J-2.

Beam J-14

Case 1:

Ultimate Moment Capacity

The procedure for the analysis is exactly the same as for the previous beam. Equilibrium is obtained for $k_u d = 4$ in and $\varepsilon_s = 0.075 \frac{in}{in}$. The numerical values are presented in the following tabulation.

layer	ε	f [psi]	Area [in^2]	F [lbs]	
1	0.01425	4809.0	2.51	12070.6	
2	0.006375	4975.9	2.51	12489.5	
3	0.00225	3477.7	4.0	13910.8	
cover	>0.004	3825.0	2.975	11379.4	
concrete at comp. rein. level	0.015	4712.7	2.87	13525.4	
comp. rein.	0.015	53263.6	0.88	46872.0	$\Sigma C = 110247.7$ lbs
ten. rein.	0.075	70306.0	1.58	111083.5	

$$\frac{\Sigma C}{T} = 0.9925 \qquad \text{difference} = 0.75\%$$

Moment with respect to the tensile reinforcement:

$$M = 1268.0 \text{ in. } - K.$$

The measured moment: $M_m = 1296.0$ in. $- K.$

$$\frac{M_{cal}}{M_m} = 0.9784 \qquad \text{difference} = 2.16\%$$

From shear analysis; $\frac{a}{d} = 5.14$, no significant shear influence.

Curvature:

$$\phi = \frac{0.075}{10} = 0.0075 \frac{rad.}{in.}$$

Case 2:

Yielding of Tensile Reinforcement

The yield strain of the tensile reinforcement is 0.001624, and the neutral axis is located at kd = 5.19 in. The numerical values are presented in the following tabulation.

layer	ε	f [psi]	Area [in^2]	F [lbs]	
1	0.000855	2651.5	8.0	21212.0	
2	0.000671	2080.1	7.56	15725.5	
3	0.000487	1508.6	7.56	11405.0	
4	0.000302	937.2	8.0	7497.6	
5	0.0001097	340.0	9.52	3236.8	
comp. rein.	0.000588	17641.0	0.88	15524.1	ΣC = 74501.0 lbs
ten. rein.	0.001624	47100.0	1.58	74418.0	

$$\frac{\Sigma C}{T} = 1.0025 \qquad \text{difference} = 0.25\%$$

The moment with respect to the tensile reinforcement:

$$M = 909.5 \text{ in. } - K.$$

The measured moment: M_m = 956.0 in. - K.

$$\frac{M_{cal}}{M_m} = 0.951 \qquad \text{difference} = 4.9\%$$

Here too the experiment was loaded, probably, beyond the yield stage, and therefore the measured moment is larger than the calculated moment.

The curvature:

$$\phi = \frac{0.001624}{8.81} = 0.0001843 \frac{\text{rad.}}{\text{in.}}$$

Case 3:

This case represents a loading stage at which the tensile reinforcement has reached a strain of $\varepsilon_s = 0.01 \frac{in}{in}$ and kd = 2.95 in. The numerical values of the analysis are presented in the following tabulation. At this stage $\varepsilon_y < \varepsilon_s < \varepsilon_{sh}$.

layer	ε	f [psi]	Area [in^2]	F [lbs]	
1	0.002305	3230.9	6.8	21970.1	
2	0.001535	2619.3	6.8	17811.2	
3	0.000284	744.5	4.0	2978.0	
concrete at comp. steel level	0.000861	1808.8	5.12	9261.0	
comp. rein.	0.000861	24969.0	0.88	21972.7	$\Sigma C = 73993.1$ lbs
ten. rein.	0.01	47100.0	1.58	74418.0	

$$\frac{\Sigma C}{T} = 0.9943 \qquad \text{difference} = 0.57\%$$

The moment with respect to the tensile reinforcement:

$$M = 935.5 \text{ in.} - K.$$

The curvature:

$$\phi = \frac{0.01}{11.05} = 0.000905 \frac{rad.}{in.}$$

Case 4:

This case represents a loading stage at which the tensile reinforcement reached strain hardening (i.e., $\varepsilon_s = \varepsilon_{sh} = 0.0175$). Equilibrium is obtained when the neutral axis shifts to kd = 2.5 in. The numerical values are presented in the following tabulation.

layer	ε	f [psi]	Area [in^2]	F [lbs]	
1	0.00327	3731.5	6.0	22389.0	
2	0.00281	3513.0	6.0	21078.0	
concrete at comp. steel level	0.00076	1654.1	7.12	11777.2	
comp. rein.	0.00076	22040.0	0.88	19395.2	ΣC = 47639.4 lbs
ten. rein.	0.0175	47100.0	1.58	74418.0	

$$\frac{\Sigma C}{T} = 1.0029 \qquad \text{difference} = 0.29\%$$

The moment with respect to the tensile reinforcement:

$$M = 950.5 \text{ in. } - K.$$

The curvature:

$$\phi = \frac{0.0175}{11.5} = 0.00152 \frac{\text{rad.}}{\text{in.}}$$

Case 5:

This case represents a loading stage at which the tensile reinforcement reaches a strain $\varepsilon_s = 0.03 \frac{in}{in}$. Equilibrium is obtained when the neutral axis shifts to kd = 2.6 in. The numerical values are presented in the following tabulation.

layer	ε	f [psi]	Area [in^2]	F [lbs]	
1	>0.004	2250.0	8.6	19350.0	
2	0.00329	3792.3	4.4	16686.1	
3	0.00039	983.4	1.8	1770.1	
concrete at comp. steel level	0.00158	2577.4	5.12	13196.3	
comp. rein.	0.00158	45820.0	0.88	40321.6	ΣC = 91324.1 lbs
ten. rein.	0.03	57953.9	1.58	91567.2	

$$\frac{\Sigma C}{T} = 0.9974 \qquad \text{difference} = 0.26\%$$

The moment with respect to the tensile reinforcement:

$$M = 1132.3 \text{ in. - K.}$$

The curvature:

$$\phi = \frac{0.03}{11.4} = 0.00263 \frac{rad.}{in.}$$

A summary of the points that have been calculated for the M-ϕ curve is presented in the following tabulation.

Case	M [in. - K.]	ϕ $[\frac{rad}{in}]$
yield	909.5	0.000184
3	935.5	0.000905
4	950.5	0.00152
5	1132.3	0.00263
ultimate	1268.0	0.0075

The M-ϕ curve is shown in Fig. 2.3.9.

Beam J-22

Case 1:

Ultimate Moment Capacity

This case represents the values of moment and curvature when the beam reached its ultimate load. Equilibrium is obtained when the tensile reinforcement reached a strain $\varepsilon_s = 0.15 \frac{in}{in}$, and the neutral axis shifts to $k_u d = 3.5$ in. The numerical values are presented in the following tabulation.
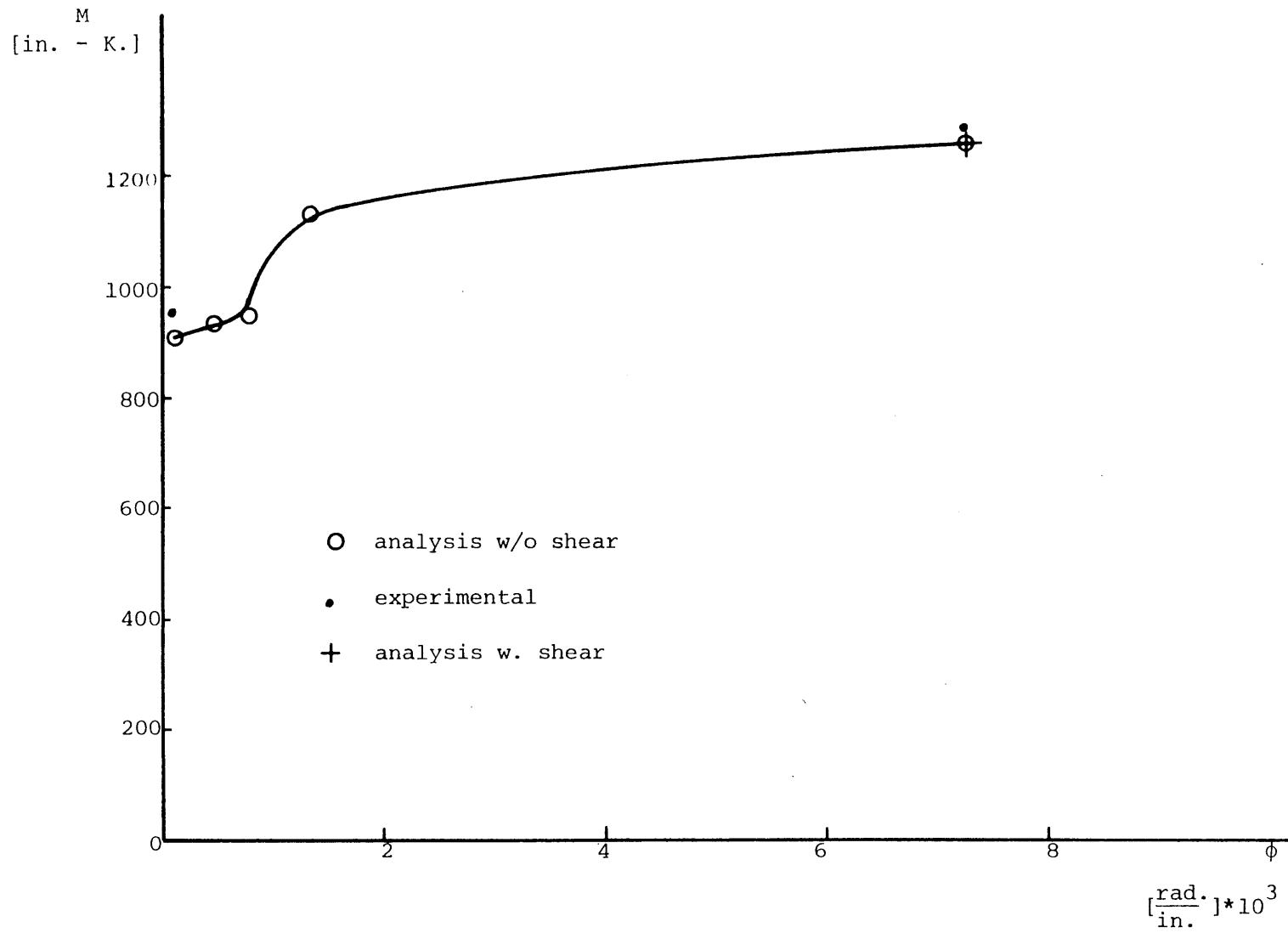
FIG. 3.2.9 Moment-curvature diagram for Beam J-14.

layer	ε	f [psi]	Area [in^2]	F [lbs]	
1	0.0072	4745.1	3.33	15801.2	
2	0.002	3266.3	3.097	10102.0	
concrete at comp. steel level	0.0155	3331.6	3.44	11477.4	
cover	>0.004	3750.0	1.53	5750.6	
comp. rein.	0.0155	46400.0	1.58	73312.0	ΣC = 116443.2 lbs
ten. rein.	0.15	73400.0	1.58	115972.0	

$$\frac{\Sigma C}{T} = 1.0040 \qquad \text{difference} = 0.4\%$$

The moment with respect to the tensile reinforcement:

$$M_{cal} = 1829.5 \text{ in. - K.}$$

This beam has a shear span to depth ratio $\frac{a}{d} = 4.0$, and #2 hoops at a 6 in. spacing. When this information is used to calculate the moment reduction factor, as proposed in Chapter 2 (program TKSH4), the following value is obtained:

$$\frac{M_u}{M_{fl}} = 0.889$$

from which:

$$(M_{cal})_{modified} = 1829.5 * 0.889 = 1626.4 \text{ in. - K.}$$

The measured moment:

$$M_m = 1650.0 \text{ in. - K.}$$

$$\frac{M_{cal}}{M_m} = 0.986 \qquad \text{difference} = 1.4\%$$

The curvature:

$$\phi = \frac{0.15}{14.5} = 0.010345 \frac{\text{rad.}}{\text{in.}}$$

Case 2:

Yielding of Tensile Reinforcement

This case represents a loading stage at which the tensile reinforcement reached a strain ε_s = 0.00181. Equilibrium is obtained when the neutral axis shifts to kd = 5.6 in. The numerical values are presented in the following tabulation.

layer	ε	f [psi]	Area [in^2]	F [lbs]	
1	0.000744	2022.2	8.0	16177.6	
2	0.000598	1660.2	7.21	11970.0	
3	0.000452	1280.5	7.21	9232.4	
4	0.000306	883.8	8.0	7070.4	
5	0.00016	458.3	8.0	3666.4	
6	0.0000438	130.7	4.8	627.4	
comp. rein.	0.0005255	15239.5	1.58	24078.4	ΣC = 72822.6 lbs
ten. rein.	0.00181	46200.0	1.58	72996.0	

$$\frac{\Sigma C}{T} = 0.9976 \qquad \text{difference} = 0.24\%$$

The moment with respect to the tensile reinforcement:

$$M = 1169 \text{ in. } - \text{ K.}$$

The measured moment:

$$M_m = 1204 \text{ in. } - \text{ K.} \qquad \frac{M_{cal}}{M_m} = 0.971 \qquad \text{difference} = 2.9\%$$

The curvature:

$$\phi = \frac{0.00181}{12.4} = 0.000146 \frac{\text{rad.}}{\text{in.}}$$

Case 3:

This case represents a loading stage at which the tensile reinforcement reaches a strain $\varepsilon_s = 0.009 \frac{in}{in}$. Equilibrium is obtained when the neutral axis shifts to kd = 3.1 in. The numerical results are presented in the following tabulation.

layer	ε	f [psi]	Area [in^2]	F [lbs]	
1	0.00157	2717.6	8.0	21740.8	
2	0.000966	2000.8	7.21	14425.8	
3	0.000332	863.7	8.01	6918.2	
comp. rein.	0.000664	19268.4	1.58	30444.1	ΣC = 73528.9 lbs
ten. rein.	0.009	46200.0	1.58	72996.0	

$\frac{\Sigma C}{T} = 1.0073$ difference = 0.73%

The moment with respect to the tensile reinforcement:

$\qquad$ M = 1212.5 in. - K.

The curvature:

$$\phi = \frac{0.009}{14.9} = 0.000604 \frac{rad.}{in.}$$

Case 4:

This case represents a loading stage at which the tensile reinforcement reaches a strain $\varepsilon_s = 0.0168 \frac{in}{in} = \varepsilon_{sh}$. Equilibrium is obtained when the neutral axis shifts to kd = 2.575 in. The numerical values are presented in the following tabulation.

layer	ε	f [psi]	Area [in^2]	F [lbs]	
1	0.00226	3140.7	8.0	25125.6	
2	0.00117	2195.85	7.21	15832.1	
3	0.000313	808.7	3.81	3081.1	
comp. rein.	0.000625	18151.35	1.58	28679.1	$\Sigma C = 72717.9$ lbs
ten. rein.	0.0168	46200.0	1.58	72996.0	

$$\frac{\Sigma C}{T} = 0.9962 \qquad \text{difference} = 0.38\%$$

Moment with respect to the tensile reinforcement:

$$M = 1208.2 \text{ in. } - \text{ K.}$$

The curvature:

$$\phi = \frac{0.0168}{15.425} = 0.001089 \frac{\text{rad.}}{\text{in.}}$$

Case 5:

This case represents a loading stage at which the tensile reinforcement reaches a strain of $\varepsilon_s = 0.1 \frac{\text{in}}{\text{in}}$. Equilibrium is obtained when the neutral axis shifts to $kd = 3.4$ in. The numerical values are presented in the following tabulation.

layer	ε	f [psi]	Area [in^2]	F [lbs)	
1	0.0051	4574.3	1.754	8022.4	
2	0.002	3216.2	4.572	15026.1	
concrete at comp. steel level	0.0096	4893.0	3.445	16856.4	
cover	>0.004	2210.0	0.809	1787.9	
comp. rein.	0.0096	46400.0	1.58	73312.0	C = 115004.8 lbs
ten. rein.	0.1	72650.5	1.58	114787.8	

$$\frac{\Sigma C}{T} = 1.0019 \qquad \text{difference} = 0.19\%$$

Moment with respect to the tensile reinforcement:

$$M = 1817.0 \text{ in. } - K.$$

The curvature:

$$\phi = \frac{0.1}{14.6} = 0.00685 \frac{\text{rad.}}{\text{in.}}$$

A summary of the points obtained from the analysis of Beam J-22 is presented in the following tabulation.

	M [in. - K.]	ϕ $[\frac{\text{rad.}}{\text{in.}}]$
yield	1169.0	0.000146
3	1212.5	0.000604
4	1208.2	0.001089
5	1817.0	0.00685
ultimate	1829.5 (w/o shear influence)	0.010345
	1626.4 (w. shear influence)	

The M-ϕ curve is illustrated in Fig. 3.2.10.

The behavior of the beams that have been analyzed previously is presented in Fig. 3.2.11. The results demonstrate that the analytical behavior is close to the experimental data. Unfortunately only the behavior at the yield and ultimate stages can be compared to the experimental data. The corrections due to the shear influence at ultimate shows a significant improvement. However, there is no experimental data to evaluate the influence of shear at intermediate loading stages.
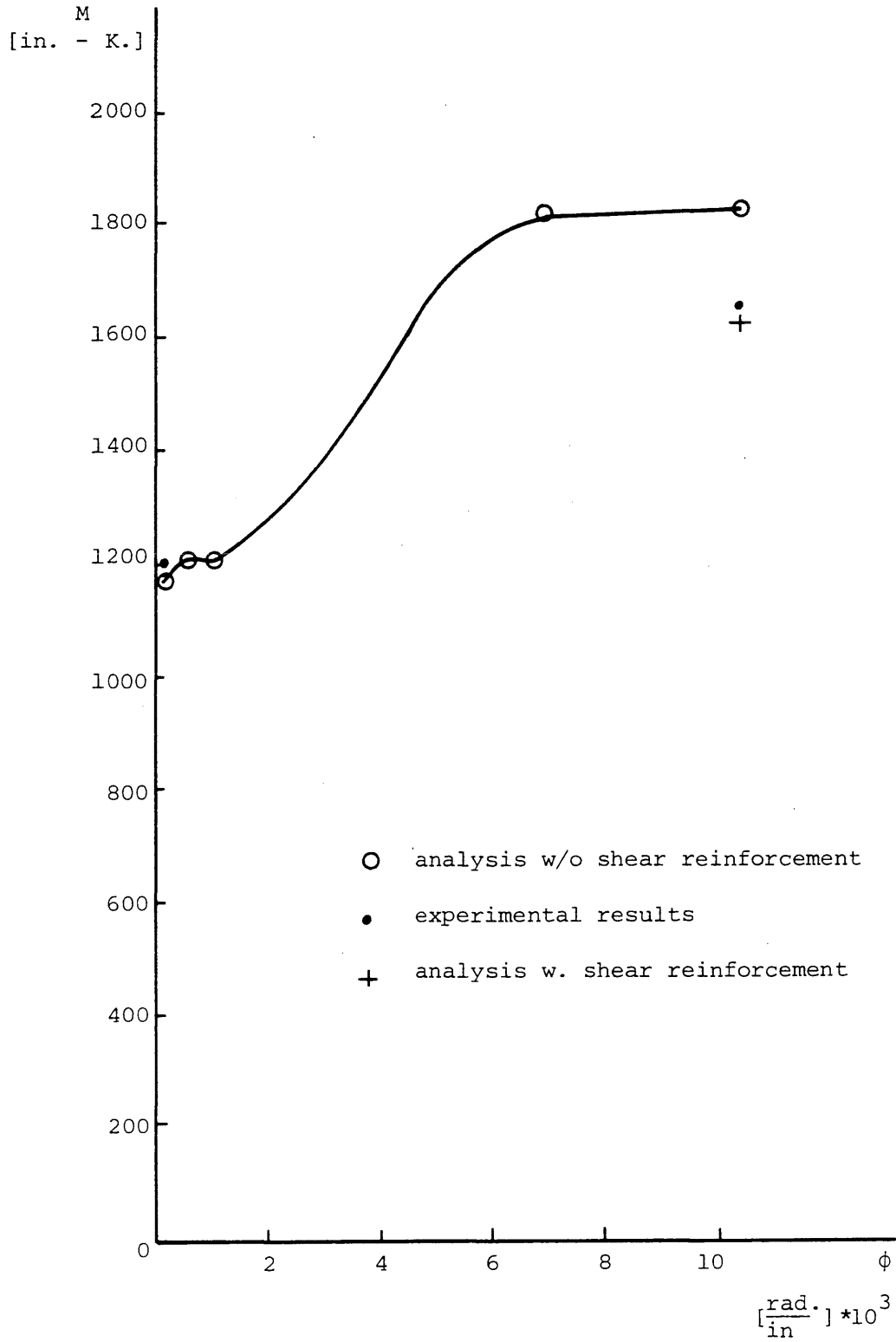
FIG. 3.2.10 Moment-curvature diagram for Beam J-22.
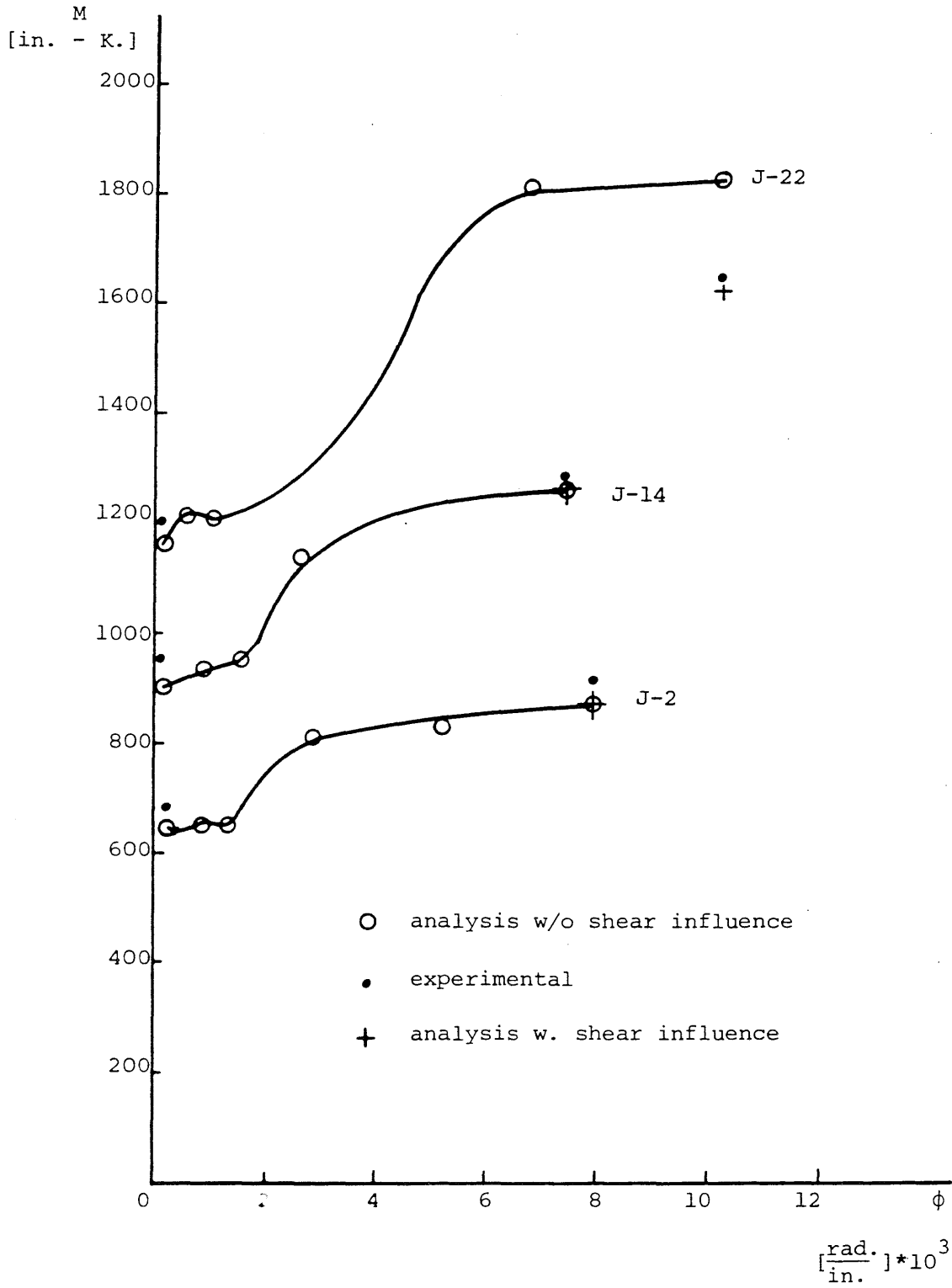
FIG. 3.2.11 Moment-curvature diagrams.

Beam J-20

In order to demonstrate once more the effectiveness of the proposed
method to analyze reinforced concrete beams, another case is examined. Beam
J-20 was tested and analyzed by Burns and Siess [12]; the analytical results
are different by more than 9.5% from the experimental (when only the ultimate
moment stage is considered).

Here, the ultimate moment capacity is evaluated, and the influence of
shear is taken into consideration. Equilibrium is obtained when the tensile
reinforcement reaches a strain $\varepsilon_s = 0.14 \frac{in}{in}$, and the neutral axis shifts to
$k_u d = 3.5$ in. The numerical results are presented in the following tabulation.

layer	ε	f [psi]	Area [in^2]	F [lbs]	
1	0.00867	4759.7	3.9	18562.8	
2	0.002	3268.9	2.4	7845.4	
cover	>0.004	2190.2	3.445	7545.2	
concrete at comp. steel level	0.02	2190.0	1.75	3832.5	
comp. rein.	0.02	48960.0	1.58	77357.3	$\Sigma C = 115143.2$ lbs
ten. rein.	0.14	71673.6	1.58	113244.3	

$$\frac{\Sigma C}{T} = 1.016 \qquad \text{difference} = 1.6\%$$

A small reduction in the value of kd should bring the system to a better
equilibrium condition, however for demonstration this system is used to
evaluate the ultimate moment.

$$M = 1352.0 \text{ in.} - K.$$

The measured moment:

$$M_m = 1238.0 \text{ in. - K.}$$

The moment that was calculated in Ref. [12]: M = 1356 in. - K.

Now, the influence of shear is considered.

Beam J-20 has a shear span to depth ratio: $\frac{a}{d} = 5.14$.

Shear reinforcement: #2 bars at a 6.0 in spacing.

When this information is used as explained in Chapter 2 (program TKSH4),

the moment reduction factor is $\frac{M_u}{M_{f\ell}} = 0.9$, therefore:

$$M_{cal} = 1352.0 * 0.9 = 1216.8 \text{ in. - K.}$$

$$\frac{M_{cal}}{M_m} = \frac{1216.8}{1238.0} = 0.983 \qquad \text{difference} = 1.7\%$$

Here again the calculated moment is quite close to the experimental value, and as in the cases that have been discussed previously the analytical result is smaller than the experimental result (i.e., the analysis is quite accurate, but still on the safe side).

3.2.3 <u>General Remarks and Observations</u> -- The results obtained in the previous section illustrate quite clearly that the analysis, based on the proposed model, makes it possible to obtain numerical solutions which are within 5% of the experimental data.

The results that had been obtained by Burns and Siess [12] for ultimate moment conditions, when corrected by the shear reduction factor (SRF) as presented in Table 3.2.3, come somewhat closer to the experimental data. When the results obtained in the previous section are considered it is clear

that even   the range of the ratio $\dfrac{(M_u)_{cal}}{(M_u)_m}$ becomes narrower than for the

uncorrected results. Based on the results from the proposed analysis this

range should be 0.95 to 1.05. The narrowing of the range, in which the ana-

lytical results fall, is illustrated in Fig. 3.2.12.

The results presented in Table 3.2.3 clearly indicate that the shear

reduction factor (SRF) alone can change the results only by a small amount.

Therefore, the combined contribution of the methods developed in this study

should be considered.

Table 3.2.3: Numerical results from Ref. [12], and their modification.

beam	$(M_u)_m$ Ref. [12] [in - K]	$(M_u)_{cal}$ Ref. [12] [in - K]	$\dfrac{(M_u)_{cal}}{(M_u)_m}$ Ref. [12]	S.R.F. present	$(M_u)_{corrected}$ Ref. [12] [in - K]	$\dfrac{(M_u)_{cal}}{(M_u)_m}$	$(M_u)_{cal}$ present [in - K]	$\dfrac{(M_u)_{cal}}{(M_u)_m}$
J-1	739	688	0.93	1.0	688	0.93		
J-11	617	595	0.96	1.0	595	0.96		
J-2	919	829	0.9	1.0	829	0.9	877.0	0.954
J-8	878	894	1.02	1.0	894	1.02		
J-17	892	896	1.0	1.0	896	1.0		
J-18	876	879	1.0	1.0	879	1.0		
J-10	943	938	0.99	1.0	938	0.99		
J-14	1296	1294	1.0	1.0	1294	1.0	1268.0	0.978
J-13	1392	1391	1.0	1.0	1391	1.0		
J-19	937	942	1.0	1.0	942	1.0		
J-20	1238	1356	1.09	0.9	1220.4	0.986	1216.8	0.983
J-4	1488	1511	1.01	0.98	1480.8	0.99		
J-9	1356	1493	1.10	0.97	1448.2	1.07		
J-5	1800	1781	0.99	0.98	1745.4	0.97		
J-6	1740	1845	1.06	0.94	1734.3	1.0		
J-21	1363	1469	1.08	0.89	1307.4	0.96		
J-22	1650	1856	1.12	0.89	1651.8	1.0	1626.4	0.986

mean: 1.015   mean: 0.987

range: 0.9 to 1.12   range: 0.9 to 1.07

x Beams of McCollister's Test Program

o Beams of the Burns Test Program

+ Present Analysis
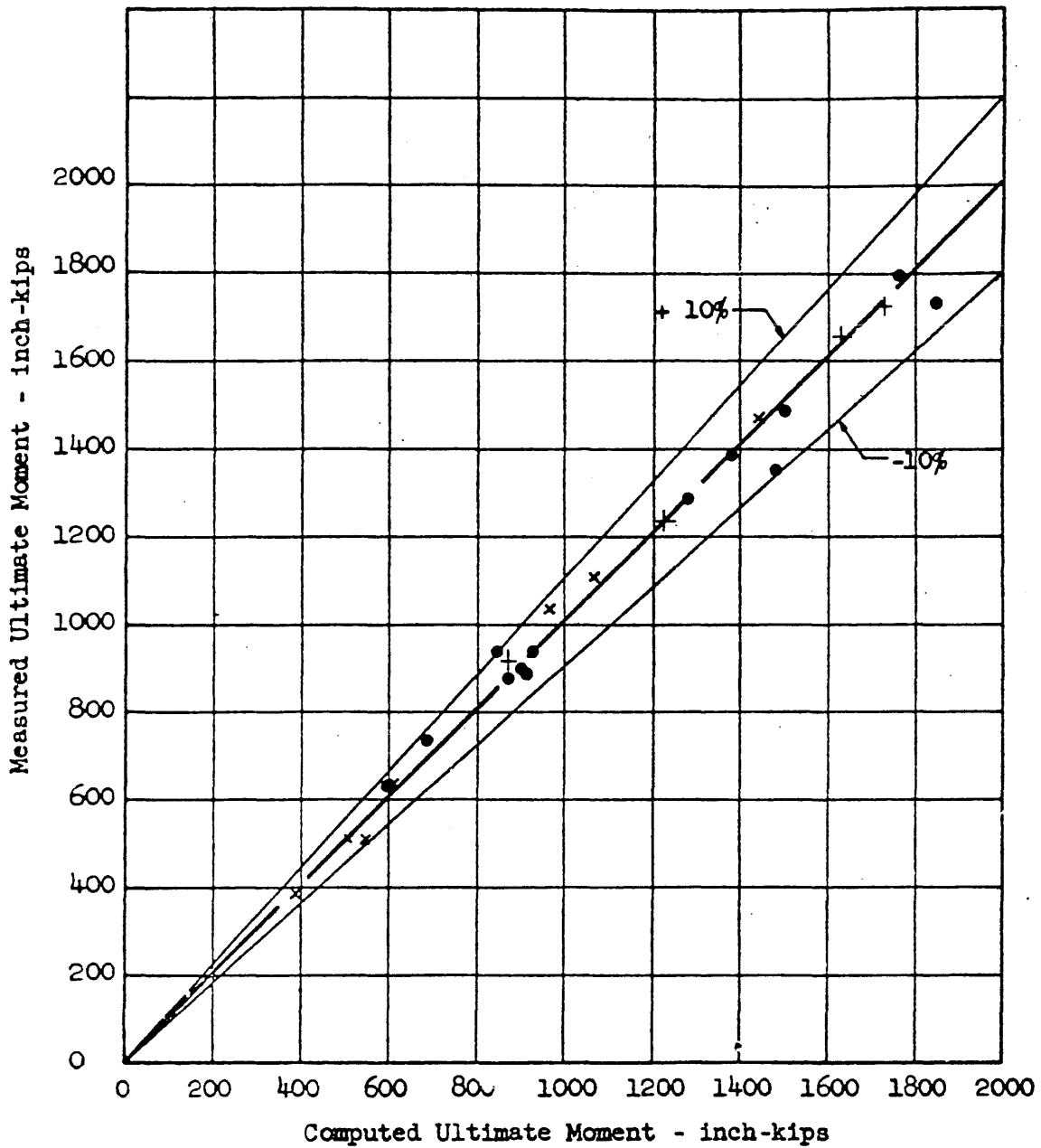
FIG. 3.2.12 Plot of measured versus computer ultimate moments.
Source Ref. [12]

3.3 Analysis by the ACI Method

It is interesting to compare the results obtained by the proposed method with results obtained by the ACI rectangular stress block method.

Beam J-2

The linear strain distribution, and the forces are illustrated in Fig. 3.3.1.
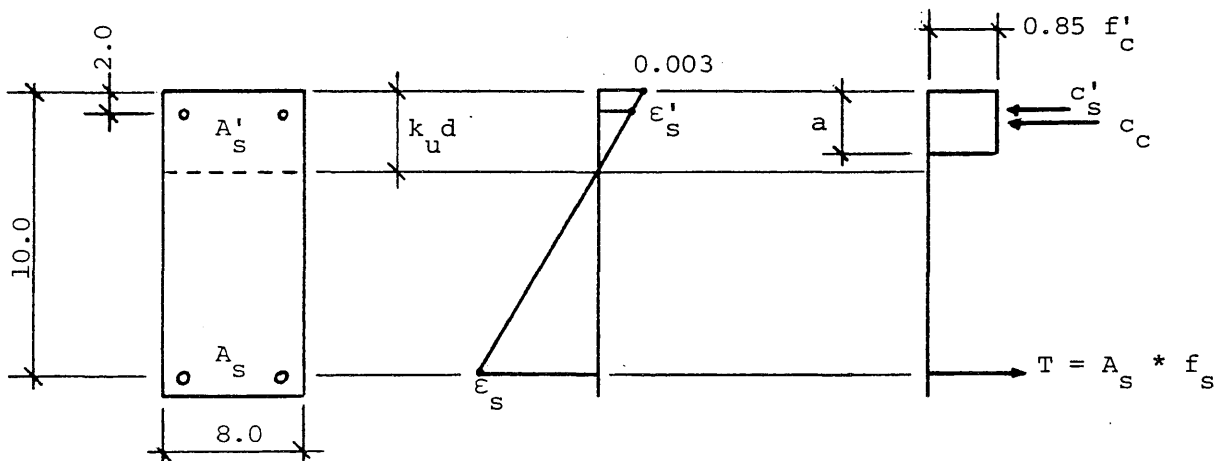
Fig. 3.3.1: The ACI method

$A_s = 1.58$ in.^{2}

$A'_s = 0.88$ in.^{2}

When equilibrium is reached the following values are obtained.

$f_s = f_y = 48000$ psi

$k_u d = 2.595$ in. $\Sigma C = 75403.3$ lbs

$\varepsilon'_s = 0.000688 < \varepsilon'_y$ $T = 75840.0$ lbs

$f'_s = 1.99433 * 10^4$ psi $\dfrac{\Sigma C}{T} = 0.994$ difference = 0.6%

$M_u = C_c * (d - \dfrac{a}{2}) + C'_s * (d - d') = 631.6$ in. - K.

where:

$$a = \beta_1 * k_u d = 0.846 * k_u d$$

$$\beta_1 = 0.85 - 0.05 * \frac{80}{1000} = 0.846$$

The measured moment: $M_m = 919$ in. $-$ K.

$$\frac{M_{ACI}}{M_m} = \frac{631.6}{919} = 0.687 \qquad \text{difference} = 31.3\%$$

Compared to a difference of 4.6% based upon the proposed method.

$(M_{cal} = 877.0$ in. $-$ K.$)$

Similarly, the other three beams have also been analyzed by the ACI method, and the values that were obtained are presented in the following table.

Table 3.3.1: Comparison of results from flexural analysis

Beam	Experimental moment [12] [in. - K.]	M_{ACI} [in. - K.]	ACI difference [%]	M present [in. - K.]	Present difference [%]
J-2	919.0	631.6	31.3	877.0	4.6
J-14	1296.0	901.6	30.4	1268.0	2.16
J-20	1238.0	916.4	26.0	1216.8	1.7
J-22	1650.0	1216.4	26.3	1626.4	1.4

In general, the ACI method results in significantly lower values, while the proposed method shows results which are significantly closer to the experimental data.

3.4 Analysis of Members with Axial Loads

3.4.1 <u>Introduction</u> -- The method employed to analyze reinforced concrete members, as presented in Chapter 2, and demonstrated in the previous sections of this chapter, is applied herein to flexural members with axial loads. Experimental, and analytical data from Yamashiro and Siess [38] is employed to evaluate the effectiveness of the proposed method.

Four beams (J-28, J-29, J-30, J-31) that had the same geometrical properties, and varied only by the magnitude of the axial load, are analyzed. The variation in the concrete compressive strength (f'_c), was small for these members, and therefore a value for f'_c is assumed that represents the entire group. Beam J-29 (f'_c = 4410 psi) has been chosen as a group representative. Beam J-28 had the largest difference in concrete compressive strength (f'_c = 5020 psi), and therefore this beam is analyzed separately to show that the analytical results are accurate.

The beam properties, and the geometrical configurations of the specimens and cross sections, are presented in Appendix B, Section B4.

3.4.2 <u>The Numerical Procedure</u> -- The numerical procedure has been discussed in Chapter 2, and is identical to the procedure used in the previous sections in this chapter. The major difference, however, is that for members with axial loads the compressive forces are not equal to the tensile forces. The difference between the two is the axial force. The procedure is demonstrated in the following examples.

Beams J-28 - J-31

Case 1:

<u>Ultimate Moment, No Axial Load</u>

This case represents a loading stage at which the ultimate moment is reached without the application of axial loads. Equilibrium is obtained when the tensile reinforcement reaches a strain $\varepsilon_s = 0.082 \frac{in}{in}$ and the neutral axis shifts to $k_u d = 3.6$ in. The numerical values are presented in the following tabulation. (These results are for beam J-28.)

layer	ε	f [psi]	Area [in^2]	F [lbs]	
1	0.02402	5834.35	1.01	5892.7	
2	0.01634	6075.0	1.01	6135.7	
3	0.00833	5614.7	3.48	19539.1	
4	0.002	3434.7	1.87	6422.9	
cover	>0.004	2321.0	0.91	2112.1	
concrete around comp. rein.	0.0205	5954.7	0.54	3239.3	
comp. rein.	0.0205	51276.0	2.0	102552.0	$\Sigma C = 145893.9$ lbs
ten. rein.	0.082	73083.9	2.0	146167.8	

$$\frac{\Sigma C}{T} = 1.0019 \qquad \text{difference} = 0.19\%$$

The moment with respect to the tensile reinforcement:

$$M = 1094.5 \text{ in. - K.}$$

The measured moment for beam J-28:

$$M_m = 1030.0 \text{ in. - K.}$$

If the shear reduction factor is considered by introducing the beam properties into program TKSH4, the following is obtained.

$$\frac{M_u}{M_{f\ell}} = 0.94$$

from which:

$$M_{cal} = 1094.5 * 0.94 = 1050.7 \text{ in. - K.}$$

$$\frac{M_{cal}}{M_m} = \frac{1050.7}{1030.0} = 1.02 \qquad \text{difference} = 2.0\%$$

When the same procedure is applied to beam J-29, the result for the ultimate moment, after the correction due to shear:

$$M_{cal} = 1079.9 \text{ in. - K.}$$

which is quite close to the result obtained for beam J-28.

The curvature:

$$\phi = \frac{0.082}{10-3.6} = 0.0128 \frac{\text{rad.}}{\text{in.}}$$

Case 2:

Ultimate Axial Load Capacity

This case represents the behavior of the member when no flexural moment is present, and only an axial load is acting on the cross section. At this stage the concrete cover is assumed to have spalled off. The axial strain is assumed to be ε_0 and this strain is applied uniformly on the cross section. The parameters that have been calculated for this stage are the following. (These parameters have been defined in Section 2.5.)

$$\varepsilon_0 = 0.0186$$

$$K = 1.16$$

$$Z = 48.07$$

The numerical results are presented in the following tabulation.

	ε	f [psi]	Area [in^2]	F [lbs]
concrete	0.0186	5115.6	44.0	225086.4
steel	0.0186	53745.2	4.0	214980.8

$$P_0 = \Sigma C = 440067.2 \text{ lbs} \quad \text{or} \quad P_0 = 440 \text{ K.}$$

Using the ACl procedure:

$$P_0 = 0.85 * f'_c * A_c + f_y * A_s = 449.3 \text{ K.}$$

which is remarkably close.

Assume:

$$P_0 = 440.0 \text{ K.}$$

The curvature:

$$\phi = 0$$

Case 3:

Balance Condition

A loading stage is defined as balanced if the failure of the member is caused when the tensile reinforcement yields and the extreme concrete fiber in compression crushes. Both the yielding of the tensile reinforcement, and the crushing of the concrete are simultaneous. Here, the crushing strain of concrete is taken as 0.004 $\frac{in}{in}$, and the yield strain of the tensile reinforcement (beam J-29) is 0.0018 $\frac{in}{in}$ as reported in Ref. [38]. The numerical values are presented in the following tabulation.

layer	ε	f [psi]	Area [in^2]	F [lbs]
1	0.00377	4954.0	4.35	21549.9
2	0.00333	5027.3	4.35	21868.7
3	0.00209	4680.0	6.0	28080.0
4	0.00151	3777.9	6.0	22667.4
5	0.00088	2433.9	6.0	14603.4
6	0.00028	831.5	5.55	4614.8
concrete at comp. rein. level	0.00277	5114.7	4.77	24386.9
comp. rein.	0.00277	48600.0	2.0	97200.0	ΣC = 234971.1 lbs
ten. rein.	0.0018	48800.0	2.0	97600.0

$P = \Sigma C - T = 137371.1$ lbs   (or 137.4 K.)

The moment with respect to the "plastic centroid", which for this cross section coincides with the center of the beam:

$M_b = 1243.0$ in. - K.

The curvature:

$$\phi = \frac{0.0018}{3.5} = 0.000514 \frac{rad.}{in.}$$

The ultimate moment in flexure is obtained for a neutral axis location kd = 3.5 in., the balanced moment for kd = 6.5 in. In order to obtain more points between these two, the neutral axis has to shift between the values 3.5 in and 6.5 in. The problem is to estimate the strain at the extreme concrete compressive fiber, as a function of the location of the neutral axis. By trial and error the following relationship is obtained.

$$\epsilon_{cu} = 0.046 - 0.004667 * (kd - 3.5)^2 \qquad (3.4.1)$$

Eq. (3.4.1) describes the variation of the strain ε_{cu} with respect to the shifting of the neutral axis.

Case 4:

<u>kd = 5 in</u>

From Eq. (3.4.1)

$$\varepsilon_{cu} = 0.0355 \ \frac{in}{in}$$

and the numerical values are presented in the following tabulation.

layer	ε	f [psi]	Area [in²]	F [lbs]	
1	0.01384	3615.5	4.44	16052.8	
2	0.0071	4650.2	4.44	20646.9	
3	0.002	4388.8	3.38	14385.9	
cover	>0.004	3748.0	2.4	9013.9	
concrete at comp. rein. level	0.0213	2472.0	2.51	6209.7	
comp. rein.	0.0213	55196.1	2.0	110392.2	$\Sigma C = 177151.4$ lbs
ten. rein.	0.0355	65156.4	2.0	130312.8	

$P = \Sigma C - T = 46838.6$ lbs   (or 46.8 K.)

The moment with respect to the plastic centroid:

$M = 1117.9$ in. - K.

The curvature:

$$\phi = \frac{0.0355}{5} = 0.0071 \ \frac{rad.}{in.}$$

Application of the ACI Method

When the ACI rectangular stress block is used to calculate the interaction diagram, the following values are obtained:

Case	P [Kips]	M [in. - K.]	ϕ
2	449.3	0.0	0.0
3 (balanced)	120.75	1153.2	0.00058
4	66.73	1073.16	0.001
5	85.4	1115.5	0.0008
1 (ultimate)	0.0	797.4	0.0015

Modification of the ACI Method

The ACI method assumes that the ultimate strength of the concrete is $0.85 * f'_c$. However, based upon the theoretical results that were discussed in Chapter 2, the maximum stress of the concrete is $K * f'_c$, where K is a function of geometry and the beam parameters. Therefore, the maximum stress that should be used is $0.85 * (K * f'_c)$. Based on this assumption, the following values are obtained.

Case	P [Kips]	M [in. - K.]	ϕ
1	139.4	1211.0	0.00058
2	77.12	1118.6	0.001
3	66.22	1087.0	0.0011
4	98.7	1167.4	0.008

The results obtained by the proposed method are combined to form the interaction diagram in Fig. 3.4.1. On the same diagram are shown the results based on the ACI method, the modified ACI method, and the experimental results from Ref. [38]. There are no experimental results in Ref. [38] for the behavior of the beams under axial loads that are higher than the balance condition. Therefore the balance point and the maximum axial load point are connected by a straight line.

The analytical results from the proposed method are much closer to the observed behavior than the results from any of the other methods that have been previously discussed. Furthermore, the "modified ACI method" developed and proposed in this study, results in better numerical values than the ACI method, as illustrated in Fig. 3.4.1. However, the results from the modified ACI method approach the results for the ACI method as the magnitude of the axial load is reduced.

3.5 Deep Beams

3.5.1 Introduction -- The analysis of deep beams is based on the analytical and experimental results reported by Crist [36,39]. The analytical results reported in Ref. [36,39] have an average error of 2% (see Table 3.5.1). Furthermore, the strain distribution for deep beams is not completely predictable, as discussed in Section 2.11. Therefore, the flexural analysis of deep beams is not performed in the same way as for slender beams. Here, the numerical results that were obtained by Crist [36,39] for ultimate moment conditions are used and modified by the moment reduction factor due to the influence of shear. The modified results as presented in Table 3.5.1, are
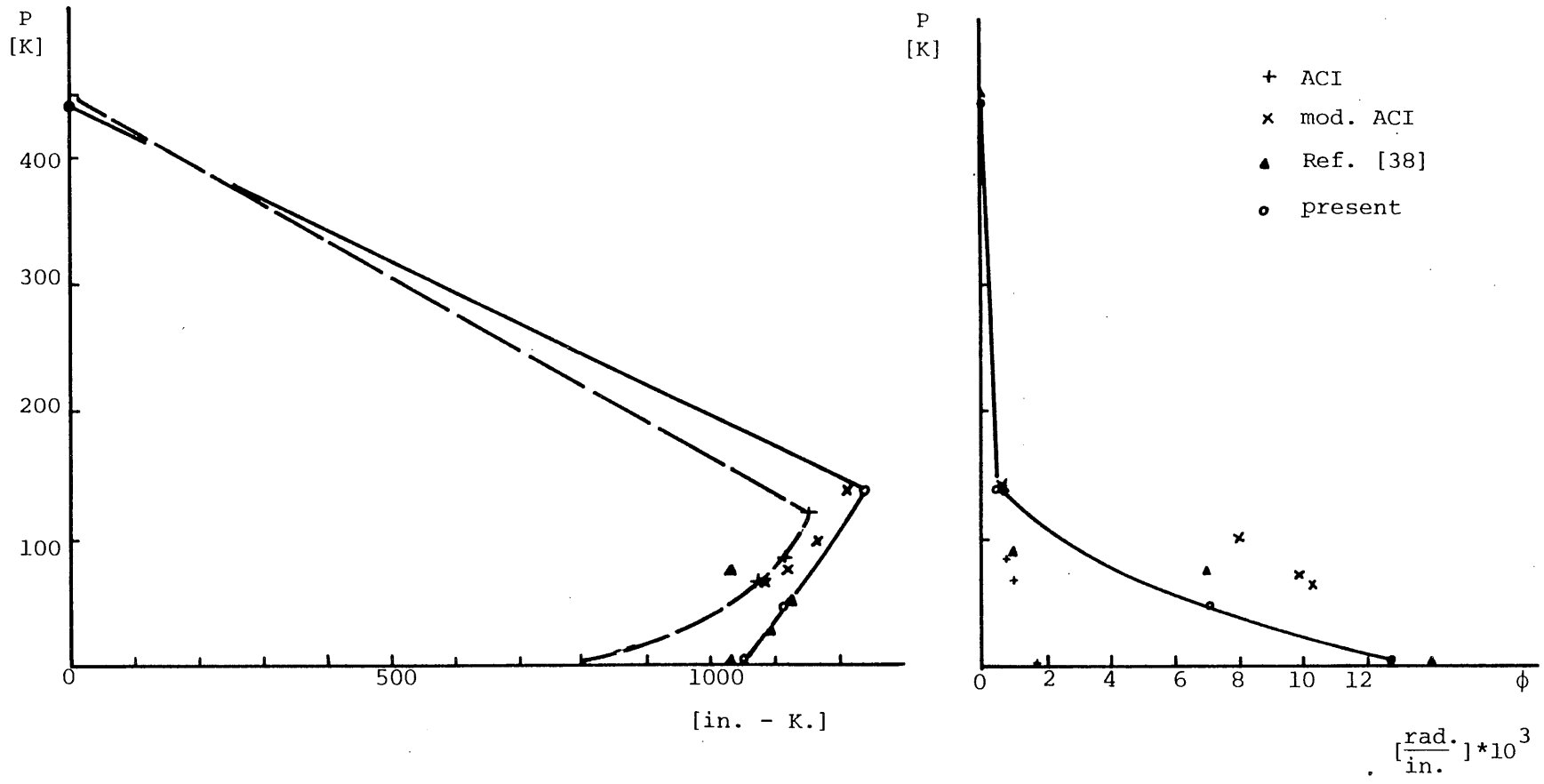
FIG. 3.4.1 Interaction diagrams.

somewhat closer to the experimental data. The important result of the present study on deep beams is that the ACI method of analysis for singly reinforced beams gives an average error smaller than any of the previous methods, as illustrated in Table 3.5.2.

3.5.2 Numerical Results -- The numerical results based on the studies by Crist [36,39], and the modification of these results by the proposed shear analysis are presented in Table 3.5.1. The results based on the ACI method are presented in Table 3.5.2. The beam properties and the geometrical configurations of the experimental specimens are presented in Appendix B, Section B4.

The results for deep beams are based on a very small number of beams that have been tested. Furthermore, only beams with a shear span to depth ratio less than 3.0 were considered as deep. The results in Table 3.5.1 show clearly that except beams S-6, and 2S1.6-3C all other beams behaved nearly as predicted. The application of the shear reduction factor (SRF) improves the average accuracy of the analysis. When the beams S-6 (no shear reinforcement), and 2S1.6-3C (identical to beam 2S1.6-3 but had a significantly lower moment capacity) are excluded from the analysis the following accuracy is obtained:

1. Prediction of ultimate moment:

$$-5\% < \text{difference} < +5\%$$

$$\text{difference} = \frac{(M_u)_{cal}}{(M_u)_m} - 1.0$$

(for all beams $-10.7\% \leq \text{difference} \leq +7.8\%$)

Table 3.5.1: Numerical results for deep beams.

beam no	$\frac{a}{d}$	$(M_u)_m$ [in. - K.]	$(M_u)_{cal}$ [in. - K.]	$\frac{(M_u)_{cal}}{(M_u)_m}$		S.R.F.	$(\alpha)_m$ [deg]	$(\alpha)_{cal}$ [deg]	$(M_u)_{cal}$ [in. - K.]	$\frac{(M_u)_{cal}}{(M_u)_m}$	$\frac{(\alpha)_{cal}}{(\alpha)_m}$
S6	2.67	6289.0	5734.0	0.91	no shear rein.	0.979	63.0	60.0	5613.6	0.893	0.952
S8	2.67	6849.0	6649.0	0.97		0.982	84.0	82.8	6529.3	0.953	0.986
S9	2.67	6248.0	6688.0	1.07		0.981	84.0	85.3	6560.9	1.05	1.015
2S1.6-1	1.6	7879.0	8152.0	1.035		1.0	80.0	83.7	8152.0	1.035	1.046
2S1.6-2A	1.6	8479.0	8589.0	1.013		1.0	83.0	82.5	8589.0	1.013	0.994
2S1.6-2B	1.6	7726.0	8116.0	1.05		1.0	87.0	82.9	8116.0	1.05	0.953
2S1.6-3	1.6	7838.0	8163.0	1.041		1.0	80.0	82.0	8163.0	1.041	1.02
2S1.6-3C	1.6	7566.0	8158.0	1.078		1.0	88.0	83.1	8158.0	1.078	0.944

average 1.0209

average 1.014   0.989

difference range: -9% to +7.8%

moment difference range: -10.7% to +7.8%

angle difference range: -5.6% to +4.6%

Table 3.5.2: Numerical results from the ACI method.

beam	f'_c [psi]	A_s [in.^{2}]	f_s [psi]	$(k_u d)_{cal}$ [in.]	a_{cal} [in.]	M_{cal} [in. - K]	$\dfrac{M_{cal}}{M_m}$
2S1.6-1	4160	2.37	61468	6.11	5.15	8074.3	1.025
2S1.6-2A	4373	"	64770	6.2	5.16	8507.0	1.003
2S1.6-2B	3829	"	61138	6.54	5.56	8000.8	1.035
2S1.6-3	5023	"	61400	5.13	4.26	8130.0	1.037
2S1.6-3C	3586	"	61623	7.04	5.99	8033.3	1.062
S-6	4129	3.81	46100	7.42	6.25	5774.2	0.92
S-8	3796	"	51732	8.98	7.64	6343	0.93
S-9	3521	"	52559	9.84	8.36	6371.5	1.02

average 1.004

moment difference range: -8% to +6.2%

Table 3.5.3: Neutral axis location.

beam	$(k_u d)_m$ [36,39] [in]	$(k_u d)_{cal}$ ACI [in]
2S1.6-1	3.9	6.11
2S1.6-2A	5.8	6.2
2S1.6-2B	8.1	6.54
2S1.6-3	8.0	5.13
2S1.6-3C	4.3	7.04
S-6	8.0	7.42
S-8	7.8	8.98
S-9	6.2	9.84

2. Prediction of crack inclination:

$$\text{difference} = \frac{(\alpha)_{cal}}{(\alpha)_m} - 1.0$$

-1.5% < difference < +5%

(for all beams -5.6% $\leq$ difference $\leq$ +4.6%)

However, when the ACI rectangular stress block method is used, the results for the ultimate moment are more accurate.

-8% < difference < +6.2%   (for all beams)

-7% < difference < +3.5%   (without S-6, 2S1.6-3C)

$$\text{difference} = \frac{(M_u)_{cal}}{(M_u)_m} - 1.0$$

Nevertheless, the differences in the results are not significant, and the range of differences is almost the same for all methods.

3.6 Summary and Discussion of the Analytical Results

3.6.1 Introduction -- The analytical procedure that was presented in Chapter 2 has been applied to the analysis of structural members. The analytical results have been compared to experimental data, and the accuracy of the method has been evaluated. Some observations have been made during the analytical procedure. However, the analytical results must be studied and evaluated with regard to the behavior of all the members that have been analyzed. Three types of structural members have been analyzed by the proposed method. The results are discussed separately for each type, and then the method is evaluated in terms of applicability to the design of structural members in general.

3.6.2 Slender Beams without Axial Loads -- The analytical method that had been proposed in Chapter 2 was applied to analyze three beams in detail,

and a fourth beam for ultimate moment capacity only. The numerical results have been given in Sections 3.2, and 3.3. The behavior of three beams has been illustrated in Figs. 2.3.8, 3.2.9, 3.2.10, and 3.2.11. The procedure to evaluate the flexural behavior without the influence of shear results in moment-curvature diagrams do compare well with the expected behavior. All three cases show a significant increase in moment capacity when the strains in the longitudinal reinforcements enter the strain hardening region on the steel stress-strain curves.

The analytical results for the yield stage of the tensile reinforcement are in the range of 2.9 percent to 6.1 percent from the measured values. However, the higher measured values can be explained by a load higher than needed to cause yielding of the tensile reinforcement. It is possible that in order to detect the yield stage the investigator had to load slightly higher than required to cause the steel to yield. If this assumption is correct then the analytical results are closer to the real yield moment. In any case, the accuracy of the results for the yield stage is quite good.

The results for the ultimate stage show that the proposed method is quite consistent and accurate. The incorporation of the procedure to account for the shear influence into the flexural analysis, brings the results within 5 percent from the experimental data. The results for the ultimate moment capacity obtained by Burns [12], when corrected by the shear reduction factor, as presented in Table 3.2.3, also show a significant improvement. The convergence of the analytical results to the experimental data is illustrated in Fig. 3.2.12, which is a graphical representation of Table 3.2.3, and the corrected values for the beams that have been analyzed in this chapter.

The beams that have been analyzed by the proposed method have also been analyzed by the ACI rectangular stress block method. The results are presented in Table 3.3.1, and show very clearly that the ACI method considerably underestimates the ultimate moment capacity.

The results obtained for slender beams in this study show that the proposed method is accurate and reliable. The moment-curvature diagrams have the expected shape, and the numerical values for the yield and ultimate stages represent quite accurately the experimental data.

As a result of these findings the assumptions that have been made in Chapter 2, on which the proposed method is based, appear justified. Furthermore, the numerical procedure of the analysis is relatively simple and only few iterations are needed in order to obtain an acceptable solution.

3.6.3 <u>Slender Beams with Axial Loads</u> -- The method that was used to analyze slender beams without axial loads has been applied to the analysis of beams with axial loads. The numerical procedure is demonstrated in Section 3.4, and the results are presented graphically in Fig. 3.4.1.

The analytical results clearly show that the accuracy of the method is quite high. This is the only method that could approximate the experimental data so well. The ACI method, the modified ACI method, and the procedure that was used in Ref. [38], have been found less accurate.

The correction of the numerical results by the shear reduction factor was performed only for the ultimate moment stage without axial loads. In other loading stages the axial force improved the shear resistance of the members, and the full moment capacity was reached. This result confirms

the observation at the end of Section 2.8 that axial loads tend to influence the behavior of slender structural members similarly to the influence by shear reinforcement.

Unfortunately, the experiments that are reported in Ref. [38] do not give information about the behavior of the members for axial loads that are larger than $\frac{1}{2}P_b$ (one half of the axial load at the balance condition).

The assumption that the strain at the extreme concrete fiber in compression has a parabolic variation between the pure flexural mode and the balance mode has been found to be correct. This behavior is described by Eq. (3.4.1), and should be evaluated for other structural members under similar loading conditions.

The proposed method is effective and quite simple to apply. The numerical results are accurate, and the analytical behavior of the members represents the experimental data quite well.

3.6.4 <u>Deep Beams</u> -- The proposed method was applied to analyze the ultimate moment capacity of deep beams. The numerical results which are quite close to the results that have been reported by Crist [36,39], and therefore they have not been presented in Table 3.5.1. In general, the results that have been reported by Crist [36,39] are within 10 percent of the experimental data. The results show a small average improvement when corrected by the shear reduction factor, but the error range shows almost no change.

The ACI method shows somewhat better results, the error range is narrower by about 2.5 percent and the average is less than 0.5 percent.

The numerical results from all three methods are quite close. The proposed method and the method that was used in Ref. [36,39], are almost identical

in terms of accuracy, while the ACI method gives slightly improved results. The average result of all three methods is within 2 percent of the experimental values, which is quite good for engineering purposes. However, results for individual members could be within 10 percent from the experimental data.

These findings indicate that the strain distribution across the depth of deep structural members is not completely understood. Without a good approximation of the strains, the calculated stresses are not accurate, and the resulting moments less accurate and less consistent than for the case of slender beams. The numerical values for the neutral axis location ($k_u d$) show significant differences when calculated by the various methods. This too confirms the observation that the strain distribution is not yet understood. (see Table 3.5.3.).

The prediction of the crack inclination is quite accurate, and all the results are within 5 percent or less of the experimental values.

In general the proposed method is capable of analyzing deep members. For most cases the results are within 5 percent from the experimental data, and for only a few cases the results are within 10 percent from the experimental data. The influence of shear reinforcement is accountable, and the results for the crack angles are within 5 percent from the experimental data.

3.6.5 <u>General Remarks</u> -- The results that were obtained by the proposed method, and discussed in this chapter, confirm the basic assumption on which the proposed method is founded. The stress-strain curves for reinforced and confined concrete, depend on the geometry of the confined area and the material properties of concrete and steel. The changes in the stress-strain curves, as a function of the loading stage, and the location of the neutral

axis have been found to contribute to the improvement of the results. The method has shown that it is applicable for the analysis of slender beams, with or without axial loads, and deep beams.

The influence of shear on the behavior can be evaluated from the model that accounts for the reduction in flexural capacity due to shear at the ultimate moment conditions. Furthermore, the method makes it possible to evaluate the effectiveness of the shear reinforcement, and to predict the inclination of cracks at the ultimate moment conditions. The evaluation of the effectiveness of the shear reinforcement, without relying on the unpredictable shear strength of the concrete, will hopefully result in safer design procedures.

4. OBSERVATIONS FROM STRUCTURAL BEHAVIOR

4.1 Introduction

The theoretical and analytical study that was conducted in the pre-
vious chapters considered the behavior of isolated structural elements.
When such elements are combined to form a complete structure their behavior is
no longer independent. The interaction between adjoining members may cause
a change in the behavior of individual members. Furthermore, a weak joint
between structural members may prevent the structure from performing as expected.
Therefore, it is important to discuss the requirements for the design of
joints between structural members. Here, only connections between beams
are discussed in detail. However, information about other types of connec-
tions can be found in the references that are mentioned during the discus-
sion.

The present chapter contains a discussion of two subjects. The first
topic discussed concerns the design of structural connections, as reported
in the literature. The second topic discussed concerns the behavior of
structures, and structural elements, as presented in the literature, and
relates to the design of protective structures.

4.2 Structural Connections

4.2.1 Introduction -- A reinforced concrete structure is composed of
many structural elements (i.e., beams, columns, walls, slabs). Individual
elements are connected to become a structural frame. When a frame is ana-
lyzed, the joints are assumed to be "rigid". The analysis determines the
detailing of individual members, and of the joints between members. In the

past, the detailing of the joint was determined by the requirements for the anchorage of the reinforcement in the members forming the joint, which could be quite unsafe in many cases. It is very important to ensure that the joints will not become "weak links" in the frame. In general, joints have to perform under the same loading conditions as the adjoining members. Therefore, the problems of strength and serviceability should be considered. It is important to prevent the joints from governing the behavior of the frame; this way the structural elements forming the joint can reach their ultimate capacity. Joints should fit the nature of the expected loads (i.e., static, loading in one or more directions, reversal, etc.). An important factor in the design of joints, is simplicity. A complicated design may cause problems during construction.

The present discussion will concentrate on knee joints and beam column connections, and is based on studies by other investigators, as reported in the literature. An extensive discussion on structural connections is found in Ref. [3].

4.2.2 <u>Knee Joints Under Closing Loads</u> -- There are several ways to design a knee joint under closing loads. In all cases, there are two locations for possible splitting or crushing of the concrete, which may reduce the load capacity of a joint. The first location is the outer corner of the joint, where concrete may split. If this splitting can be avoided, no major problems should be expected, because anchorage is almost always ensured. At the inner corner, the concrete may crush, but the biaxial state of stress at this location improves the behavior of the concrete. Mayfield

et al. [40], found that the corner detailing is unimportant in the case of closing loads.

From a free body diagram, Fig. 4.2.1, the splitting stress of the concrete in the corner, can be calculated as follows.

$$f'_t = \frac{T}{bd} = \frac{A_s * f_y}{bd} = \rho * f_y \cong 6 * \sqrt{f'_c} \quad \text{[psi]} \quad \quad (4.2.1)$$

where:

T = magnitude of tensile force

b = width of joint

d = depth of joint

A_s = area of bars in tension

f_y = yield strength of bars in tension

Swann [41] found that to avoid splitting of the joint, the percentage of steel content should be limited by the following equation.

$$\rho \leq 1.2 * \frac{f'_t}{f_y} \quad\quad\quad (4.2.2)$$

A more conservative value is given by Park and Paulay [3].

$$\rho \leq \frac{f'_t}{f_y} \quad\quad\quad (4.2.3)$$

A recommended detailing of a joint under closing loads is presented in Ref. [3], as illustrated in Fig. 4.2.2.

Park and Paulay [3], also recommended the following:

1. Provide continuous tension steel around the corner, without lapping in the joint.

2. Bend bars in sufficient radius, and support the reinforcement, if possible, as shown in Fig. 4.2.1g, to improve behavior.

3. Limit the amount of steel in a joint according to Eq. (4.2.3).

4. Provide confinement to the concrete in the joint, as illustrated by Fig. 4.2.2, which will also prevent crack growth.

4.2.3 <u>Knee Joints Under Opening Loads</u> -- When the loads, acting on a knee joint, tend to open the joint, the generated stresses cause splitting of the concrete at the inner corner, and spalling of the concrete at the outer corner. The detailing of opening joints is very important, in order to ensure the full capacity of the adjoining members.

Nilsson [42] studied the behavior of joints, and recommended a procedure for the detailing of opening knee joints, as illustrated in Fig. 4.2.3. Based on the results from Ref. [42], Park and Paulay [3] calculate the amount of radial hoops, to prevent the diagonal tension crack, across the joint, by the following equation.

$$a_{sj} = [\frac{f_y}{f_{yj}} \sqrt{1 + (\frac{h_1}{h_2})^2}] \frac{A_{sl}}{n} \tag{4.2.4}$$

where:

a_{sj} = cross section area of one radial hoop

f_{yj} = yield stress of radial hoop

n = number of radial hoop legs (see Fig. 4.2.3)

h_1, h_2 = total depth of adjoining members

A better performance is obtained when the loop of the main reinforcement is continuous. In this case, radial hoops are required only if the flexural steel content exceeds 0.5%, and calculated from Eq. (4.2.4), multiplied by the following parameter.

$$\rho* = \frac{\rho - 0.005}{\rho} \qquad\qquad (4.2.5)$$

where the flexural steel content is defined as follows.

$$\rho = (\frac{A_s}{bd}) \quad \text{(for member 1)}$$

The cross section area of the diagonal bar across the inner corner of the joint, should be at least one half of the value A_{sl}.

The introduction of a haunch at the inner corner, will improve the behavior. This recommendation was confirmed by Conner and Kaar [43].

Hanson [44] recommended a similar approach, but used rectangular ties instead of radial hoops, and did not use a diagonal bar across the inner corner.

Balint and Taylor [45] proposed to use a mesh reinforcement instead of rectangular ties, or radial hoops.

The methods proposed in Refs. [42,44,45] ensure that the joint will not prevent the adjoining members to reach their full flexural capacity.

Further recommendations, regarding the design of joints are found in the report by the ACI-ASCE Committee 352 [46].

All three methods, that are recommended for the design of joints, provide reinforcement that increases the confinement of the concrete in the

joint, and resists the shear stress due to the deformation of the frame. The amount of shear reinforcement in a joint, should be sufficient to resist the shear stresses, without relying on the contribution of the concrete.

4.2.4 <u>Summary</u> -- The experimental results for knee joints that have been discussed previously, and further studies on the behavior of T joints and column-slab joints that are discussed in Refs. [42,47], provide information on the required design of joints. It is recommended that reinforcing bars acting in tension should be continuous in order to avoid crack initiation at the cut-off or lapping zones. Anchorage of the steel bars ensures that the reinforcement will act in the whole loading range, and will not be pulled-out to weaken the joint.

Special attention should be given to the shear reinforcement. It is recommended to provide enough shear reinforcement so that the entire shear is resisted by the reinforcement, and neglect the contribution of the concrete. An upper limit should be placed on the joint shear, to avoid excessive diagonal compression. Park and Paulay [3] recommend that this limit should be in the range $10\sqrt{f'_c}$ to $11.5\sqrt{f'_c}$, in psi units.

The confinement of the concrete in the joints is as important as in the adjoining members. The shear reinforcement alone may not be able to provide the required confinement, and additional reinforcement should be provided in the form of wire meshes, or rectangular hoops at right angles, as described in Refs. [44,45].

Careful design and detailing of joints ensures that the adjoining members can develop their ultimate capacity, and behave as the experimental isolated members under similar loading conditions.

4.3 Structures Designed for Large Load Capacity

4.3.1 Introduction -- The information from analytical and experimental
studies on the behavior of structures under dynamic high intensity loads
is usually not available in the literature. Some information can be found
in the literature that is discussed in Appendix A. However, most of the
information includes design recommendations and not many details on the
behavior. Therefore, this discussion of the behavior of structures under
high intensity loads is restricted to only two cases, for which the informa-
tion was published. The first structure is a missile silo closure, and
the second is a thick-walled multiple opening conduit.

4.3.2 Missile Silo Closure Systems -- The discussion of the behavior
of missile silo closure systems is based on the studies of Iten [48], and
Gamble et al. [49].

Itan [48] studied the behavior of closure slabs to resist impact loads
in the range of 1000 psi to 2000 psi. Two types of slabs were investigated.
The first type was a bar reinforced slab, which was a concrete slab rein-
forced by steel bars. The second type was a plate reinforced slab, which
was a concrete slab with a steel plate bottom. Both types had a circular
geometry.

The results of the study showed that both types provided the required
resistance. When shear reinforcement was included the behavior became
more ductile. The plate reinforced slab could be used with or without
shear reinforcement, while the bar reinforced slab required shear reinforce-
ment to provide similar results. A significant improvement in the capacity

of the slabs was obtained by providing lateral confinement for the concrete in the form of steel rings or steel hoops. The lateral confinement improved the bearing capacity, the shear strength, and the flexural resistance of the slabs. The failure of the slabs at loads higher than the operational range was governed by shear or bearing stresses.

Gamble et al. [49] studied the behavior of launch facility closures. (The study by Iten [48] was part of the study by Gamble et al. [49].) The specimens were of the same types, as in the previous study. It was found that the plate reinforced slab had a better performance than the bar reinforced slab, and that shear reinforcement improved the ductility but not the load capacity. The friction induced compressive forces at the supports improved the flexural strength of the slabs. Unreinforced slabs could reach almost the same load capacity as the reinforced slabs, but had a brittle mode of failure and very little ductility.

A recommendation for the analysis of such slabs, was to separate the analysis into two parts. In the first part, to include the effect of the compressive forces at the supports, while in the second part these forces are ignored. The two parts of the analysis consider the case where the slabs maintain contact with the supports, and also the case where the contact is lost due to the vibration of the slab.

These studies show quite clearly that the confinement of the concrete and the shear reinforcement are two major factors that determine the behavior of the slabs.

4.3.4 <u>Thick-Walled Multiple Opening Conduits</u> -- Studies of thick-walled

multiple opening conduits, at the University of Illinois [50,51,52,53], pro-

vide valuable information about the behavior of massive reinforced concrete

structures. The scaled models of the structures were designed to resist a

uniform distributed load equivalent to 250 psi, which is in the load range

designated for certain protective structures.

The results of the experimental and numerical studies indicated that

the deep beams which are parts of the frame are very sensitive to shear.

The models that were designed to resist the equivalent load of 250 psi

actually were loaded up to an equivalent load of 1050 psi. The shear

strength of the members governed the behavior, and a lower bound for the

shear strength was proposed.

Gamble [53] applied the results of the studies to design procedures.

He showed that conventional methods for frame analysis, when modified to

comply with the experimental results, would give reasonable design parameters.

The behavior of these structural models indicate that it is quite dif-

ficult to evaluate the actual resistance of a structure. Again, the shear

strength governed the behavior, and an improved method to evaluate the

amount of shear strength was needed.

4.4 Conclusion

The experimental data on the behavior of structures, discussed in this

chapter, indicate that the behavior could be evaluated by analytical methods.

The behavior is governed by the "weak link" concept, which means that the

structure will not be able to perform as required if the resistance of

individual structural members is lost. The design should ensure that all structural members and joints are able to perform under the expected loading conditions. It is clear that joints have to be designed carefully in order to prevent them from becoming the cause of failure.

It is important to use reliable analytical methods to evaluate the performance of the individual members. All the results show that the confinement of the concrete and the shear resistance of the members are critical parameters that govern the behavior. The shear resistance of concrete is too unpredictable. Therefore it is recommended that shear reinforcement be provided in critical members and critical locations in the structure, so that shear can be resisted by the shear reinforcement alone. This approach for the requirements of shear reinforcement complies with the European design methods that have been discussed in Chapter 2.

The analytical method for the analysis of reinforced concrete members that has been proposed in Chapter 2 and demonstrated in Chapter 3 provides the capability to account for the confinement of concrete, and to evaluate the influence of shear on the behavior of structural members. This study demonstrates the importance of confinement provided by the transverse reinforcement in beams. The combined contribution of the transverse reinforcement confining the concrete and resisting shear stresses intuitively explains the improved behavior of structural joints when such reinforcement is introduced. However, further study is required to develop an analytical procedure to describe the behavior of a joint and the influence of transverse reinforcement on the behavior.
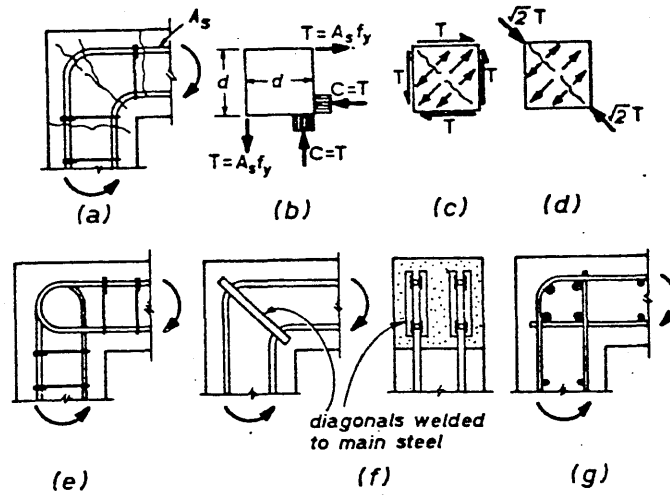
FIG. 4.2.1 Actions and details of knee joints subjected to
closing moments. (a) Typical cracks. (b) Internal
forces. (c) Crack due to shear. (d) Splitting
crack. (e) Overlapping hoops. (f) Diagonal
stiffeners. (g) Transverse bearing bars. Source
Ref. [3]
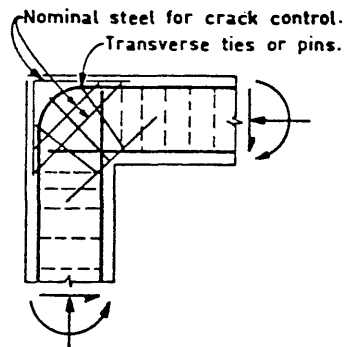
FIG. 4.2.2 Secondary reinforcement at knee of portal frame.
Source Ref. [3]
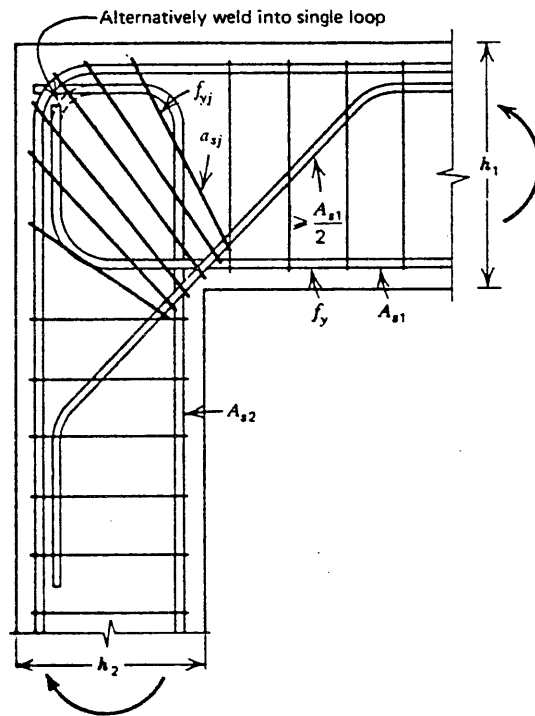
FIG. 4.2.3 Suggested details for large opening knee joint.
Source Ref. [3]

5. CONCLUSIONS AND RECOMMENDATIONS

5.1 Conclusions

The conclusions drawn in this study are summarized herein under several general categories. The first category relates to the general behavior of structures, and structural members under high intensity dynamic loading conditions. The second category relates to the nature of the stress-strain curves of reinforced and confined concrete, and the numerical procedure to analyze flexural reinforced concrete members. The third category relates to the influence of shear on the behavior and moment capacity of reinforced concrete beams. It also relates to the influence of shear reinforcement on the behavior of flexural members, and the procedure to evaluate the efficiency of shear reinforcement in terms of ultimate moment capacity and crack inclination angles.

5.1.1 <u>Structural Behavior Under High Intensity Loading Conditions</u> -- This study is concerned with a specific range of dynamic loading conditions. These loading conditions correspond to the detonation of nuclear weapons in the megaton range of yields. The loading function applied to the structure under consideration usually has a time duration considerably longer than the natural period of the structure and structural elements. Therefore, in most cases of this type only a static analysis is necessary to determine the proportions and detailing of the structure. Furthermore, the design procedure, as presented in Appendix A, calls for a preliminary static design from which it is determined if a dynamic analysis is necessary. The experimental and theoretical evidence   presented and discussed in Appendix A indicate that a static

analysis of protective structures should always be performed as a preliminary step. In the event that the structure has to resist the loading from large nuclear weapons, usually no dynamic modification is necessary. Therefore, as a result of these recommendations only the static aspect of the behavior is considered in this study. However, the material properties for the "equivalent static analysis" are not the same as for static conditions. The results presented in Appendix A indicate that the performance of concrete and steel under the expected dynamic loads improves by as much as between 20 percent to 30 percent. Therefore the material properties should be modified accordingly for the equivalent static analysis, and the design procedure should follow the general steps, as presented in Appendix A. However, the increase in strength and improved performance of protective structures reported in the literature cannot be explained by only the improved material properties under dynamic loading conditions. Other factors, unidentified at present, contribute to the apparent "overdesigned" performance.

5.1.2 <u>The Analysis of Flexural Behavior</u> -- As a result of the present study the following conclusions are drawn about the analytical procedure to analyze reinforced concrete beams in flexure.

1. The stress-strain curves for reinforced and confined concrete are studied in Section 2.3. As a result of the discussion in that section a modified model is proposed in Section 2.5. The new model developed in the present study is characterized as follows.

   a. The stress-strain curve of reinforced and confined concrete applies only to that portion of the cross section which is in compression.

b. Because the neutral axis shifts during the loading process and causes the compressive zone of the member to change its geometry, the shape of the stress-strain curve changes accordingly.

Therefore, a family of stress-strain curves describe the stress-strain relationship in a flexural member, as illustrated in Fig. 2.6.

2. The numerical procedure to evaluate the flexural behavior of beams is presented in Section 2.6, and applied successfully in Chapter 3. The numerical results indicate that the numerical method and the proposed stress-strain relationships for reinforced concrete and steel can approximate the behavior of beams with or without the presence of axial loads.

3. The assumptions about the behavior of the concrete cover, as presented in Sections 2.5.1 and 3.2.2, increase the accuracy of the numerical results. This study concentrates on the effects of monotonic high intensity loads on reinforced concrete beams. This load system closely simulates the loading conditions generated by the detonation of nuclear weapons in the megaton range of yields. Under these loading conditions the effect of reversal loading and rebound can be disregarded without affecting the design procedure. Therefore, the behavior of the concrete cover, as presented in this study indicates that parts of the concrete cover do sustain compressive stresses even though the concrete strain is larger than $0.004 \frac{in}{in}$.

4. The application of the method developed in this study to analyze
   deep reinforced concrete beams is presented in Section 3.5. The
   analytical results indicate that the procedure is less effective
   in this case. Nevertheless, the degree of accuracy of the pro-
   posed method is virtually equal to the accuracy obtained by other
   recommended procedures, as discussed in Sections 3.5 and 3.6.
   The major problem that affects the analysis of deep beams is
   the different type of strain distribution across the depth of
   these beams. Experimental results indicate that the strain
   distribution in deep beams is not linear. However, the lack
   of accurate experimental data on the strain distribu-
   tion introduces impractical strain values into the analysis,
   and as a result the analytical procedure becomes less rational.
   The relatively high accuracy, despite the impractical strain
   values, indicates that better results can be expected when ac-
   curate experimental data is used.

5.1.3 The Influence of Shear and Shear Reinforcement -- The influence
of shear on the behavior of slender beams is presented in Section 2.7, and
the influence of shear on the behavior of deep beams is presented in Section
2.11. A procedure is developed in this study to account for the influence
of shear on the ultimate moment capacity, and the contribution from shear
reinforcement. The procedure is presented in Section 2.8 for slender beams,
and in Section 2.12 for deep beams. The procedure is applied to the analysis
of slender and deep beams in Chapter 3. As a result of the present study,
the following conclusions are drawn:

1. The proposed method to account for the influence of shear on the behavior of flexural members improves significantly the accuracy of the numerical procedure to analyze beams in flexure. The analytical values for the ultimate moment are within 5 percent of the experimental data.

2. The proposed method can be applied to predict the crack inclination angles, and the results are quite close to the experimental data.

3. It is possible to evaluate the efficiency of shear reinforcement by applying the proposed method to analyze slender or deep beams. Here the shear resistance of the concrete is considered in a different way than recommended by other procedures, and the results are considerably improved. The evaluation of the efficiency of shear reinforcement makes it possible to calculate the optimum amount of shear reinforcement to ensure a desired performance of the members under consideration.

4. In slender beams an increase in the amount of provided shear reinforcement results generally in an improved moment capacity. Deep beams however, show a decrease in moment capacity when the amount of shear reinforcement is increased beyond an optimum quantity, which implies that deep beams are quite sensitive to excessive amount of shear reinforcement.

5. The procedures to consider the effects of shear reinforcement on the behavior and performance of beams as presented in this study are based on a limited amount of experimental data. These procedures should be further studied and modified before they become reliable design methods.

5.1.4 <u>General</u> — The combined numerical procedure that considers both
flexure and shear, as presented and evaluated in this study, improves the
results obtained from the analysis of beams. The improvement of the results
confirms the assumptions about the stress-strain relationships for reinforced
concrete and steel, and the influence of shear reinforcement on beam behavior.

It is expected that the proposed procedure will be applicable to the
analysis of reinforced concrete members other than beams. However, it is
possible that some modification of the procedure will be necessary before
it can be employed for such purposes.

The procedure developed and demonstrated in this study is quite simple
to apply. Almost all numerical steps, as discussed in Chapters 2 and 3,
can be performed without a computer and do not require complicated calcula-
tions. Nevertheless, the use of a digital computer for all, or part of the
analysis, is recommended if many similar structural members have to be analyzed.
The flow diagrams of the programs are presented in Appendix C.

5.2 <u>Recommendations for Future Studies</u>

The procedure developed in this study has been applied successfully to
the analysis of reinforced concrete beams. The presence of axial loads and
shear reinforcement does not alter the procedure, nor does it influence the
accuracy of the results. However, several questions concerning basic assump-
tions employed in this study still remain unanswered. Therefore, it is
recommended that the following topics be studied to improve the understanding
of reinforced concrete structures, and develop reliable design methods.

   1. The general procedure to account for the shear influence, and

      the contribution of shear reinforcement to the performance of

reinforced concrete structural members, as developed and pre-
sented in this study, defines three characteristic points, as
illustrated in Fig. 2.23.

point 1 is located in the range $\quad 1.0 \leq \frac{a}{d} \leq 1.5$

point 2 is located in the range $\quad 2.0 \leq \frac{a}{d} \leq 3.0$

point 3 is located in the range $\quad \frac{a}{d} \geq 5.0$

These locations were determined experimentally by other investi-
gators. The following questions have not been answered yet,
and the problems should be investigated in the future.

a. What determines the locations of the characteristic points?
    It is clear that an error in defining the locations of
    these points may result in significant differences between
    experimental and analytical results.

b. In the analysis of deep beams, what is the influence of
    shear reinforcement if the corresponding crack angles
    are smaller than 45 degrees?

c. When both slender and deep beams are concerned, the
    influence of the shear reinforcement on the moment
    capacity when the applied loads are smaller than the
    ultimate load is unclear. Further studies are neces-
    sary to provide the answers for this problem.

2. The strain distribution across the depth of deep beams is impor-
    tant for the analytical procedure developed in the present study.
    Therefore, better experimental data is necessary in order to
    improve the approximate strain values used in the analysis.

3. The general procedure developed in this study may improve the results obtained from finite element programs. The stress-strain relationships for reinforced concrete, as presented herein, provide a better way to account for the influence of the internal geometry of reinforced concrete members on the state of stress and the performance under various loading conditions. A flow diagram of a combined procedure is presented in Fig. C3 of Appendix C.

4. Many structures are subjected to dynamic loading conditions that cannot be simulated by equivalent static force systems. Therefore, the procedure proposed in this study, including the finite element analysis mentioned in item 3, should be modified to high frequency loading conditions. When protective structures are considered these loading conditions may result from the detonation of conventional explosives.

173

APPENDIX A

DYNAMIC BEHAVIOR
AND
DESIGN CONSIDERATIONS

Appendix A: Dynamic Behavior and Static Design

Introduction

Dynamic loading conditions could be a result of various sources, for example: earthquakes, winds, vibrations related to machines and transportation systems, conventional or nuclear explosives.   In this study, only one source of dynamic loads is considered, namely dynamic loads from nuclear detonations.   Unfortunately, the information of which this study is based is limited to unclassified material only.   Furthermore, some results that have been studied were obtained by simulating nuclear detonations in a laboratory, and therefore some inaccuracy could be involved.

The experimental and theoretical research in the effects of nuclear detonations on structures is quite extensive.   Nevertheless, some related problems have not been solved yet, while other problems have only empirical solutions.

One of the questions that has to be answered, before designing a structure to resist dynamic loads, is if the structure has to be analyzed, dynamically, or if static design procedures could satisfy the requirements.   The results from previous studies by other investigators, as reported in the literature, show that in certain cases, a static analysis will give the required results.   Some of the studies concerning this problem are discussed in the following section.

Results of Previous Studies

Newmark [56] presented a design approach, based upon simplified assumptions, concerning nuclear blast and structural behavior.   The dynamic behavior was transformed into a statically equivalent behavior, thus simplifying the

design procedure. The statically equivalent loads depended on the natural

period of vibration of the structural elements, the permissible deflections,

and the duration of the applied load.

Merritt and Newmark [57] studied the effect of a nuclear blast on under-

ground structures, and recommended a design procedure for such structures.

A static design for the peak values of the expected loads is the first step

in the procedure. Based on the preliminary design one could proportion the

structural members. The next step was to estimate the natural period of each

member, and to compare these values to the rise time of the applied load.

If the ratio of the rise time to the natural period was greater than 2, the

structural member need   not to be redesigned. However, if the ratio was

smaller than 2, a dynamic design method was required. The dynamic analysis can be

performed by applying a triangular pulse to simulate the load, to a single

degree of freedom (SDF) system simulating the structure. From the dynamic

analysis the resistance of the members was evaluated, and compared to the

resistance of the proportioned members, from the preliminary design. The

procedure is iterative, until the analytical values and the values for the

proportioned members are reasonably close. It also was recommended to elimi-

nate structural components that have a brittle influence by limiting the percentage

of the main reinforcement (ρ) to between 0.25% to 1.5%, and the percentage of

web reinforcement (ρ_w) to not less than 0.5%. The use of high strength

steel was not recommended. It also was recommended to assume a 25% increase

in steel strength under blast loading, but no increase in concrete strength

because of the relatively large range of concrete quality. For flexural

members where flexure dominates the behavior, it was recommended to neglect

the influence of axial loads and to provide a minimum of 0.25ρ for compressive reinforcement. For members where axial loads have a relatively large influence, the amount of compressive reinforcement should equal the amount of tensile reinforcement.

Newmark et al. [58] studied the various aspects of protective structure design. That report was written as a handbook for design of protective structures. The loads for which the structure was designed had been evaluated from the amount of protection that was required. The transformation of the dynamic loading conditions to equivalent static conditions was performed by a method similar to the one in Ref. [57]. In general, when the duration of the positive overpressure phase was long compared to the natural period of vibration of the structural elements, a static design was justified. Only small errors were expected for weapons in the 1 MT range, and for smaller weapons the design was expected to be conservative. As for the material properties under dynamic loading conditions, an increase of about 25% was recommended for both the yield strength of steel and compressive strength of concrete.

Keenan [59] investigated the behavior of reinforced concrete beams under blast loading. His findings supported the recommendations in the previous studies. The ratio of the duration of the load (T_e) to the natural period (T_n) effected the ultimate deflection of the beam, and the degree of damage. This ratio also affected the amount of rebound that was observed. Large $\frac{T_e}{T_n}$ ratios, and high damping, decreased the amount of rebound. An important result was that a beam could absorb approximately the same amount of energy regardless of how many times it had been loaded, as long as the loading

conditions had not been close to causing a complete collapse. Damping was found to be between 10% to 28% for reinforced concrete beams, and only 11% for pre-stressed beams.

Newmark [60] discussed the problems related to the design of protective structures. It was recommended to increase the yield strength of structural carbon steel (A-7) by about 30%, but only by 10% for high strength steel. It was also recommended to increase the compressive strength of concrete by about 25%. The theoretical background was based on previous studies (that have been discussed in this section).

Fuss [61] confirmed the recommendations for higher compressive strength of concrete under dynamic loads. He found an average increase of 26%. Similar results were reported by Cowell [62].

Seabold [63], and Fuss [65] found that the increase in the shear strength of concrete was considerably smaller than the compressive strength.

Iten [48], and Gamble et al. [49] found that deep slabs under dynamic loading conditions behaved as if under static loads when the duration of the impulse was longer than the natural period of the slab.

Furlong et al. [65] investigated the shear strength of reinforced concrete beams, and the bond between the reinforcing bars and the concrete under impact loads. When the mode of failure was flexure the beams showed an increase of 27% to 30% in their strength. However, when shear governed the behavior the increase in strength was in the range of 5% to 86% (37% on the average). Furthermore, they found no indication that the bond between the steel bars and the concrete was influenced by the nature of the loading.

Keenan [66] found that an increase of about 40% in the strength of slabs under dynamic loads.

Seabold [67] found that the strength of reinforced concrete beams increased under dynamic loading conditions. This increase could be explained by an average increase in material strength of 20% for concrete, and 30% for steel. It also was found that low strength materials showed a larger increase than high strength materials.

Criswell [47] found an increase of 18% in the strength of reinforced concrete specimens failing in flexure, and an increase of 26% in strength when failure was governed by shear. These increases were contributed to an increase in material strength under dynamic loads.

Brown and Black [68] found that slabs tested under dynamic conditions were 23.7% to 24.6% stronger than slabs tested under static conditions. The deflections measured under dynamic conditions were larger, and the cracking patterns of these slabs had a better similarity to the cracking patterns based upon the yield line theory.

Watt [69] investigated the behavior of slabs with a span to thickness ratio of 4.12, under dynamic loading conditions. He found an increase of about 35%, compared to slabs tested under static conditions.

Keenan [70] studied the behavior of one-way slabs under static and dynamic conditions. He found that the behavior was determined by the dynamic properties of the load, and the members. Furthermore, the increase in strength due to the dynamic conditions, determined the mode of failure.

The result of these studies clearly show that under dynamic loading conditions an increase in material properties is noticed. This increase is in the range of 20% to 30%. Another important finding is that for loads of long durations compared to the neutral period of the structural members,

a dynamic design procedure is usually not required. However, the dynamic material properties should be considered in the design. In the cases where a dynamic analysis is required, a single degree of freedom (SDF) model of the structural member will give reasonably good results. The values of mass, stiffness, and damping are obtained by empirical formulation.

Design Procedures

The design procedures of protective structures are based on results that have been obtained by extensive research. A representing part of these results have been discussed in the previous section. The basic approach is very similar to the procedures that were described by Newmark [56,60], Newmark et al. [57,58]. In general, there are two principal stages in the design. In the first stage certain assumptions must be made concerning the following parameters: required probability of survival of the structure and its content, required ductility, type of structure, expected loading conditions, etc. These assumptions and the information from design manuals [54,55,71,72], result in an "equivalent static condition", for which a preliminary design is made. From the dimensions of the structure, and the structural elements, an approximate value of the natural periods (T_n), is obtained, as described in Refs. [54,57,58,60]. The natural period is then compared to the duration of the positive phase of the load function (T_e). It is recommended, in Ref. [54], that if the ratio $\frac{T_e}{T_n} > 3$, no dynamic analysis is required, and the preliminary design is used for the structures. However, if the ratio $\frac{T_e}{T_n} \leq 3$, a dynamic analysis of the structure is recommended.

The dynamic analysis of structural members is usually performed by applying the load function to a SDF system. In many cases, the shape of the

load function (which is the variation of the pressure, as a function of time, at the location of the structure due to the passing of the shock wave) is simplified to a triangle. However, in some cases it is recommended to use a bi-linear behavior for the part of the function that describes the decline in pressure. The actual load function shape, as described in Refs. [55,56], is used only for exact solutions, and theoretical studies. The use of multi-degree of freedom systems (MDF), is recommended only if it will better repre-sent the behavior of the structure under consideration. The resistances of the structural members are calculated by the dynamic analysis, and used to modify the proportioning of these members. The procedure is repeated until convergence of the results is obtained.

Detailing of protective structures are discussed in Swiss Codes [71,72]. When the information from Refs. [54,55,71,72] is applied to the design the results will be compatible with current understanding of nuclear weapons effects.

APPENDIX B

EXPERIMENTAL RESULTS AND DATA

B.1 Properties and Experimental Data for Slender Beams Without Axial Loads

The beams that are analyzed in this study are illustrated in Fig. B1. The dimensions of the cross sections are described by Fig. B2. The material properties, and the type of reinforcement are presented in Table B1. The experimental results that describe the properties of the longitudinal reinforcement are presented in Table B2.

B.2 Shear Reinforcement and the Angles of Cracks - Slender Beams

The relationship between the amount of shear reinforcement and the angle of cracks α, has been developed based upon the experimental results of Burns and Siess [12]. The angles of cracks were measured on pictures of four beams, that have been taken during the experiments. Because no more data was available, the equations that result from this empirical study should be reevaluated when more data is available.

The parameters employed for the analysis are defined in Section 2.8, and their numerical values are presented in the following tabulation.

beam	b [in]	d [in]	$\frac{a}{d}$	s [in]	A_v [in^2]	f'_c [psi]	f''_y [psi]	$\rho^*_2 * \frac{a}{d}$	$\rho^*_2 * \frac{a}{d}$	α [deg]	tan α
J-13	8.0	14.0	5.14	6.0	0.22	4800.0	50000.0	0.2454	17.0	45.0	1.0
J-20	8.0	14.0	5.14	6.0	0.1	4380.0	50000.0	0.1222	8.088	71.9	3.059
J-6	8.0	18.0	4.0	6.0	0.22	5160.0	50000.0	0.1776	12.76	61.8	1.865
J-22	8.0	18.0	4.0	6.0	0.1	4420.0	50000.0	0.9424	6.266	84.5	10.385

These results have been plotted in the following figures:

1. $\rho^*_1 * \frac{a}{d}$ vs. α (Fig. B3)

2. $\rho^*_2 * \frac{a}{d}$ vs. α (Fig. B4)

3. $\rho_1^* * \frac{a}{d}$ vs. $\tan \alpha$ (Fig. B5)

4. $\rho_2^* * \frac{a}{d}$ vs. $\tan \alpha$ (Fig. B6)

The linear relationships, corresponding to the first two cases, are the following:

1. $\alpha = -261.3 * (\rho_1^* * \frac{a}{d}) + 109.1$

2. $\alpha = -3.68 * (\rho_2^* * \frac{a}{d}) + 107.46$

B.3   Shear Reinforcement and the Angles of Cracks - Deep Beams

The beams that had been tested by Crist [36,39], have been used to develop the relationship between the crack angle α, and the beam parameters. The variables ρ_1^*, and ρ_2^* have been defined in Section 2.8. The numerical values of the parameters are presented in Table B3. Various possible relationships have been considered, and finally the following two equations are proposed to describe the linear relationships.

from Fig. B7:

    $\log \alpha = 0.039396 * \log(\rho_1^* * \frac{a}{d}) + 1.97558$

from Fig. B8:

    $\log \alpha = 0.042 * \log(\rho_2^* * \frac{a}{d}) + 1.903$

B.4   Properties of Beams With Axial Loads

The properties of the beams that were tested by Yamashiro and Siess [38] are presented as follows.

The dimensions of the beams and material properties are presented in Table B4.

The beams geometry is illustrated in Fig. B9.

The properties of the stress-strain curve for reinforcing bars are presented in Table B5.

B.5 Properties of Deep Beams from Refs. [36,39]

The deep beams analyzed in this study are described in Refs. [36,39]. The geometry of the specimens is illustrated in Figs. B10, B11, B12. The numerical values of beam properties are presented in Tables B6, B7, B9. Experimental results are presented in Tables B8, B9.

P/2

6"

12", 16", or 20"   d = 10", 14", or 18"

P/2

6"

12"

P/2   P/2

6"   12'-0" Span   6"
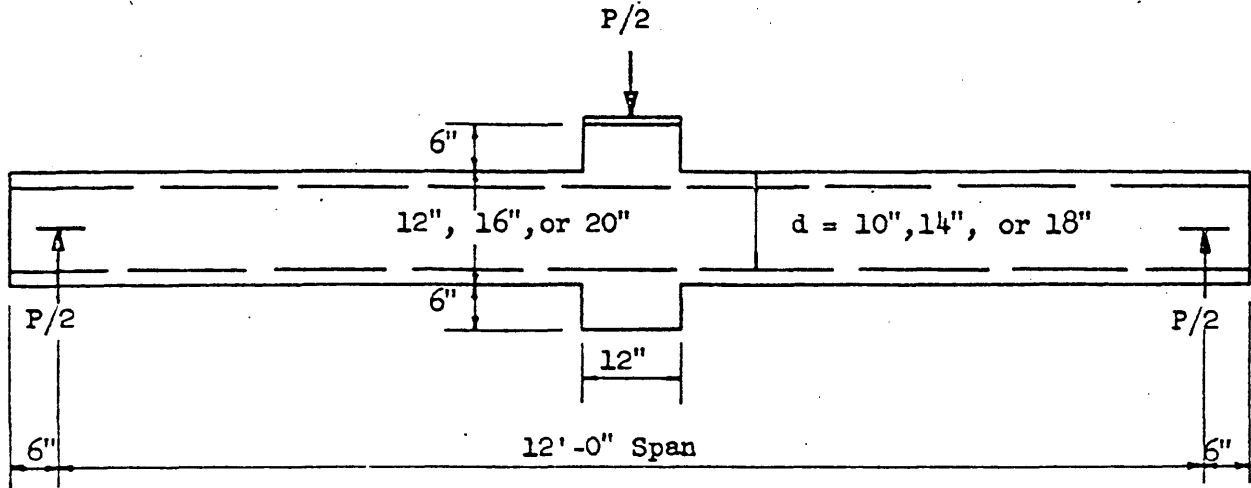
FIG. B1 Test specimen used in Ref. [12].

8"   8"

1-1/2"   5"   1-1/2"   1-1/2"   5"   1-1/2"

2"

1-1/2"   D'/2

d   d

D/2   D/2

2"   2"

(a) Beams Without   (b) Beams With
    Compression Steel   Compression Steel

6"   8"

1"   4"   1"   1-1/2"   2" 1" 2"   1-1/2"

2"   1-1/2"

3-1/2"

d   d

D/2   D/2

2"   2"

(c) Beams With b = 6 in.

(d) Beams With U-Stirrups
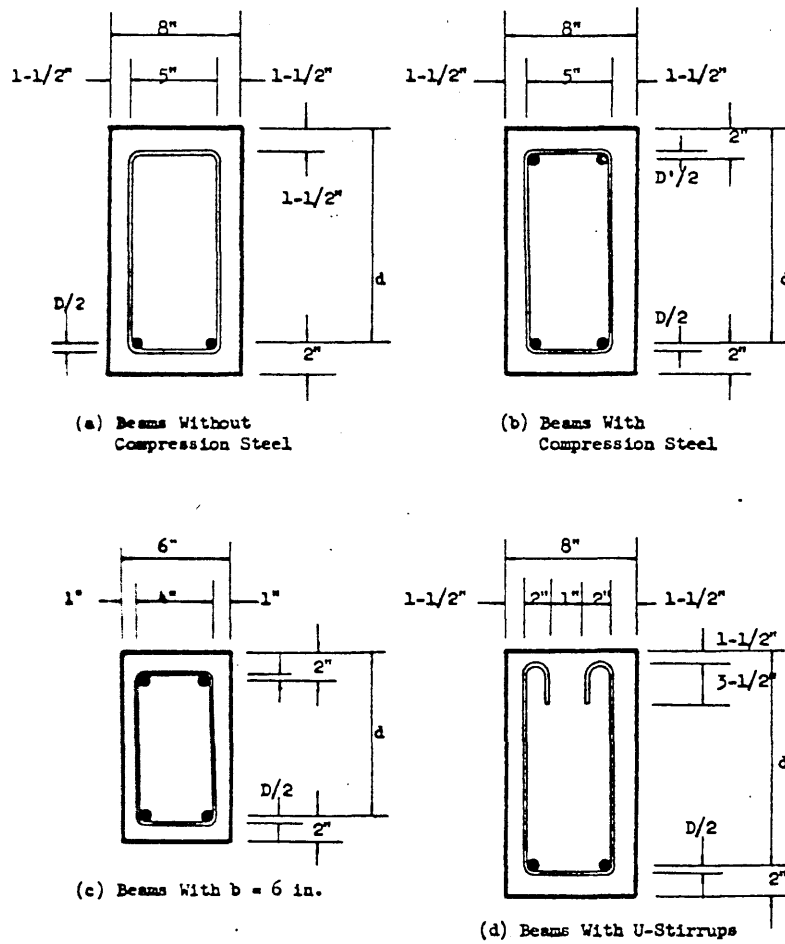
Note: All closed stirrups welded at the top with
       approximately 1-1/2 in. lap of bar.

FIG. B2 Details of stirrups used in beams of the current
         test program. Source Ref. [12]

TABLE B1

PROPERTIES OF BEAMS FROM THE CURRENT TEST PROGRAM.

Source Ref. [12]

(b = 8 in. for all beams except as noted)

Beam Number	Cylinder Strength f'_c (psi)	Reinforcement Quantity and Size		Yield Point of Reinforcement (ksi)		d in.	d' in.	Stirrup Size and Spacing
		Tens.	Comp.	Tens.	Comp.			
J-1	4930	2-#8	--	47.6	--	10.0	2.0	#3 at 6 in.
J-11	4110	2-#8	--	46.9	--	10.0	2.0	#3 at 6 in.
J-2	4080	2-#8	2-#6	48.0	48.6	10.0	2.0	#3 at 6 in.
J-3	4900	2-#8	2-#8	48.3	48.0	10.0	2.0	#3 at 6 in.
J-8	4680	2-#8	2-#8	45.4	45.5	10.0	2.0	#3 at 6 in.
J-17	3900	2-#8	2-#8	46.9	46.8	10.0	2.0	#3 at 6 in.
J-18*	4410	2-#8	2-#8	45.4	47.1	10.0	2.0	#3 at 6 in.
J-24*	5000	2-#4	2-#4	48.5	47.8	10.0	2.0	#3 at 6 in.
J-10	3590	2-#8	--	45.1	--	14.0	2.0	#3 at 6 in.
J-14	4500	2-#8	2-#6	47.1	50.0	14.0	2.0	#3 at 6 in.
J-13	4800	2-#8	2-#8	45.6	46.0	14.0	2.0	#3 at 6 in.
J-19	3900	2-#8	--	45.8	--	14.0	2.0	#2U at 6 in.
J-20	4380	2-#8	2-#8	45.8	46.5	14.0	2.0	#2 at 6 in.
J-4	4820	2-#8	--	44.9	--	18.0	2.0	#3 at 6 in.
J-9	4190	2-#8	--	47.0	--	18.0	2.0	#3 at 6 in.
J-5	5000	2-#8	2-#6	45.1	48.9	18.0	2.0	#3 at 6 in.
J-12	4550	2-#8	2-#6	45.1	49.7	18.0	2.0	#3 at 6 in.
J-6	5160	2-#8	2-#8	46.2	46.4	18.0	2.0	#3 at 6 in.
J-7	4450	2-#8	2-#8	46.5	46.3	18.0	2.0	#3 at 6 in.
J-21	4350	2-#8	--	47.6	--	18.0	2.0	#2U at 6 in.
J-22	4420	2-#8	2-#8	46.2	46.4	18.0	2.0	#2 at 6 in.

*b = 6 in.

TABLE B2

PROPERTIES OF REINFORCING BARS

SOURCE REF. [12]

(#8 Bars Except as Noted)

Beam No.	Tension Reinforcement						
	f_y ksi	ϵ_{sy} %	ϵ_{sh} %	f_{ult} ksi	ϵ_{ult} %	f_{fract} %	$\epsilon_{fract.}$ %
J-1	47.6	0.172	0.77	87.6	12.5	84.1	--
J-2	48.0	0.181	0.96	87.3	--	84.5	--
J-3	48.3	0.170	0.75	88.5	12.5	87.1	--
J-4	44.9	0.152	1.86	71.0	15.0	64.5	20.0
J-5	45.1	0.195	1.77	73.7	16.3	69.2	19.5
J-6	46.2	0.178	1.84	73.6	15.0	68.5	18.7
J-7	46.5	0.182	1.71	74.0	15.0	68.6	18.1
J-8	45.4	0.178	1.92	72.1	16.3	67.0	18.8
J-9	47.0	0.175	1.66	74.0	15.0	69.3	19.5
J-10	45.1	0.195	1.79	73.0	15.0	68.0	18.5
J-11	46.9	0.188	1.57	75.4	15.0	70.5	18.8
J-12	45.1	0.174	1.86	71.8	15.0	66.7	18.8
J-13	45.6	0.188	1.61	73.3	15.0	69.2	18.8
J-14	47.1	0.183	1.75	74.0	15.0	69.2	17.5
J-17	46.9	0.188	1.69	73.6	15.0	70.5	18.8
J-18	45.4	0.191	1.58	73.2	15.0	69.2	17.5
J-19	45.8	0.178	1.85	72.0	16.3	65.4	18.8
J-20	45.8	0.185	1.76	71.8	16.3	65.4	18.3
J-21	47.6	0.186	1.80	72.1	15.0	66.7	18.8
J-22	46.2	0.181	1.68	73.4	15.0	69.2	17.5
J-24[*]	48.5	0.180	1.90	77.8	16.0	68.1	24.1

* #4 bars.

TABLE B2 (Continued)

PROPERTIES OF REINFORCING BARS

SOURCE REF. [12]

(#8 Bars Except as Noted)

Beam No.	Tension Reinforcement						
	f_y ksi	ϵ_{sy} %	ϵ_{sh} %	f_{ult} ksi	ϵ_{ult} %	f_{fract} %	ϵ_{fract} %
J-2*	48.6	0.180	1.33	78.6	13.8	67.5	17.8
J-3	48.0	0.165	0.73	89.5	12.5	86.0	--
J-5*	48.9	0.170	1.22	82.6	12.5	78.4	13.8
J-6	46.4	0.192	1.73	75.0	15.0	69.3	19.5
J-7	46.3	0.186	1.57	75.1	13.8	70.5	18.0
J-8	45.5	0.162	1.73	72.3	15.0	66.6	18.8
J-12*	49.7	0.180	1.45	82.3	12.5	79.4	14.0
J-13	46.0	0.173	1.98	71.8	15.0	66.7	18.8
J-14*	50.0	0.170	1.22	81.2	12.5	74.4	--
J-17	46.8	0.188	1.55	74.9	15.0	70.5	18.8
J-18	47.1	0.191	1.68	74.7	15.0	70.5	17.5
J-20	46.5	0.180	1.74	73.7	15.0	69.2	18.8
J-22	46.4	0.161	1.83	72.3	15.0	66.6	17.5
J-24**	47.8	0.180	1.55	76.9	16.0	65.2	22.8

* #6 bars.
** #4 bars.
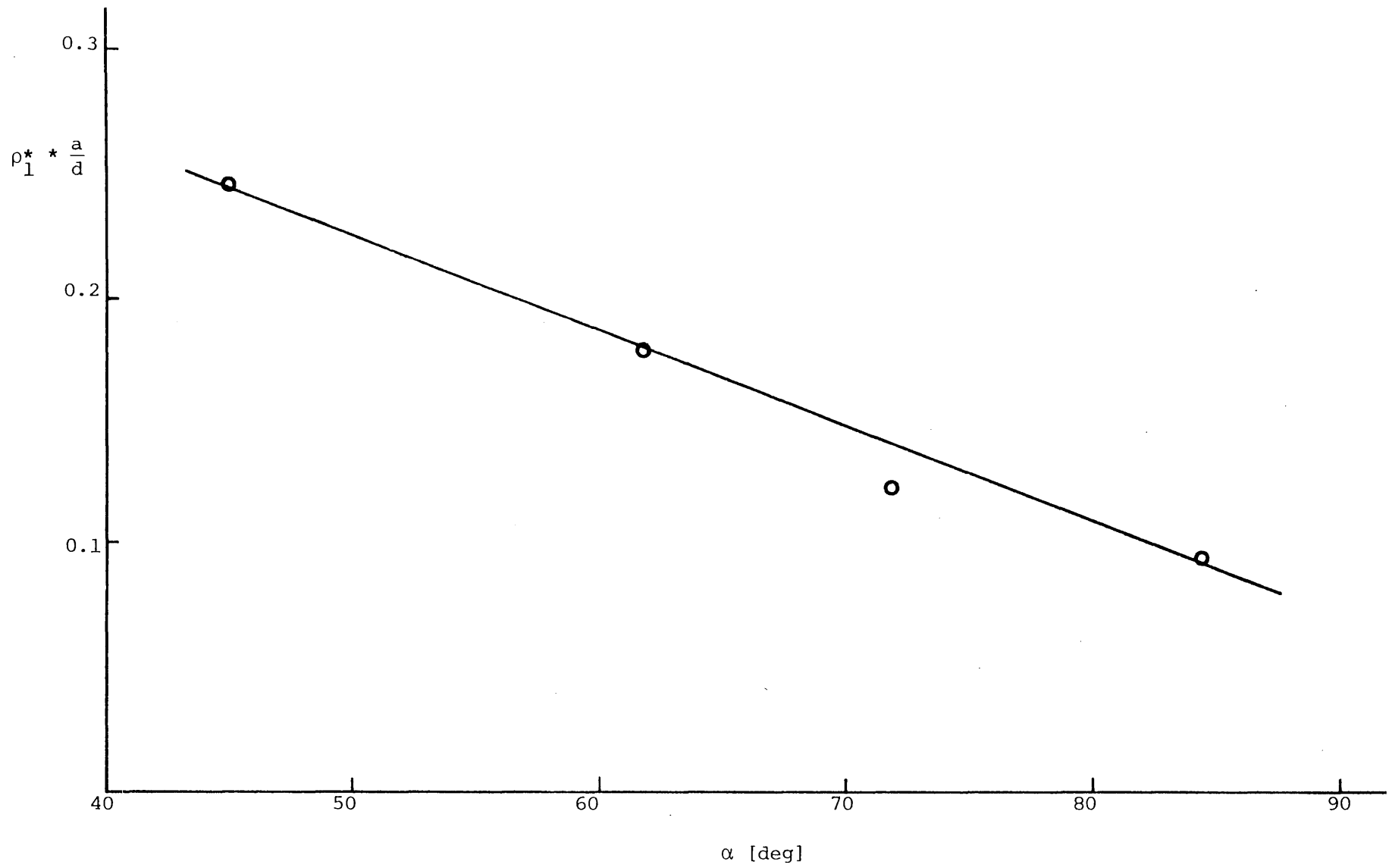
FIG. B3 Shear reinforcement and crack angle.
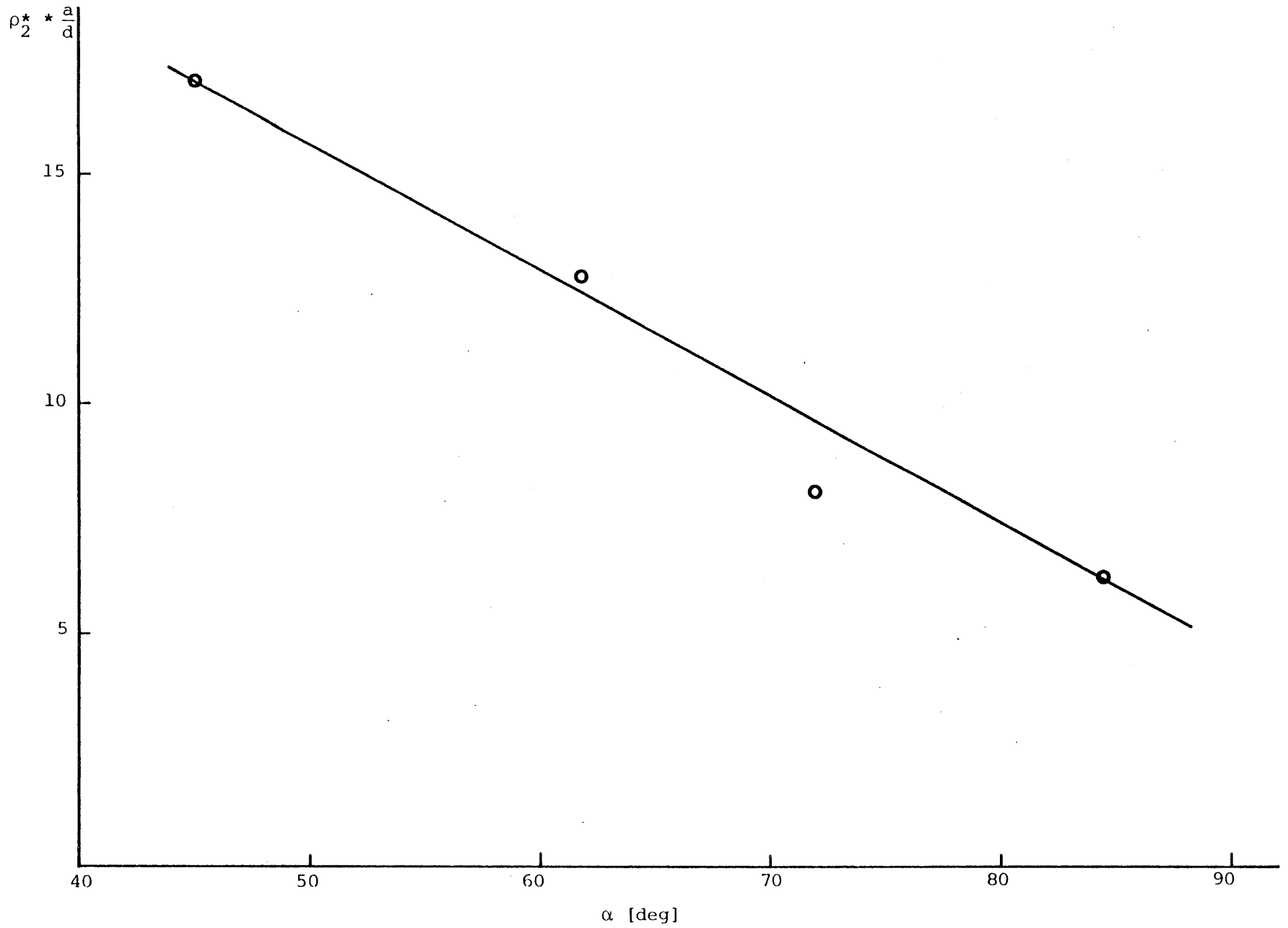
FIG. B4   Shear reinforcement and crack angle.
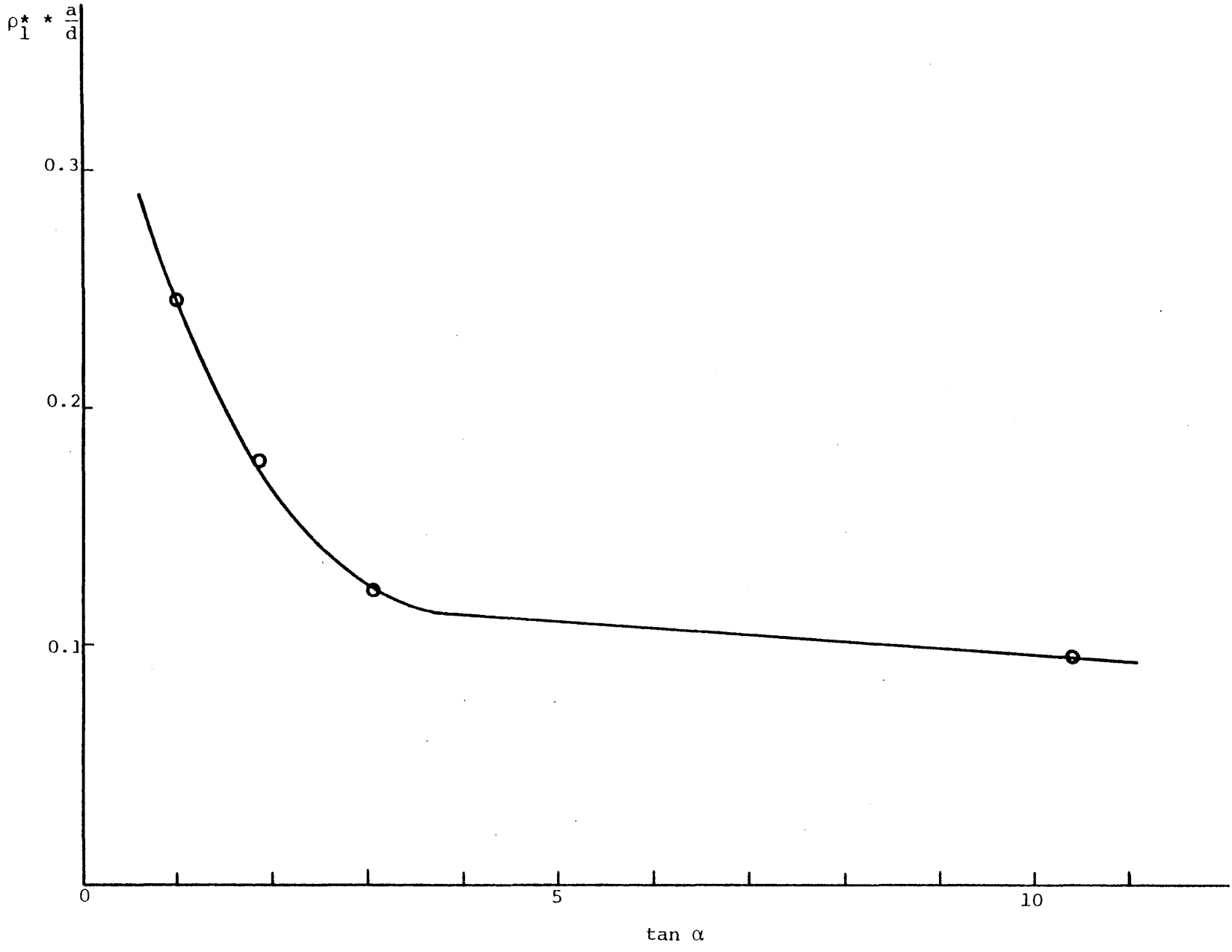
FIG. B5 Shear reinforcement and crack angle.
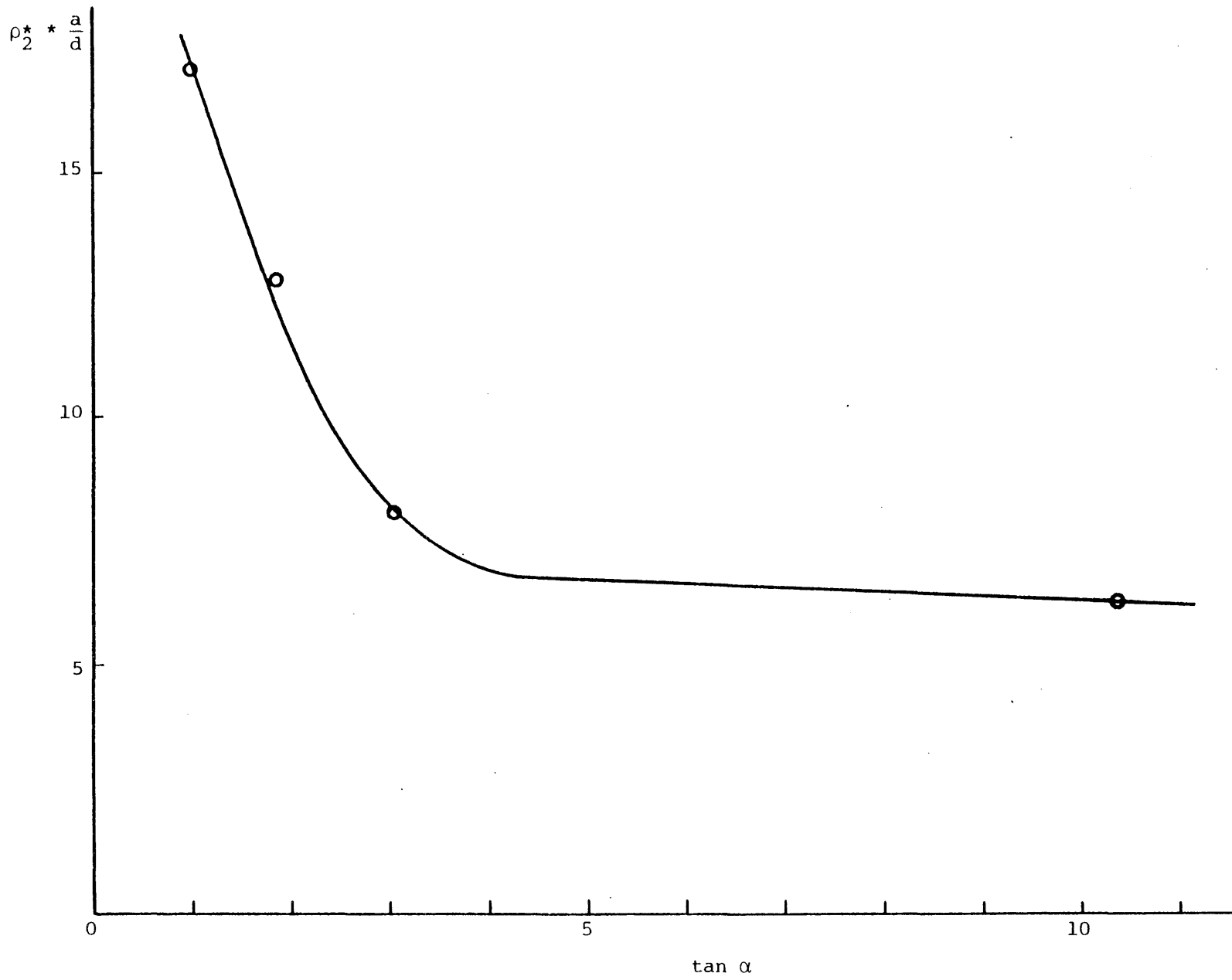
FIG. B6   Shear reinforcement and crack angle.

Table B3: Influence of deep beam properties on crack inclinations

Beam No.	a/d,L/d	b [in]	d [in]	A_s [in²]	ρ	A_v [in²]	s [in]	f'_c [psi]	f''_y [psi]	ρ^*_1	ρ^*_2	α [deg]	ρ^*_1(a/d)	ρ^*_2(a/d)
S1	1.66	8.0	58.0	3.12	0.006724	/	/	3339	/	/	/	50.0	/	/
	"	"	"	"	"	/	/	3341	/	/	/	"	/	/
S2	1.66	8.0	58.0	3.12	0.006724	/	/	3260	/	/	/	60.0	/	/
	"	"	"	"	"	/	/	3097	/	/	/	"	/	/
S3	1.66	8.0	58.0	3.12	0.006724	0.22	24.0	3468	51846	0.01713	1.00878	62.0	0.02844	1.6746
	"	"	"	"	"	"	"	3392	"	0.01751	1.020	"	0.02907	1.6932
S4	1.66	8.0	58.0	3.12	0.006724	0.22	8.0	3647	51846	0.04887	2.9511	59.0	0.08112	4.8989
	"	"	"	"	"	"	"	3607	"	0.04941	2.9675	"	0.08202	4.9260
S5	1.66	8.0	58.0	3.12	0.006724	0.22	8.0	2287	51846	0.07793	3.7267	84.0	0.12935	6.1863
	"	"	"	"	"	"	"	2637	"	0.06758	3.4706	"	0.1122	5.7612
S6	2.67	8.0	36.0	3.81	0.0133	/	/	4129	/	/	/	63.0	/	/
	"	"	"	"	"	/	/	4018	/	/	/	"	/	/
S7	2.67	8.0	36.0	3.81	0.0133	/	/	3449	/	/	/	53.0	/	/
	"	"	"	"	"	/	/	3263	/	/	/	"	/	/
S8	2.67	8.0	36.0	3.81	0.0133	0.22	9.0	3796	51545	0.0415	2.5563	84.0	0.11078	6.8253
	"	"	"	"	"	"	18.0	"	"	0.0209	1.2781	"	0.0558	3.413
	"	"	"	"	"	"	18.0	3605	"	0.02184	1.3116	"	0.0583	3.502
	"	"	"	"	"	"	9.0	"	"	0.0437	2.6231	"	0.1166	7.004
S9	2.67	8.0	36.0	3.81	0.0133	0.22	9.0	3521	51545	0.0447	2.654	84.0	0.1194	7.087
	"	"	"	"	"	"	"	3388	"	0.0465	2.706	"	0.124	7.224
S10	2.67	8.0	36.0	3.81	0.0133	0.22	9.0	3940	51600	0.040	2.512	70.0	0.1068	6.707
	"	"	"	"	"	"	"	3874	"	0.0407	2.533	"	0.1087	6.763
2S1.6-1	1.6	8.0	58.0	2.37	0.00511	0.22	13.0	4160	54000	0.0274	1.771	80.0	0.0439	2.834
	"	"	"	"	"	"	20.0	"	"	0.0178	1.151	"	0.0286	1.842
	"	"	"	"	"	"	13.0	4021	"	0.0284	1.801	"	0.0454	2.882
	"	"	"	"	"	"	20.0	"	"	0.0185	1.171	"	0.0295	1.873
2S1.6-2A	1.6	8.0	58.0	2.37	0.00511	0.22	18.0	4373	53910	0.0188	1.245	83.0	0.0301	1.993
	"	"	"	"	"	"	36.0	"	"	0.00942	0.6227	"	0.0151	0.996
	"	"	"	"	"	"	18.0	4742	"	0.0174	1.196	"	0.0278	1.914
	"	"	"	"	"	"	36.0	"	"	0.0087	0.0598	"	0.0139	0.957

Beam no.	a/d,L/d	b [in]	d [in]	A_s [in^2]	ρ	A_v [in^2]	s [in]	f'_c [psi]	f''_y [psi]	$\rho^\star_1$	$\rho^\star_2$	α [deg]	$\rho^\star_1$(a/d)	$\rho^\star_2$(a/d)
2S1.6-2B	1.66	8.0	58.0	2.37	0.00511	0.22	18.0	3829	53837	0.0215	1.329	87.0	0.0344	2.127
	"	"	"	"	"	"	36.0	"	"	0.0107	0.665	"	0.172	1.063
	"	"	"	"	"	"	18.0	4069	"	0.0202	1.29	"	0.0323	2.063
	"	"	"	"	"	"	36.0	"	"	0.0101	0.645	"	0.0162	1.031
2S1.6-3	1.6	8.0	58.0	2.37	0.00511	0.1	8.0	5023	53670	0.0167	1.183	80.0	0.0267	1.893
	"	"	"	"	"	"	"	4903	"	0.0171	1.197	"	0.0274	1.916
2S1.6-3C	1.6	8.0	58.0	2.37	0.00511	0.1	8.0	3586	52925	0.0231	1.381	89.0	0.0369	2.21
	"	"	"	"	"	"	"	3801	"	0.0217	1.341	"	0.0348	2.146
2S1.6-5	1.6	8.0	58.0	3.12	0.00672	/	/	3248	/	/	/	62.0	/	/
	"	"	"	"	"	/	/	3697	/	/	/	"	/	/
2S2.6-1	2.7	8.0	35.1	4.34	0.01546	/	/	3840	/	/	/	90.0	/	/
	"	"	"	"	"	/	/	3966	/	/	/	"	/	/
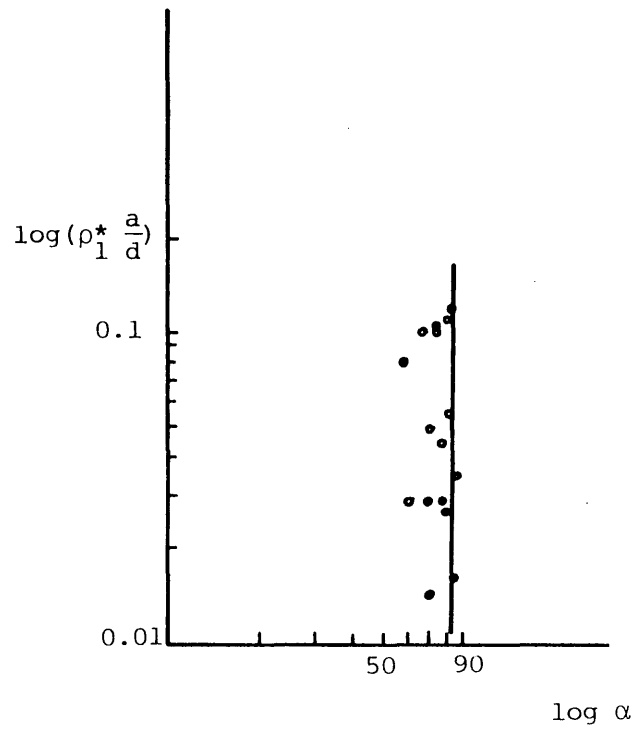
FIG. B7   Shear reinforcement and crack
          angle, deep beams.
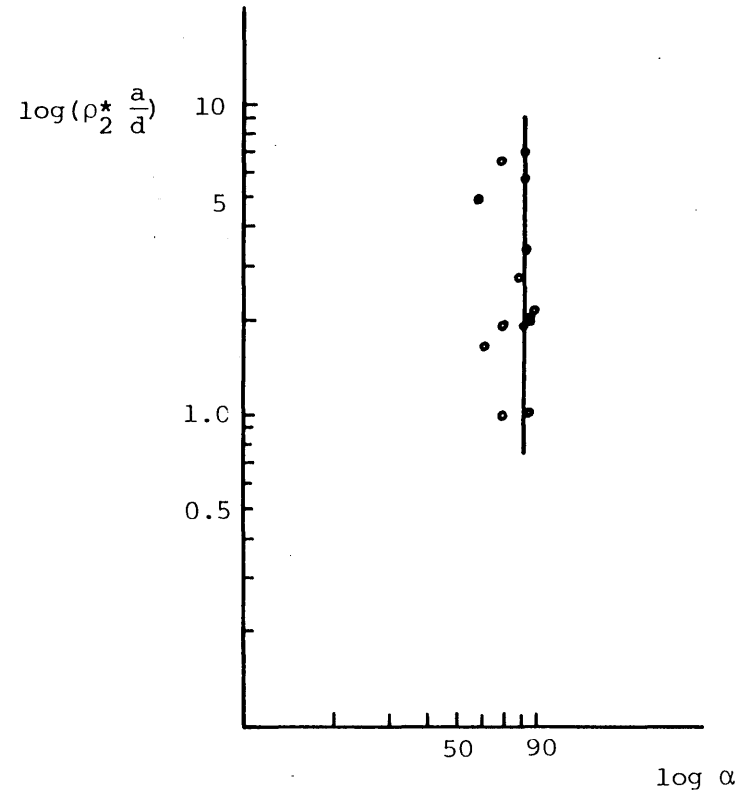
FIG. B8   Shear reinforcement and crack
          angle, deep beams.

TABLE B4

PROPERTIES OF SPECIMENS TESTED IN THIS PROGRAM

SOURCE REF. [38]

Mark	Nom. Axial Load	Cylinder Strength	Reinforcement				
			Amt. and Size	Ratio Tens. and Comp.	Column Ratio	Yield Stress Tens.	Comp.
	P	f'_c	Each	$p = p'$	p_g	f_y	f'_y
	kips	psi	Face	%	%	ksi	ksi
J-24	0	5060	2-#4	0.67	1.11	48.5	47.8
J-25	25	5050	2-#4	0.67	1.11	49.2	49.2
J-26	50	4600	2-#4	0.67	1.11	49.9	49.0
J-27	75	4920	2-#4	0.67	1.11	50.0	50.1
J-34*	75	4520	2-#4	0.67	1.11	48.8	50.3
J-16**	25	4550	2-#8	1.98	3.29	45.9	44.7
J-15**	50	4400	2-#8	1.98	3.29	46.9	47.3
J-28	0	5020	2-#9	3.33	5.55	46.9	46.7
J-29	25	4410	2-#9	3.33	5.55	48.8	48.6
J-30	50	4500	2-#9	3.33	5.55	47.0	47.2
J-31	75	4280	2-#9	3.33	5.55	48.3	47.9

* Tie spacing 3 in.; all others 6 in.; see Fig. 2.2.

** b = 8 in.; all others 6 in.;

#3 ties at 6" throughout

J-15, J-16

(a) Specimens J-15, J-16, J-24 through J-31

#3 ties at 6" except
as shown

J-24 through J-31,
and J-34

(b) Specimen J-34
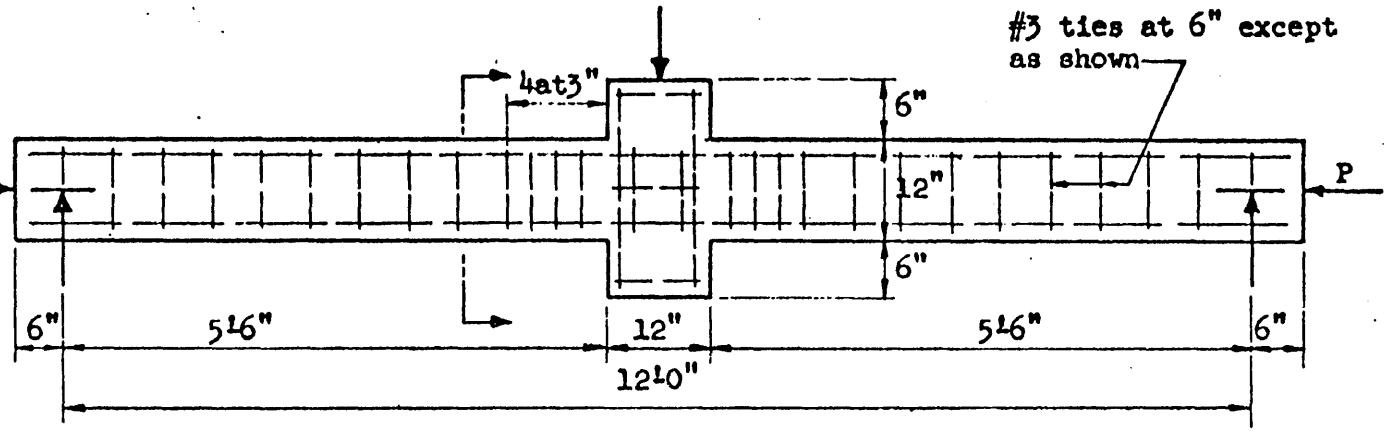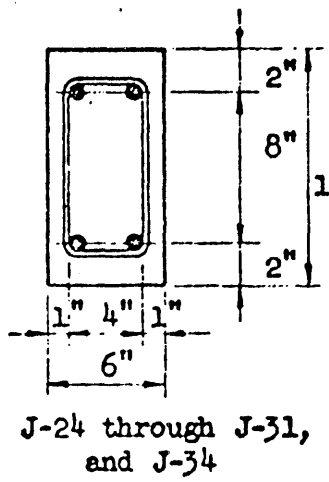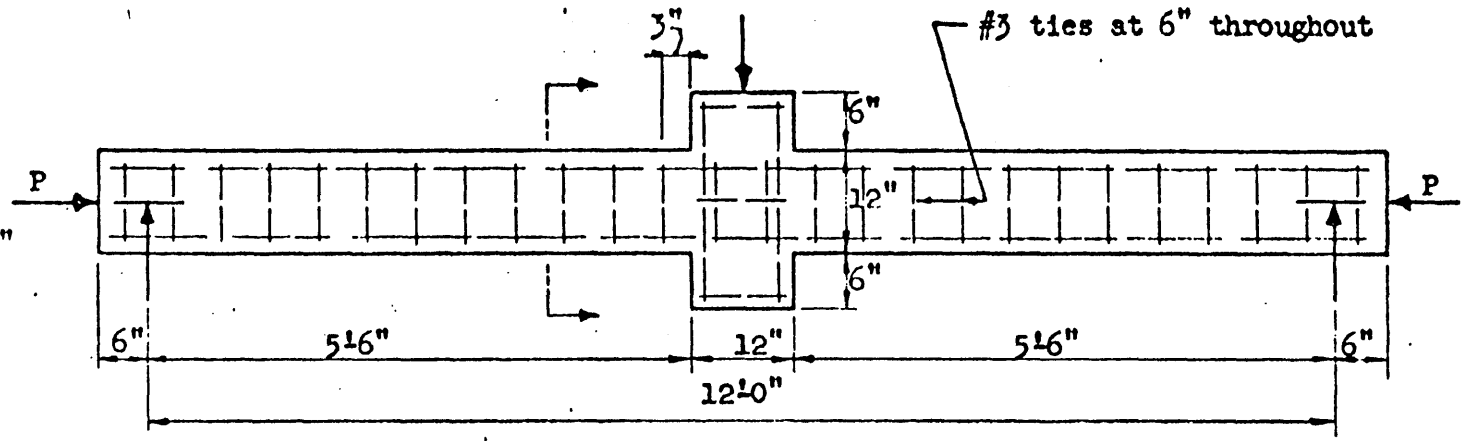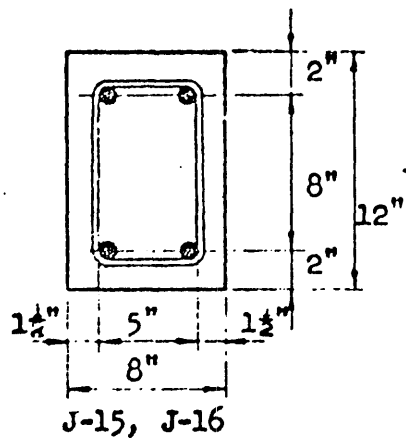
FIG. B9 Test specimens. Source Ref. [38]

TABLE B5

PROPERTIES OF REINFORCING BARS

SOURCE REF. [38]

Mark	Size	Yield Stress f_y ksi	Yield Strain ϵ_y %	Work Hard. Strain ϵ_{sh} %	Ult. Stress f_{su} ksi	Ult. Strain ϵ_{su} %	Rupt. Stress ksi	Rupt. Strain %	Young's Modulus $E_s \times 10^{-3}$ ksi
				Tension Reinforcement					
J-24	#4	48.5	0.180	1.61	77.8	16.0	68.1	24.1	27.0
J-25	#4	49.2	0.175	1.80	78.8	17.0	73.5	19.5	28.1
J-26	#4	49.9	0.175	1.44	81.9	16.0	71.9	17.4	28.5
J-27	#4	50.0	0.175	1.50	80.1	15.5	68.5	19.9	28.6
J-34	#4	48.8	0.175	1.40	81.2	14.0	73.5	17.0	27.9
J-15	#8	46.9	0.170	1.57	75.3	14.5	71.8	17.5	27.6
J-16	#8	45.9	0.150	1.68	72.8	15.0	67.9	18.8	30.6
J-28	#9	46.9	0.160	1.53	77.6	17.0	76.0	19.9	29.3
J-29	#9	48.8	0.180	1.36	80.2	16.0	75.8	24.3	27.1
J-30	#9	47.0	0.150	1.62	77.5	16.0	75.0	17.9	31.3
J-31	#9	48.3	0.145	1.39	78.3	18.0	74.5	24.3	33.3
				Compression Reinforcement					
J-24	#4	47.8	0.175	1.55	76.9	17.5	65.2	22.8	27.4
J-25	#4	49.2	0.175	1.77	78.0	15.5	68.0	22.3	28.1
J-26	#4	49.0	0.170	1.42	80.3	16.0	69.0	20.6	28.8
J-27	#4	50.1	0.175	1.48	81.3	18.0	69.7	21.4	28.6
J-34	#4	50.3	0.175	1.40	81.9	16.0	74.0	20.4	28.7
J-15	#8	47.3	0.160	1.57	75.3	15.0	71.8	18.1	29.6
J-16	#8	44.7	0.150	1.69	71.4	15.0	67.9	18.8	29.8
J-28	#9	46.7	0.170	1.62	77.6	17.5	75.0	23.4	27.5
J-29	#9	48.6	0.160	1.50	80.4	15.6	76.2	25.0	30.4
J-30	#9	47.2	0.145	1.00	80.2	15.8	75.0	24.1	32.5
J-31	#9	47.9	0.160	1.44	80.2	18.7	75.5	24.5	29.9
								Mean	29.1
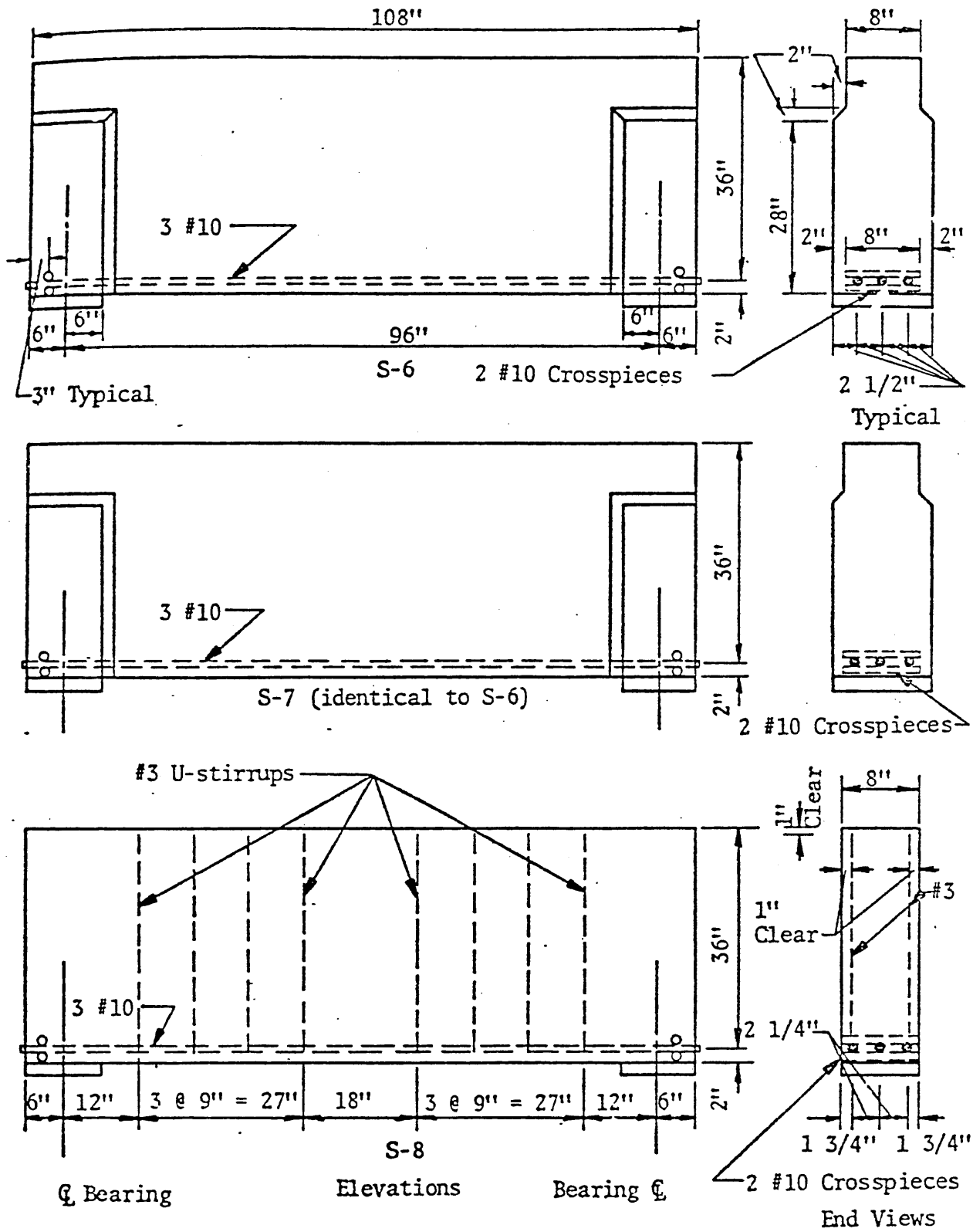
FIG. B10 Geometry of static beams S-6, S-7, and S-8, L/d = 2.67 series.
Source Ref. [39]
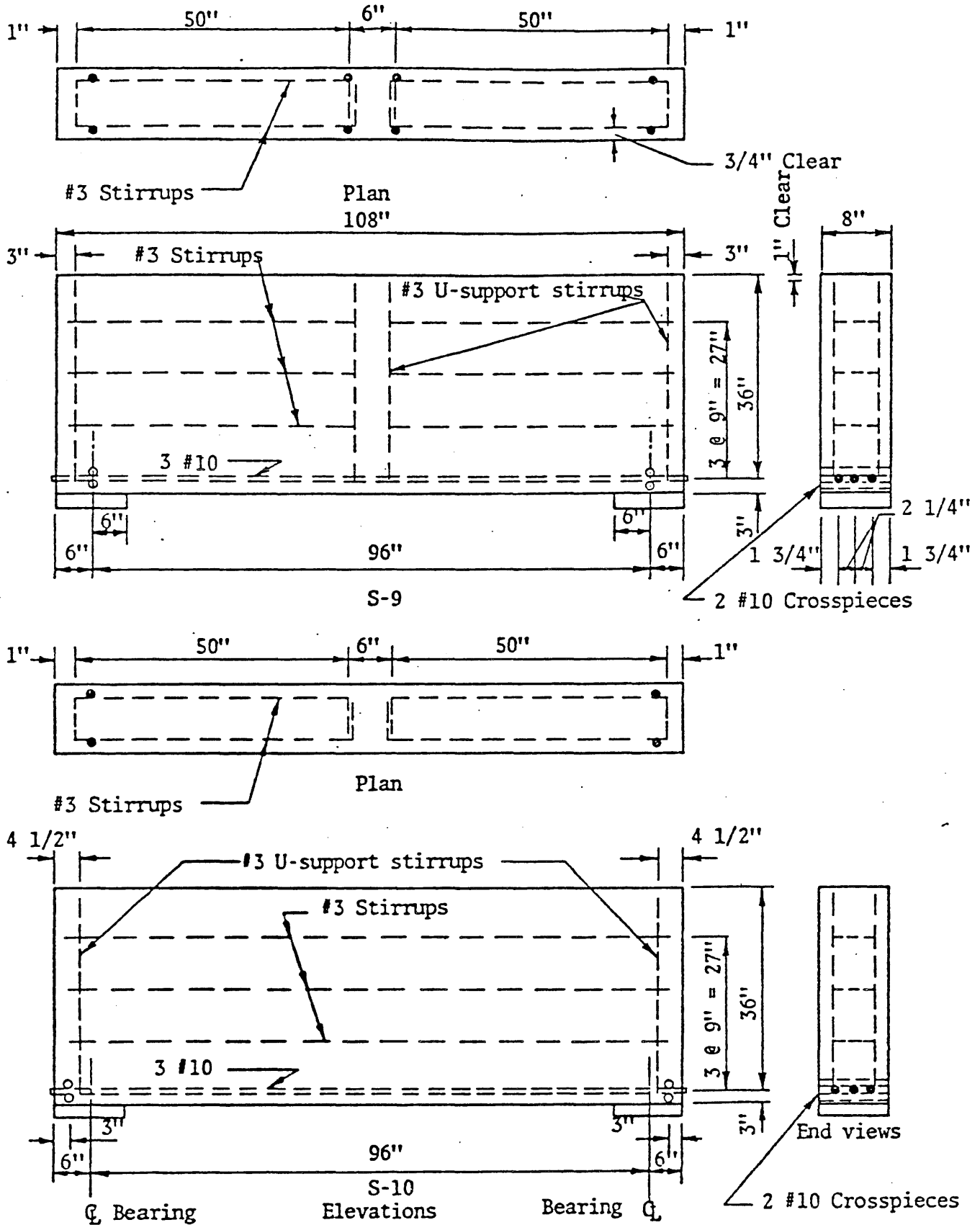
FIG. B11 Geometry of static beams S-9 and S-10, L/d = 2.67 series.
Source Ref. [39]
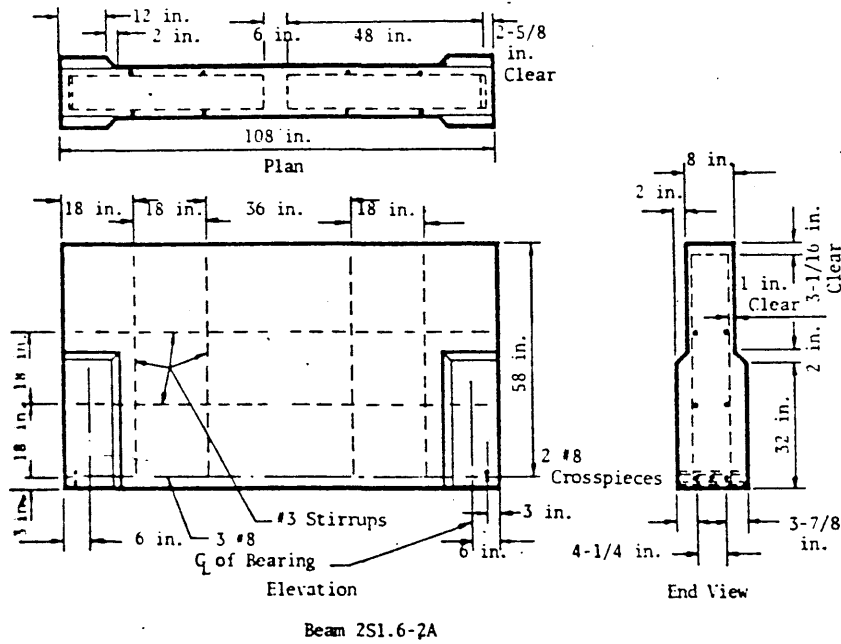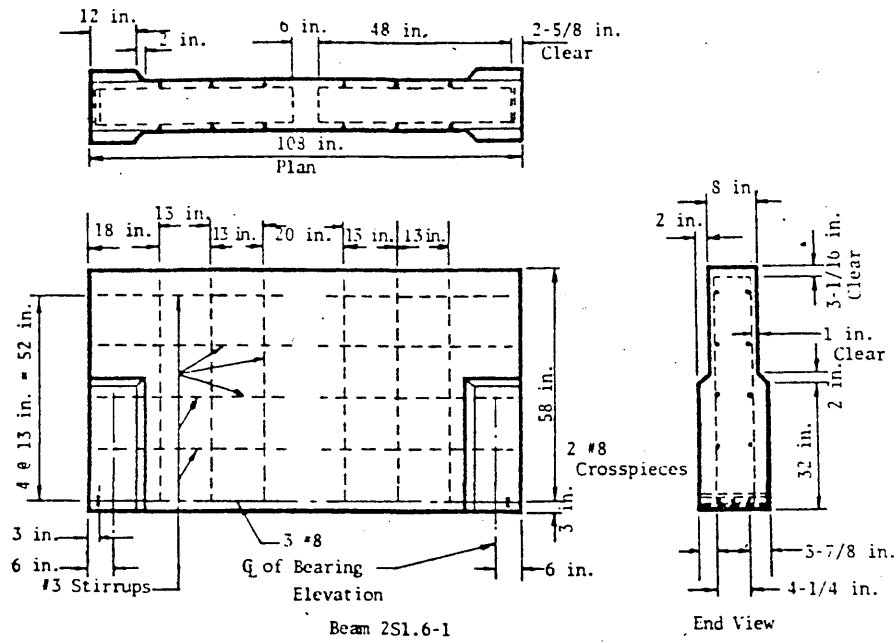
FIG. B12 Geometry of static test series L/d = 1.6.
Source Ref. [36]

Beam 2S1.6-2B

Beam 2S1.6-3
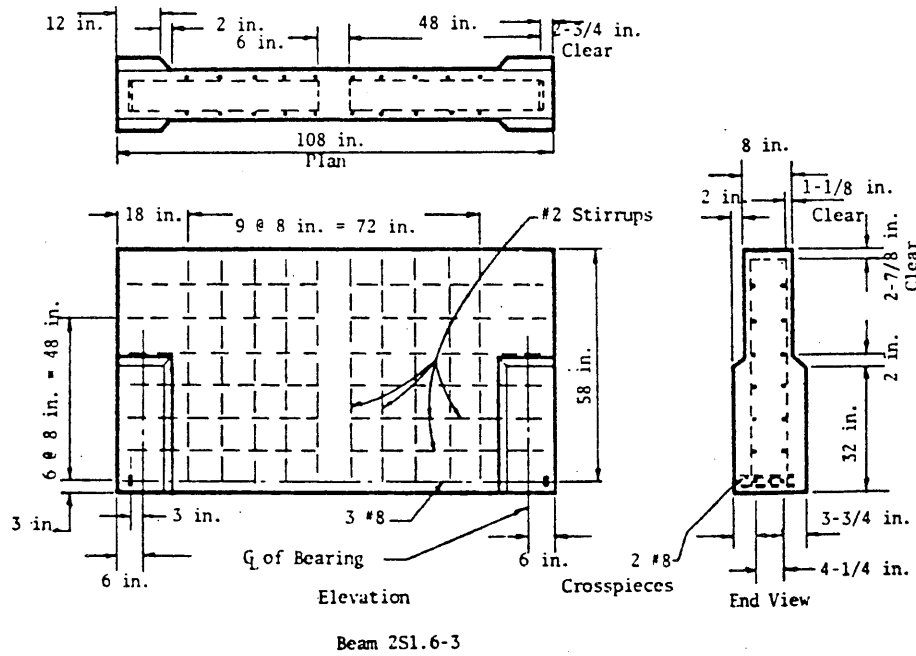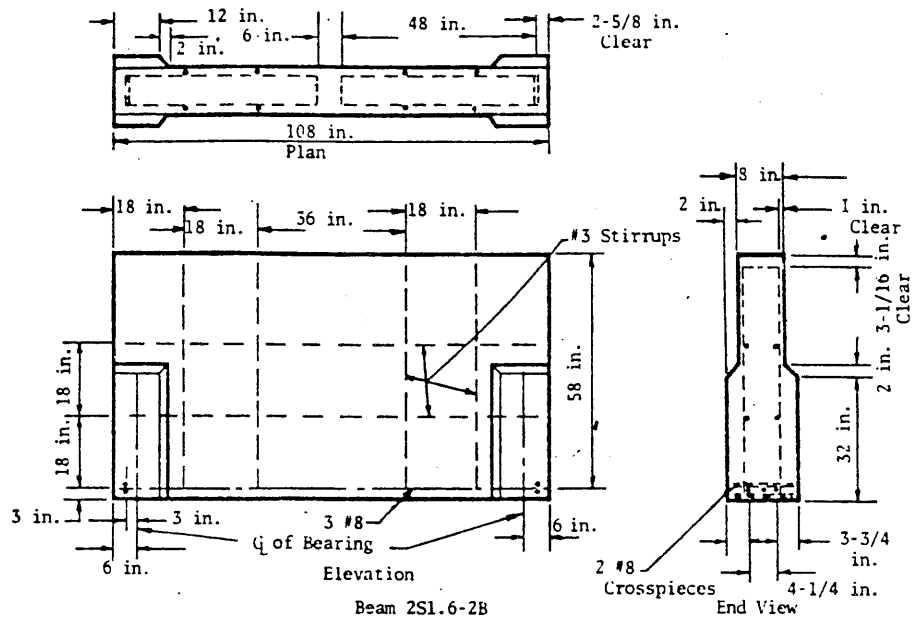
FIG. B12 Continued.
Source Ref. [36]

Note: Lapped end of horizontal stirrup placed at alternate positions.

Beam 2S1.6-3C

Beam 2S1.6-5
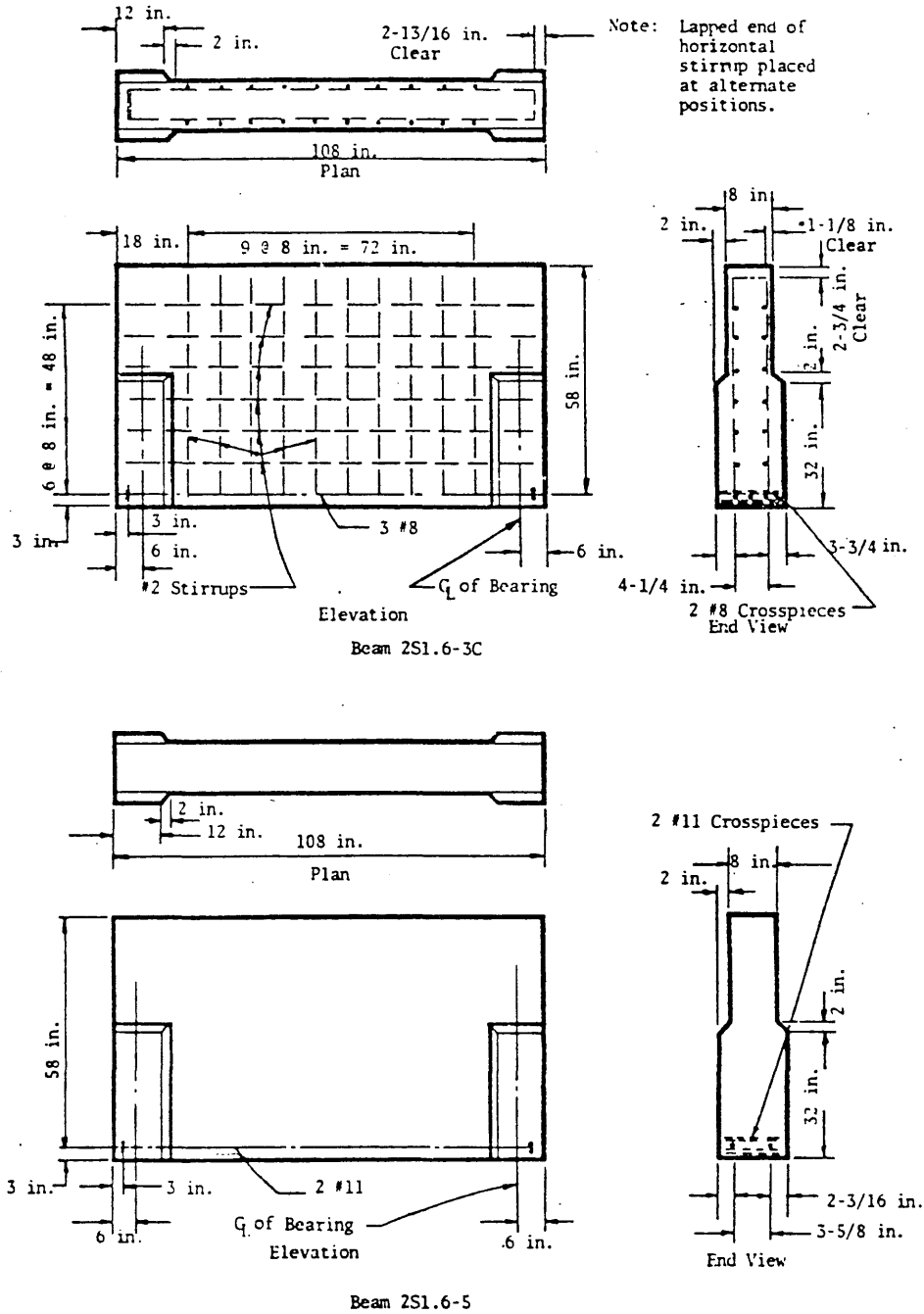
FIG. B12 Concluded.
Source Ref. [36]

BEAM DIMENSIONS AND CONCRETE STRENGTH PARAMETERS. SOURCE REF. [39]

Beam	L/d series	Casting orientation	b, in.	d, in.	Flexure			Shear			Tensile splitting			Test age, days	Method of cure
					f'_c, flexure, psi	Number specimens	c_v	f'_c, shear, psi	Number specimens	c_v	f'_{sp}, psi	Number specimens	c_v		
S-1	1.66	Side	8	58	3,339	3	4.37	3,341	6	3.04	257	4	19.80	7	Room
S-2	1.66	Side	8	58	3,260	4	1.72	3,097	8	5.05	263	12	12.50	8	Room
S-3	1.66	Side	8	58	3,468	4	7.18	3,392	8	5.31	301	12	14.60	7	Room
S-4	1.66	Side	8	58	3,647	3	4.94	3,607	6	3.33	371	12	4.50	6	Room
S-5	1.66	Side	8	58	2,287	3	0.48	2,637	6	12.05	284	12	12.90	7	Room
S-6	2.67	Side	8	36	4,129	3	4.03	4,018	6	4.04	323	12	14.37	14	Room
S-7	2.67	Vertical	8	36	3,449	3	5.00	3,263	6	7.59	364	12	7.67	15	Room **
S-8	2.67	Vertical	8	36	3,796	3	3.84	3,605	6	5.52	347	12	7.18	15	Moist R.
S-9	2.67	Side	8	36	3,521	3	3.86	3,388	6	6.79	340	12	9.06	13	Room
S-10	2.67	Side	8	36	3,940	3	9.01	3,874	6	6.99	333	6	8.86	31	Room
S-11	3.62	Side	8	26.5	2,419 †	3	4.08	3,681	3	4.08	329	7	7.38	52	Room
S-12	3.62	Side	8	26.5	4,191	3	2.94	4,191	3	2.94	380	6	13.91	50	Room
S-13	3.62	Side	8	26.5	3,787	3	3.25	3,787	3	3.25	308	10	8.24	47	Room

* Cured at approximately 70°F., 50% relative humidity.

** Cured at approximately 70°F., 100% relative humidity.

† Concrete in compression region from second batch of this beam only for L/d = 3.62 series.

TABLE B7

ULTIMATE MOMENTS--BASED ON MEASURED f_s, $k_u d$. SOURCE REF. [39]

Beam	L/d	A_s, sq in.	p	d, in.	f'_c-flex, psi	Measured at Ultimate								
						ϵ_s, μin./in.	f_s, psi	$k_u d$, in.	$k_1 k_3$	k_2	$(M_u)_{calc}$, in.-kips	$(W_u)_{meas}$, kips	$(M_u)_{meas}$, in.-kips	$\frac{(M_u)_{meas}}{(M_u)_{calc}}$
S-6	2.67	3.81	.01322	36	4129	1,712	46,100	8.0	0.665	.42	5734	444.9	6289	1.10
S-8	2.67	3.81	.01322	36	3796	14,471	51,732	7.8	0.832	.42	6649	484.5	6849	1.03
S-9	2.67	3.81	.01322	36	3521	15,534	52,559	6.2	1.147	.42	6688	442.0	6248	0.93
S-12	3.62	3.00	.01415	26.5	4191	16,677	62,850	4.3	1.308	.42	4656	298.9	4225	0.91
S-13	3.62	3.00	.01415	26.5	3787	17,675	51,000	5.8	0.871	.42	3682	282.3	3991	1.08
				Ave	3885				0.965					1.01

TABLE B8

PROPERTIES OF REINFORCING STEEL, STATIC BEAMS. SOURCE REF. [39]

Beam	L/d	Bars No.	Bars Size	A_s, sq. in.	p	f_y, psi	f_{ult}, psi	E_s, ksi	Bar size	A_v, sq. in.	p_v	f_y, psi	f_{ult}, psi	s, in.	Orientation
S-1	1.66	2	11	3.12	.00672	46,721	76,914	30,209	--	--	--	--	--	--	--
S-2	1.66	2	11	3.12	.00672	46,151	76,442	28,414	--	--	--	--	--	--	--
S-3	1.66	2	11	3.12	.00672	46,703	77,067	29,501	3	.22	.0011	51,846	75,409	24	V*
S-4	1.66	2	11	3.12	.00672	48,651	82,596	28,022	3	.22	.0034	51,846	75,409	8	V
S-5	1.66	2	11	3.12	.00672	50,481	--	30,543	3	.22	.0034	51,846	75,409	8	V
S-6	2.67	3	10	3.81	.01322	46,100	76,654	28,820	--	--	--	--	--	--	--
S-7	2.67	3	10	3.81	.01322	49,600	79,606	29,000	--	--	--	--	--	--	--
S-8	2.67	3	10	3.81	.01322	44,646	75,354	28,804	3	.22	.0031	51,545	74,545	9	V
S-9	2.67	3	10	3.81	.01322	45,943	76,575	29,000**	3	.22	.0031	51,545	74,545	9	H†
S-10	2.67	3	10	3.81	.01322	46,600	76,600	29,000**	3	.22	.0031	51,600	75,200	9	H
S-11	3.62	3	9	3.00	.01415	53,850	85,350	29,000**	--	--	--	--	--	--	V
S-12	3.62	3	9	3.00	.01415	51,450	84,300	29,000**	3	.22	.0055	54,545	77,727	5	V
S-13	3.62	3	9	3.00	.01415	50,250	82,200	29,550	3	.22	.0034	55,295	82,057	8	V

*V = vertical.
**Assumed modulus.
†H = horizontal.

TABLE B9

CALCULATED AND MEASURED ULTIMATE MOMENTS FOR UNIFORMLY LOADED BEAMS FAILING IN FLEXURE (STATIC TESTS). SOURCE REF. [36]

Beam	Reference	Beam Properties c, in.	Beam Properties A_s, in.²	Beam Properties p	Beam Properties f'_c, psi	Calculated $k_1 k_3$ eq. (47)	Calculated Fc_u eq. (104)	Calculated k_2	Calculated $1 - \frac{k_2}{k_1 k_3} \frac{p f_s}{f'_c}$	Calculated f_s, psi	Calculated $(M_u)_{calc}$, in.-kips	Measured $(M_u)_{avg}$, kips	Measured $(M_u)_{meas}$, in.-kips	$\frac{(M_u)_{meas}}{(M_u)_{calc}}$
2S1.6-1	This Report	58.0	2.37	0.00511	4160	0.9	0.003	0.42	0.965	61,468	8152	578	7879	0.97
2S1.6-2A	This Report	58.0	2.37	0.00511	4373	0.9	0.003	0.42	0.965	64,770	8589	622	8479	0.99
2S1.6-2B	This Report	58.0	2.37	0.00511	3829	1.0	0.003	0.42	0.966	61,138	8116	566	7716	0.95
2S1.6-3	This Report	58.0	2.37	0.00511	5023	0.8	0.003	0.42	0.967	61,400	8163	575	7838	0.96
2S1.6-3C	This Report	58.0	2.37	0.00511	3586	1.0	0.003	0.42	0.963	61,623	8158	555	7566	0.93
S-6	14	36.0	3.81	0.01322	4129	0.9	0.003	0.42	0.925	50,371	6390	445	6066	0.95
S-8	14	36.0	3.81	0.01322	3796	1.0	0.003	0.42	0.928	49,050	6246	485	6605	1.06
S-9	14	36.0	3.81	0.01322	3521	1.0	0.003	0.42	0.922	49,468	6257	442	6025	0.96
S-12	14	26.5	3.00	0.01415	4191	0.9	0.003	0.42	0.914	54,382	3953	299	4075	1.03
S-13	14	26.5	3.00	0.01415	3787	1.0	0.003	0.42	0.920	50,919	3725	282	3848	1.03
													Avg	0.98

APPENDIX C

THE NUMERICAL METHOD FLOW-CHARTS
AND COMPUTER PROGRAMS

start

Input beam properties, geometrical and material
include σ-ε curve of steel reinforcements

Assume value for ε_s
$\varepsilon_s \geq \varepsilon_y$

Assume value for kd

Evaluate σ-ε curve for concrete
using the proposed model for
confined concrete

Divide compression zone into layers
while steel remains in exact location

Calculate layer strain
Calculate layer stress
Calculate layer force
Do the same for A_s and A_s'

Calculate $\Sigma C = C$
Calculate $\Sigma T = T$

$C \overset{?}{=} T$ No

Yes

Calculate M, ϕ
Include "shear reduction":

$M \overset{?}{=} M_u$ No

Yes

End

Fig. C1:   Moment-curvature in flexure, w/o shear influence

```
                              ( start )
                                  │
        ┌─────────────────────────┴──────────────────┐
        │                                             │
┌───────┴──────────────────────────────┐             │
│ Input:  Beam properties, geometrical  │             │
│ and material                          │             │
└───────┬───────────────────────────────┘            │
        │                                             │
┌───────┴───────────────────────────────┐            │
│ Calculate main reinforcement ratio     │            │
└───────┬───────────────────────────────┘            │
        │                                             │
┌───────┴───────────────────────────────┐            │
│ Calculate max. reduction w/o shear     │            │
│ reinforcement                          │            │
└───────┬───────────────────────────────┘            │
        │                                             │
      ╱   ╲                                           │
     ╱ crack ╲          Yes                           │
    ╱ inclination?╲───────────────────────────────────┤
     ╲  known  ╱                                      │
      ╲     ╱                                          │
        │ No                                           │
┌───────┴───────────────────────────────┐            │
│ Calculate crack inclination            │            │
└───────┬───────────────────────────────┘            │
        │                                             │
  slender ┌──────────────┐                            │
 ┌────────┤ check for     │                           │
 │        │ deep beam     │                           │
 │        └───────┬───────┘                           │
 │                │ deep                               │
 │        ┌───────┴────────────────────────┐          │
 │        │ Moment reduction factor for deep│         │
 │        │ beams w and w/o shear reinforce-│         │
 │        │ ment                            │         │
 │        └───────┬────────────────────────┘          │
 │                │                                    │
┌┴────────────────┴──────────────┐                    │
│ Moment reduction factor for     │                   │
│ slender beams w and w/o shear   │                   │
│ reinforcement                   │                   │
└───────┬────────────────────────┘                    │
        │                                              │
┌───────┴────────────────────────┐                    │
│ Out-put and comments            │                    │
└───────┬────────────────────────┘                    │
        │                                              │
      ╱   ╲                                            │
     ╱ Another case ╲   Yes                            │
    ╱      ?      ╲──────────────────────────────────── ┘
     ╲         ╱
      ╲     ╱
        │ No
      ( End )
```
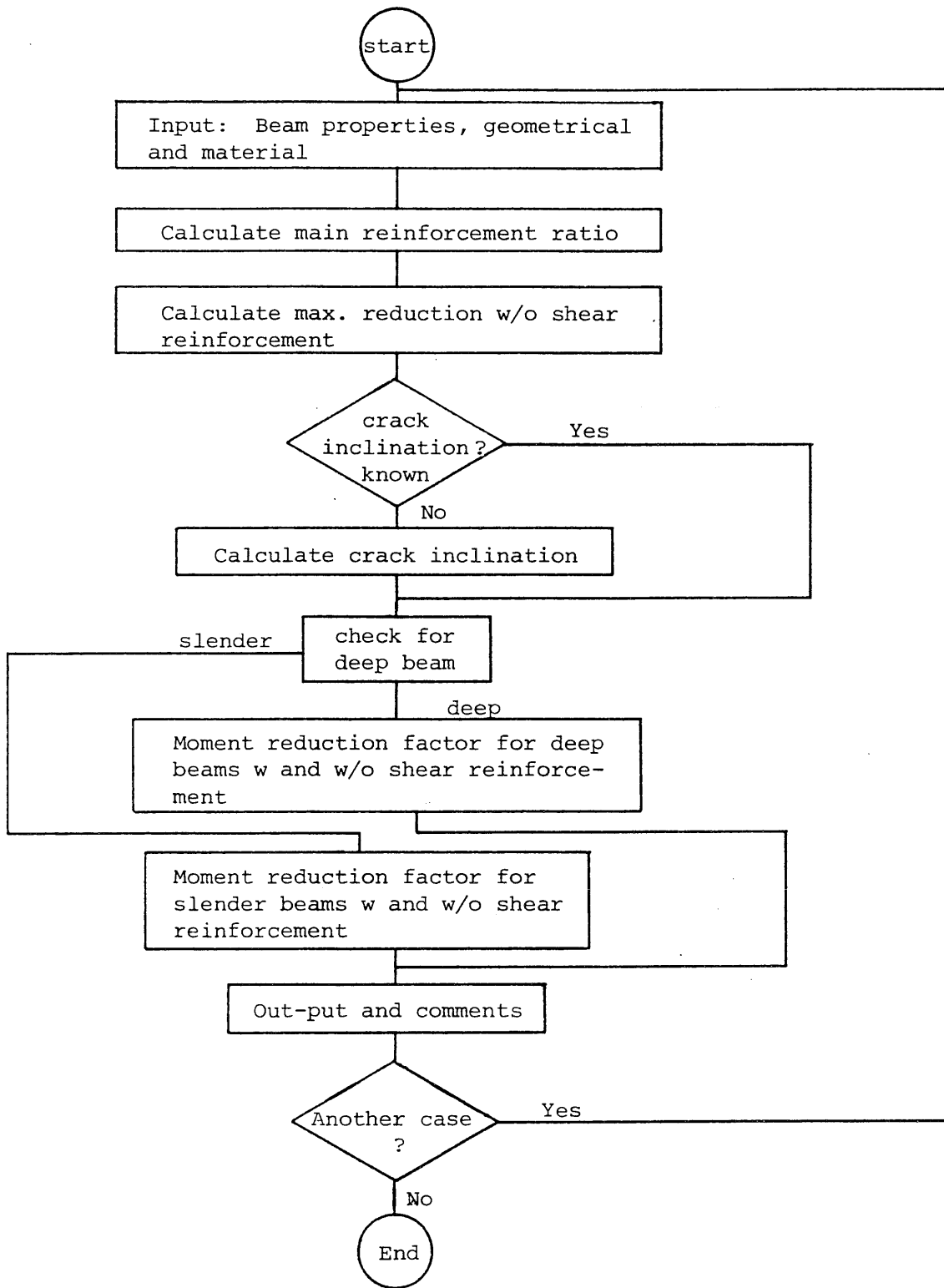
Fig. C2:   Moment reduction factor due to shear
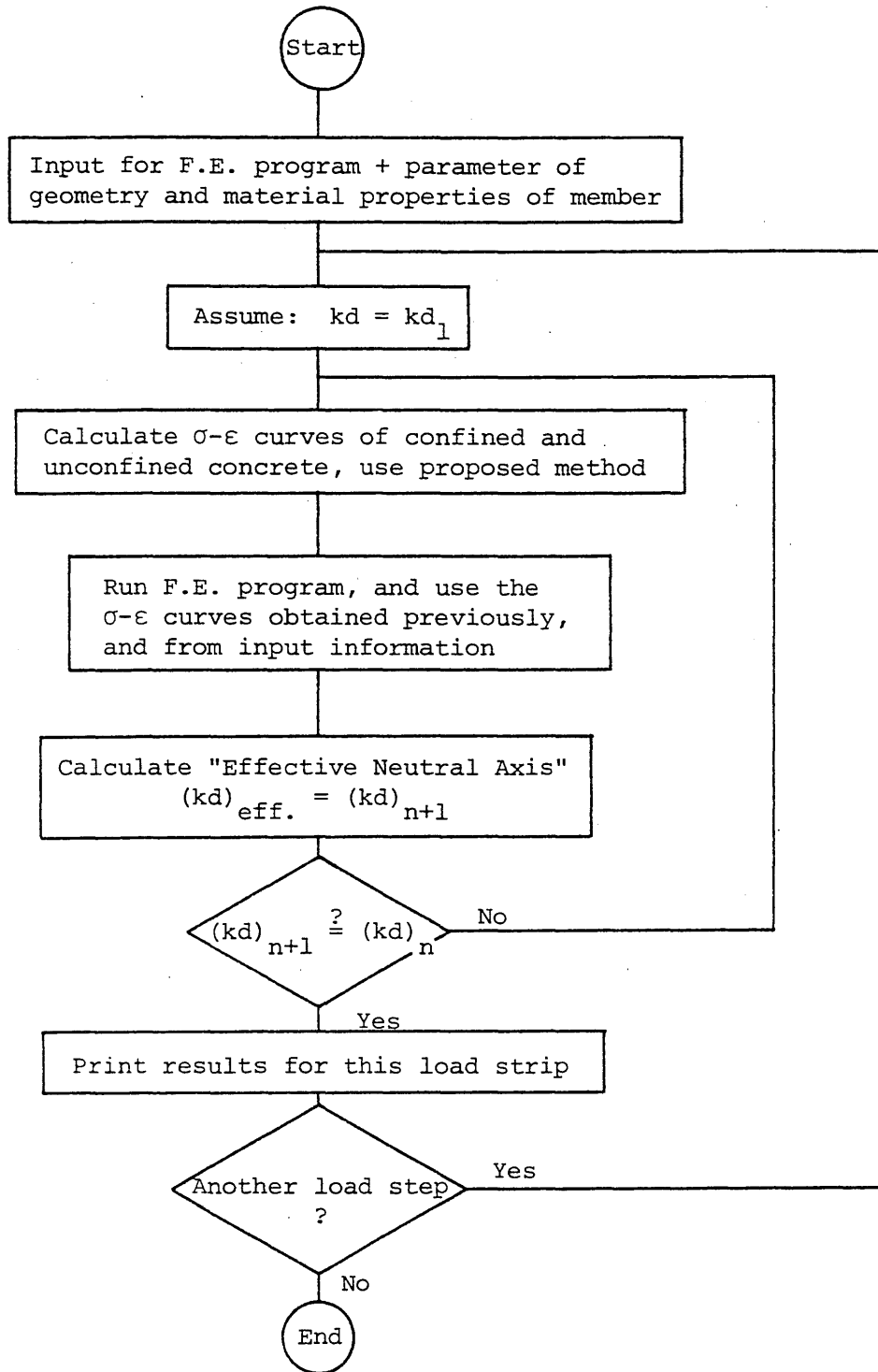
Fig. C3: Proposed finite element procedure

```
79/05/29. 08.54.21.
PROGRAM   TKPR2

10   REM - THIS PROGRAM EVALUATES THE CHANGES IN THE PARAMETERS AS A
20   REM - FUNCTION OF THE GEOMETRY OF THE CROSS SECTION, AND THE
21   REM - MATERIAL PROPERTIES
22     DIM E1( 1000 )
30   PRINT " BEAM WIDTH, [IN.]                              B=", INPUT B
40   PRINT " BEAM EFFECTIVE DEPTH, [IN.]                    D=", INPUT D
50   PRINT " THICKNESS OF CONCRETE COVER, [IN.]             T=", INPUT T
60   PRINT " WIDTH OF CONFINED CORE, [IN.]                  B1=", INPUT B1
70   PRINT " DEPTH  TO COMPRESSION REINFORCEMENT, [IN.]     D1=", INPUT D1
80   PRINT " SPACING OF STEEL HOOPS, [IN.]                  S=", INPUT S
90   PRINT " YIELD STRESS OF HOOPS, [PSI]                   F2=", INPUT F2
100  PRINT " COMPRESSIVE STRENGTH OF CONCRETE, [PSI]        F3=", INPUT F3
110  PRINT " DIAMETER OF COPRESSIVE BAR, [IN.]              D2=", INPUT D2
120  PRINT " AREA OF COMPRESSIVE BAR, [SQR. IN.]            A1=", INPUT A1
130  PRINT " NUMBER OF COMPRESSIVE BARS, [INTGE]            N1=", INPUT N1
140  PRINT " DIAMETER OF HOOP BAR, [IN.]                    D3=", INPUT D3
150  PRINT " AREA OF HOOP BAR, [SQR. IN.]                   A2=", INPUT A2
160  PRINT " INITIAL DEPTH OF NEUTRAL AXIS, [IN.]           L=", INPUT L
170  PRINT " FINAL DEPTH OF NEUTRAL AXIS, [IN.]             M=", INPUT M
180  PRINT " STEP SIZE OF DEPTH CHANGE FOR NEUTRAL AXIS, [IN.]  N=", INPUT N
200    A5 = N1 * A1
201    Y1 = SQR ( F3 )
202    J = ( M - L ) / N
203    E1(1) = 1.0
204    J1 = J + 2
210    FOR I = 2 TO J1 STEP 1
211    C = L + ( I - 2 ) * N
220    R1 = A5 / ( C * B )
225    H1 = C -T
226    H2 = B1
230    X1 = 2 * A2 * ( H1 + B1 )
240    X2 = ( H1 * B1 - A5 ) * S
250    R2 = X1 / X2
260    H3 = 0.5 * ( H1 + H2 )
270    X3 = R2 * F2 / Y1
280    X4 = ( R2 + R1 * D3 / D2 ) * F2 /Y1
281    Y2 = S / H3
283    Y5 = 1 - 0.734 * Y2
284    IF Y5 >= 0 THEN 287
285    GO TO 288
287    Y5 = Y5 - 1
288    Y6 = ABS( Y5 )
289    F9 = 0.005 * Y6 * X3
290    E1( I ) = 0.0024 + F9
291    IF E1( I ) < 0.0028 THEN 293
292    GO TO 295
293    E1( I ) = 0.0028
294    GO TO 300
295    IF  E1( I ) > E1( I - 1 )  THEN 297
296    GO TO 300
297    E1( I ) = 0.75 * E1( I - 1 )
298    GO TO 291
300    K = 1 + 0.0091 * ( 1 - 0.245 * Y2 ) * X4
310    X5 = 3 + 0.002 * F3
320    X6 = F3 - 1000.0
330    X7 = X5 / X6
334    V1 = 1 / Y2
335    Y3 = SQR ( V1 )
340    X8 = 0.75 * R2 * Y3 + X7 - 0.002
350    Z = 0.5 / X8
355    PRINT " THE DEPTH OF THE COMPRESSION ZONE IS ", C
400    PRINT" EO =",E1( I )
410    PRINT "  K =", K
420    PRINT "  Z =", Z
430    PRINT " RO =", R1
440    PRINT " RO2 =", R2
500     IF C = M  THEN  600
550     NEXT I
600    PRINT " FOR YES TYPE - 1 "
610    PRINT " FOR NO TYPE  - 0 "
620    PRINT " DO YOU WANT TO PERFORM CHANGES, AND RUN AGAIN ? ", INPUT Q
630    IF Q = 0 THEN  700
640    IF Q = 1 THEN  30
700    END
```

Fig. C4: Program TKPR2

```
   79/05/29. 08.56.23.
PROGRAM   TKSH4

00010 REM-THIS PROGRAM CALCULATES THE REDUCTION IN FLEXURAL MOMENT DUE TO SHEAR
00011 REM ***********************************************************************
00012 REM -----------------------------------------------------------------------
00100 REM - INPUT DATA
00101 REM -----------------------------------------------------------------------
00200 PRINT 'BEAM EFFECTIVE DEPTH, [ IN. ]                      ',INPUT D
00300 PRINT 'BEAM WIDTH, [IN.]                                  ',INPUT B
00400 PRINT 'AREA OF TENSILE REINFORCING BAR, [SQR. IN.]        ',INPUT A1
00500 PRINT 'NUMBER OF TENSILE REINFORCING BARS, [INTGR.]       ',INPUT N
00600 PRINT 'DO YOU KNOW THE CRACK INCLINATION ?  1=YES, 0=NO   ',INPUT M1
00610 IF M1 = 1   THEN   625
00620 IF M1 = 1   THEN   700
00625 PRINT 'IS THERE SHEAR REINFORCEMENT IN THE MEMBER ? NO = 0, YES = 1',INPUT H2
00626 IF H2 = 1   THEN   630
00627 IF H2 = 0   THEN   670
00630 PRINT 'AREA OF SHEAR REINFORCING BAR, [SQR. IN.]          ',INPUT A3
00640 PRINT 'NUMBER OF SHEAR REINFORCING BARS IN SECTION, [INTGR.]',INPUT N1
00650 PRINT 'SPACING OF SHEAR REINFORCEMENT, [IN.]              ',INPUT S
00660 PRINT 'YIELD STRESS OF SHEAR REINFORCEMENT, [PSI]         ',INPUT F2
00670 PRINT 'CONCRETE COMPRESSION STRENGTH, [PSI]               ',INPUT F3
00680 GO TO 800
00700 PRINT 'INCLINATION OF CRACK TO THE HORIZONTAL, [DEG.]     ',INPUT A5
00800 PRINT 'SHEAR SPAN, OR CLEAR SPAN LENGTH [IN.]             ',INPUT A
00900 PRINT 'A/D VALUE FOR MAX. MOMENT REDUCTION, 2.0 < A/D < 3.0 ',INPUT P2
01000 PRINT 'A/D VALUE FOR REDUCTION START, 1.0 < A/D < 1.5     ',INPUT P1
02000 P = 3.141592654
02100 A2 =   N * A1
02200 X1 = B * D
02300 X2 = A / D
02400 R1 = ( A2 / X1 ) * 100
02500 IF R1 <= 0.65   THEN   2530
02510 IF R1 <= 1.88   THEN   2550
02520 IF R1 <= 2.8   THEN   2570
02525 IF R1 > 2.8   THEN   2565
02530 Y1 = 1.0
02540 GO TO 2600
02550 Y1 = 1.0 - 0.366 * ( R1 - 0.65 )
02560 GO TO 2600
02565 PRINT 'RO > 2.8%, ASSUME BEHAVIOUR AS FOR RO = 2.8%'
02570 Y1 = 0.6
02580 GO TO 2600
02600 IF M1 = 0   THEN   2905
02610 IF M1 = 1   THEN 2990
02899 REM -----------------------------------------------------------------------
02900 REM- CALCULATE CRACK INCLINATION FROM BEAM PROPERTIES
02901 REM -----------------------------------------------------------------------
02905 IF H2 = 0   THEN   2907
02906 GO TO 2910
02907 IF X2 <= P2   THEN   2966
02908 IF X2 > P2   THEN   2980
02910 A4 = N1 * A3
02920 R5 = A4 / ( B * S )
02930 P4 = R5 * F2 / F3
02935 IF X2 = P2   THEN   2960
02940 A5 = -261.3 * R6 * X2 + 109.1
02941 IF A5 > 30.0   THEN   2943
02942 GO TO 2990
02943 A5 = 30.0
02944 GO TO 2990
02960 T1 = R6 * X2
02961 T2 = LG*( T1 )
02962 T3 = 0.0394 * T2 + 1.9756
02963 A5 = 10 ^ T3
02964 IF A5 < 50.0   THEN   2966
02965 GO TO 2990
02966 A5 = 50.0
02967 GO TO 2990
02980 A5 = 90.0
02981 GO TO 2990
02990 A6 = ( A5 / 360.0 ) * 2 * P
02995 Z2 = COT ( A6 )
```

Fig. C5: Program TKSH4

```
02997 REM ---------------------------------------------------------------
029911 REM - DIRECT CALCULATION TO SPECIFIC BEAM TYPE
02999 REM ---------------------------------------------------------------
03000 IF X2 <= P1  THEN  10000
03010 IF X2 <= P2  THEN   4100
03020 IF X2 < 7.0  THEN   6100
03030 IF X2 >= 7.0 THEN  10020
03999 REM ---------------------------------------------------------------
04000 REM- MOMENT REDUCTION FOR DEEP BEAMS
04001 REM ---------------------------------------------------------------
04100 V1 = X2 - P1
04200 V2 = Y1 - 1.0
04300 V3 = P2 - P1
04400 V4 = 1.0 + V1 * V2 / V3
04500 IF V4 > 1.0 THEN  4700
04600 GO TO 4850
04700 V4 = 1.0
04800 GO TO 4850
04850 IF H2 = 0  THEN  10500
04860 GO TO 4900
04900 Y2 = Y1 + ( 1.0 - Y1 ) * Z2
05000 V5 = Y2 - 1.0
05100 V6 = 1.0 + V1 * V5 / V3
05200 IF V6 > 1.0   THEN 5400
05300 GO TO 9100
05400 V6 = 1.0
05500 GO TO 9100
05999 REM ---------------------------------------------------------------
06000 REM- MOMENT REDUCTION FOR SLENDER BEAMS
06001 REM ---------------------------------------------------------------
06100 W1 = Y1 - 1.0
06200 W2 = X2 - 7.0
06300 W3 = P2 - 7.0
06400 W4 = 1.0 + W1 * W2 / W3
06500 IF W4 > 1.0   THEN  6700
06600 GO TO 6850
06700 W4 = 1.0
06800 GO TO 6850
06850 IF H2 = 0   THEN  10600
06860 GO TO 6900
06900 Y2 = Y1 + ( 1.0 - Y1 ) * Z2
07000 W5 = Y2 - 1.0
07100 W6 = 1.0 + W2 * W5 / W3
07200 IF W6 > 1.0   THEN  7400
07300 GO TO 9500
07400 W6 = 1.0
07500 GO TO 9500
08999 REM ---------------------------------------------------------------
09000 REM- OUT-PUT OF RESULTS AND COMMENTS
09001 REM ---------------------------------------------------------------
09100 PRINT ' THIS IS A DEEP BEAM,   A / D  < ', P2
09200 PRINT 'ULT. MOMENT REDUCTION COEFFICIENT, W/O SHEAR REINFORCEMENT =',V4
09300 PRINT 'ULT. MOMENT REDUCTION COEFFICIENT  W.  SHEAR REINFORCEMENT =',V6
09350 PRINT 'EXPECTED CRACK ANGLE TO CAUSE FAILURE, [ DEG. ]     ALFA =',A5
09400 GO TO 11000
09500 PRINT ' THIS IS A SLENDER BEAM,  A / D  >', P2
09600 PRINT 'ULT. MOMENT REDUCTION COEFFICIENT, W/O SHEAR REINFORCEMENT =',W4
09700 PRINT 'ULT. MOMENT REDUCTION COEFFICIENT  W.  SHEAR REINFORCEMENT =',W6
09750 PRINT 'EXPECTED CRACK ANGLE TO CAUSE FAILURE, [ DEG. ]     ALFA =',A5
09800 GO TO 11000
10000 PRINT ' A / D  <= ', P1
10010 GO TO 10100
10020 PRINT ' A / D  >=  7.0 '
10030 GO TO 10100
10100 PRINT ' NEGLIGABLE MOMENT REDUCTION FOR THIS CASE '
10200 GO TO 11000
10500 PRINT 'THIS IS A DEEP BEAM W/O SHEAR REINFORCEMENT'
10510 PRINT 'ULT. MOMENT REDUCTION COFFFICIENT FOR THIS CASE =           ',V4
10511 PRINT 'EXPECTED CRACK ANGLE TO CAUSE FAILURE, [ DEG. ]             ',A5
10520 GO TO 11000
10600 PRINT 'THIS IS A SLENDER BEAM W/O SHEAR REINFORCEMENT'
10610 PRINT 'ULT. MOMENT REDUCTION COEFFICIENT FOR THIS CASE =           ',W4
10620 GO TO 11000
11000 PRINT 'DO YOU WANT TO CONSIDER ANOTHER CASE ? YES = 1, NO = 0', INPUT C
11100 IF C = 0 THEN 12000
11200 IF C = 1 THEN   200
12000 END
```

Fig. C5: (Continued)

APPENDIX D

A NUMERICAL EXAMPLE

The following example is provided in order to demonstrate the procedure by which the compressive zone properties of a reinforced concrete beam are considered for the calculation of the moment-curvature relationship of such members.

Here, the application of the proposed stress-strain curve for reinforced concrete to the analysis of Beam J-2 is demonstrated. At advanced stages of loading the concrete located below the neutral axis is disregarded.

In the compressive zone of a concrete beam as illustrated in Fig. D.1, the concrete core is assumed to be confined by the transverse reinforcement from all four sides. This assumption requires the introduction of an imaginary steel bar, as an integral part of the rectangular hoop, along the neutral axis.

The percentage of the transverse reinforcement is calculated as follows.

$$\rho'' = \frac{A''_s * \{[(kd - t) + b']*2\}}{[(kd - t)*b' - A'_s]*S} \tag{D.1}$$

where:

A''_s = cross section area of hoop

kd = depth of neutral axis

t = thickness of concrete cover to outside of hoop

b' = width of confined core to outside of hoop

A'_s = area of compressive reinforcement

S = spacing of hoops along beam axis

The percentage of compressive reinforcement

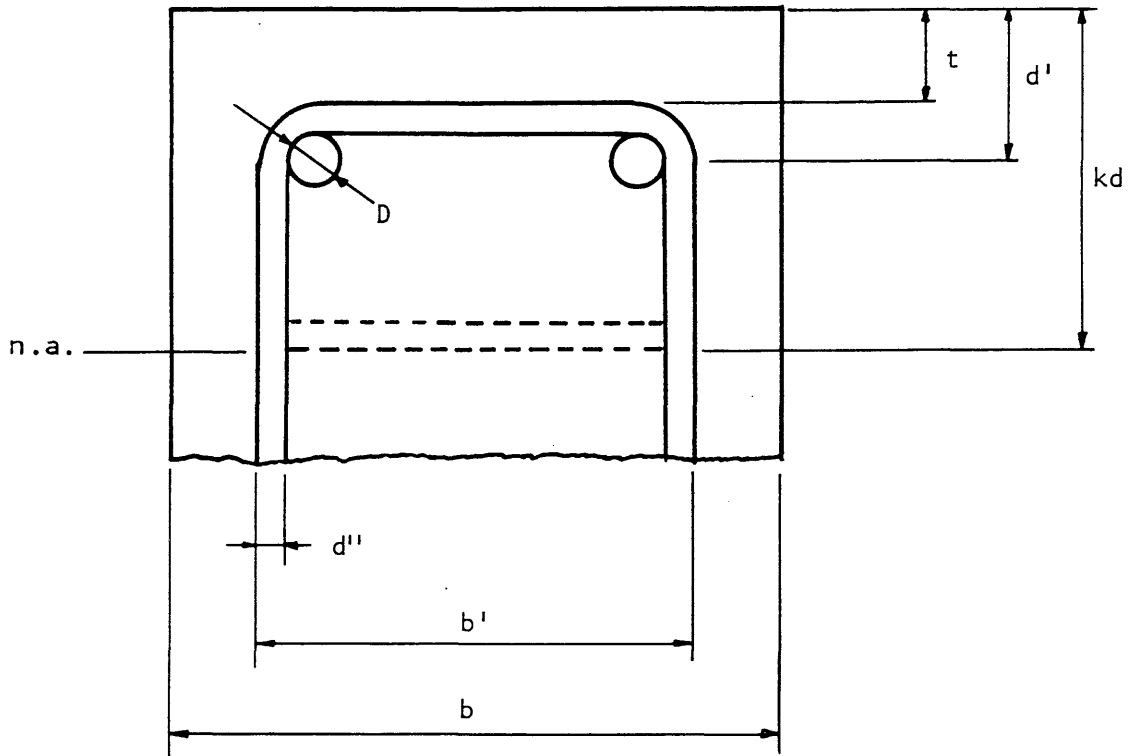$$\rho = \frac{A'_s}{kd*b} \tag{D.2}$$

Fig. D.1: Geometrical parameters of the compressive zone
           for a reinforced concrete beam.

where:

b – width of beam

The two sides of the rectangular confined core are the following:

$$h_1'' = kd - t \qquad\qquad\qquad (D.3)$$

$$h_2'' = b' \qquad\qquad\qquad (D.4)$$

The average dimension of the confined core is given by the following equation

$$h'' = 1/2 \; (h_1'' + h_2'') \qquad\qquad\qquad (D.5)$$

These parameters and dimensions are introduced into Eqs. (2.5.4) through (2.5.6) to obtain the parameters ε_o, K, Z that are used to calculate the stresses in the concrete layers. These parameters can be obtained from program TKPR1 or TKPR2 (see Appendix C). An example of how to employ programs TKPR1 or TKPR2 and the format of the results is demonstrated in Fig. D.2.

The application of the numerical procedure in the present investigation is demonstrated in the following example.

Beam J-2: Ultimate Loading Condition

A cross section of Beam J-2 is presented in Fig. 3.2.1. The dimensions of the cross section, as provided for program TKPR2, are presented in Fig. D.2. Additional information is presented in Tables B1, B2, and Fig. B.2, of Appendix B.

```
beam   J - 2


79/05/21.  12.49.35.
PROGRAM    TKPR2

   BEAM WIDTH, [IN.]                                      B=      ? 8.0
   BEAM EFFECTIVE DEPTH, [IN.]                            D=      ? 10.0
   THICKNESS OF CONCRETE COVER, [IN.]                     T=      ? 1.25
   WIDTH OF CONFINED CORE, [IN.]                          B1=     ? 5.8
   DEPTH  TO COMPRESSION REINFORCEMENT, [IN.]             D1=     ? 2.0
   SPACING OF STEEL HOOPS, [IN.]                          S=      ? 6.0
   YIELD STRESS OF HOOPS, [PSI]                           F2=     ? 50000.0
   COMPRESSIVE STRENGTH OF CONCRETE, [PSI]                F3=     ? 4080
   DIAMETER OF COPRESSIVE BAR, [IN.]                      D2=     ? 0.75
   AREA OF COMPRESSIVE BAR, [SQR. IN.]                    A1=     ? 0.44
   NUMBER OF COMPRESSIVE BARS, [INTGE]                    N1=     ? 2
   DIAMETER OF HOOP BAR, [IN.]                            D3=     ? 0.375
   AREA OF HOOP BAR, [SQR. IN.]                           A2=     ? 0.11
   INITIAL DEPTH OF NEUTRAL AXIS, [IN.]                   L=      ? 2.0
   FINAL DEPTH OF NEUTRAL AXIS, [IN.]                     M=      ? 6.0
   STEP SIZE OF DEPTH CHANGE FOR NEUTRAL AXIS, [IN.]      N=      ? 0.1




   THE DEPTH OF THE COMPRESSION ZONE IS            2
   EO =            7.57847E-2
    K =            1.37969
    Z =            12.5081
   RO =            .055
   RO2 =           6.92123E-2
   THE DEPTH OF THE COMPRESSION ZONE IS            2.1
   EO =            7.88677E-2
    K =            1.34334
    Z =            14.1895
   RO =            .052381
   RO2 =           6.02058E-2
   THE DEPTH OF THE COMPRESSION ZONE IS            2.2
   EO =            .066189
    K =            1.31545
    Z =            15.7767
   RO =            .05
   RO2 =           5.34557E-2
   THE DEPTH OF THE COMPRESSION ZONE IS            2.3
```

Fig. D.2: Reinforced concrete parameters, Program TKPR2.

The results from program TKPR2 for the case where the neutral axis is at $K_u d$ = 4.5 in. are the following:

ε_o = 0.0028

K = 1.148 (use 1.15)

Z = 36.63

The strain at the tensile reinforcement level is assumed to be ε_s = 0.044. The following strains are obtained for the various concrete and steel layers. (See Fig. 3.2.1 for details).

ε_1 = 0.015   , > ε_o , use Eq. (2.5.2) for stress calculation

ε_2 = 0.0106   , > ε_o , use Eq. (2.5.2) for stress calculation

ε_3 = 0.0062   , > ε_o , use Eq. (2.5.2) for stress calculation

ε_4 = 0.002   , < ε_o , use Eq. (2.5.1) for stress calculation

ε'_s = 0.02   , > ε_o , use Eq. (2.5.2) for stress calculation

ε_s = 0.044

The stresses for the concrete are calculated as follows.

$$f_1 = 4080 * 1.15 * [1 - 0.8 * 36.63 * 0.0028 * (\frac{0.015}{0.0028} - 1)] = 3014.5 \text{ psi}$$

$$f_2 = 4080 * 1.15 * [1 - 0.8 * 36.63 * 0.0028 * (\frac{0.0106}{0.0028} - 1)] = 3619.5 \text{ psi}$$

$$f_3 = 4080 * 1.15 * [1 - 0.8 * 36.63 * 0.0028 * (\frac{0.0062}{0.0028} - 1)] = 4224.5 \text{ psi}$$

$$f_4 = 4080 * \frac{\frac{3 * 10^6 * 0.002}{4080} - 1.15 * (\frac{0.002}{0.0028})^2}{1 + [\frac{3 * 10^6 * 0.0028}{1.15 * 4080} - 2] (\frac{0.002}{0.0028})} = 4241.5 \text{ psi}$$

For the concrete at the level of the compressive reinforcement the stress is the following:

$$F_{\varepsilon'_s} = 4080 * 1.15 * [1 - 0.8 * 36.63 * 0.0028 * (\frac{0.02}{0.0028} - 1)] = 2327.1 \text{ psi}$$

The concrete cover is at a strain greater than 0.004 therefore, the stress is assumed as follows:

$$f_{cover} = 0.605 * 4080 = 2468 \text{ psi}$$

The stresses in the longitudinal reinforcing bar can be obtained by employing either Eq. (2.4.1), or Eqs. (2.4.2). The parameters needed for the calculation are presented in Table B2 of Appendix B.

For this case Eqs. (2.4.2) are employed as follows:

Compressive reinforcement:

f_y = 48.6 ksi

ε_{sh} = 1.33%

f_u = 78.6 ksi

ε_{su} = 13.8%

$r = \varepsilon_{su} - \varepsilon_{sh} = 0.138 - 0.0133 = 0.1247$

$$m = \frac{(\frac{78.6}{48.6}) * (30 * 0.1247 + 1)^2 - 60 * 0.1247 - 1}{15 * 0.1247^2} = 119.48$$

$$f'_s = 48.6 * [\frac{119.48 * (0.02 - 0.0133) + 2}{60 * (0.02 - 0.0133) + 2} + \frac{(0.02 - 0.0133)(60 - 119.48)}{2 * (30 * 0.1247 + 1)^2}] =$$

= 56.235 ksi

Tensile reinforcement:

f_y = 48 ksi

ε_{sh} = 0.96%

f_u = 87.3 kis

ε_{su} = 15% (average value from Table B2)

$$r = 0.15 - 0.0096 = 0.1404$$

$$m = \frac{(\frac{87.3}{48}) * (30 * 0.1404 + 1)^2 - 60 * 0.1404 - 1}{15 * 0.1404^2} = 135.2$$

$$f_s = 48 * [\frac{135.2 * (0.044 - 0.0096) + 2}{60 * (0.044 - 0.0096) + 2} + \frac{(0.044 - 0.0096)(60 - 135.2)}{2 * (30 * 0.1404 + 1)^2}] =$$

$$= 76.2682 \text{ ksi}$$

The area of the concrete layers, and steel bars is the following.
(See Fig. 3.2.1).

Layer	Area [in.^{2}]
1	3.19
2	3.19
3	3.19
4	4.0
Concrete at comp. rein. level	2.89
Cover	3.795
Comp. Rein.	0.88
Ten. Rein.	1.58

The forces in the layers and the longitudinal reinforcement is obtained
by multiplying the stress in a layer by the area of the layer.

Layer	Force [lbs.]
1	3014.5 * 3.19 = 9616.25
2	3619.5 * 3.19 = 11546.2
3	4224.5 * 3.19 = 13476.15
4	4241.5 * 4.0 = 16966.0

Concrete at
    Comp. Rein. Level   2327.1 * 2.89 - 6722.4

Cover   2468.0 * 3.795 = 13161.0

Comp. Rein.   56235.0 * 0.88 = 49486.8

Ten. Rein.   76268.2 * 1.58 = 120503.7

The cross section is checked for equilibrium by comparing the sum of compressive forces to the sum (in this case only one force) of tensile forces.

ΣC = 9616.25 + 11546.2 + 13476.15 + 16966.0 + 6722.4 + 13161.0 +
      + 49486.8 = 120974.8 lbs.

Σt = 120503.7

$\dfrac{\Sigma C}{T}$ = 1.004   difference = 0.4%

Assume equilibrium, and calculate the associated moment and curvature.
The moment is obtained by the following procedure:

1. Calculate the moment of each compressive force with respect to the tensile reinforcement (i.e., multiply each compressive force by its distance from the tensile reinforcement).

2. Sum all moments.

Comp. Force [lbs.]	Lever Arm [in.]	Moment [in.-K]
9616.25	7.45	71.6
11546.2	6.85	79.1
13476.15	6.6	88.9
16966.0	5.75	97.5
6722.4	8.0	53.8
13161.0	6.85	90.1
49486.8	8.0	395.9
	Sum:	877.0

The curvature is obtained by dividing the strain at the compressive reinforcement level by the distance of that strain from the neutral axis:

$$\phi = \frac{0.02}{2.5} = 0.008 \ \frac{rad.}{in.}$$

The influence of shear is evaluated by employing program TKPR4 (see Appendix C). The required data and the result of the computation is illustrated in Fig. D3. As a result of the analysis for shear it is found that no reduction in the flexural moment capacity is detected by the analysis.

The following results were obtained for this case:

$$M_{cal.} = 877.0 \ in.-K$$

$$M_m = 919.0 \ in.-K \ (from \ Ref. \ [12])$$

$$\frac{M_{cal.}}{M_m} = \frac{877.0}{919.0} = 0.9543 \qquad difference = 4.57\%$$

The moment and curvature conditions at this stage (ultimate moment capacity) are represented on the moment-curvature diagram (M - Φ) by a single point. Additional points are calculated by the same procedure, in the loading range between the yielding of the tensile reinforcement and ultimate moment capacity. As a result the complete moment-curvature diagram is obtained, as illustrated in Fig. 3.2.8.

```
old,tksh4


SRU      0.185 UNTS.
READY.
run,mа=40000

 79/05/18. 10.24.36.
PROGRAM   TKSH4

BEAM EFFECTIVE DEPTH, [ IN. ]                                    ? 10.0
BEAM WIDTH, [IN.]                                                ? 8.0
AREA OF TENSILE REINFORCING BAR, [SQR. IN.]                      ? 0.79
NUMBER OF TENSILE REINFORCING BARS, [INTGR.]                     ? 2
DO YOU KNOW THE CRACK INCLINATION ? 1=YES, 0=NO                  ? 0
IS THERE SHEAR REINFORCEMENT IN THE MEMBER ? NO = 0, YES = 1? 1
AREA OF SHEAR REINFORCING BAR, [SQR. IN.]                        ? 0.11
NUMBER OF SHEAR REINFORCING BARS IN SECTION, [INTGR.]            ? 2
SPACING OF SHEAR REINFORCEMENT, [IN.]                            ? 6.0
YIELD STRESS OF SHEAR REINFORCEMENT, [PSI]                       ? 50000.0
CONCRETE COMPRESSION STRENGTH, [PSI]                             ? 4080.0
SHEAR SPAN, OR CLEAR SPAN LENGTH [IN.]                           ? 72.0




A/D VALUE FOR MAX. MOMENT REDUCTION, 2.0 < A/D < 3.0            ? 2.5
A/D VALUE FOR REDUCTION START, 1.0 < A/D < 1.5                  ? 1.25




 A / D  >= 7.0
 NEGLIGABLE MOMENT REDUCTION FOR THIS CASE
DO YOU WANT TO CONSIDER ANOTHER CASE ? YES = 1, NO = 0          ? 0

SRU      7.271 UNTS.

RUN COMPLETE.
```

Fig. D.3: Shear influence analysis, Program TKSH 4.

REFERENCES

1. Richart, F.E., Brandtzaeg, A. and Brown, R.L., "A Study of the Failure of Concrete Under Combined Compressive Stresses", University of Illinois Engineering Experimental Station, Bulletin No. 185, 1928.

2. Iyengar, K.T.R.J., Desayi, P. and Reddy, K.N., "Stress-Strain Character-istics of Concrete Confined in Steel Binders", Magazine of Concrete Research, Vol. 22, No. 72, September 1970, pp. 173-184.

3. Park, R. and Paulay, T., "Reinforced Concrete Structures", Wiley, 1975.

4. Kent, D.C. and Park, R., "Flexural Members with Confined Concrete", Journal of the Structural Division, ASCE, Vol. 97, ST7, July 1971, pp. 1969-1990.

5. Vallenas, J., Bertero, V.V. and Popov, E.P., "Concrete Confined by Rectangular Hoops and Subjected to Axial Loads", Report No. UCB/EERC - 77/13, University of California, Berkeley, College of Engineering, August 1977.

6. Sargin, M., "Stress-Strain Relationship for Concrete and the Analysis of Structural Concrete Sections", University of Waterloo, Ontario, 1971.

7. Sargin, M., Ghosh, S.K. and Handa, V.K., "Effect of Lateral Reinforce-ment upon the Strength and Deformation Properties of Concrete", Magazine of Concrete Research, Vol. 23, No. 75-76, June-September 1971, pp. 99-110.

8. Base, G.B. and Read, J.B., "Effectiveness of Helical Binding in the Compression Zone of Concrete Beams", ACI Journal, Vol. 62, No. 7, July 1965, pp. 763-781.

9. McDonald, J.E., "The Effect of Confining Reinforcement on the Ductility of Reinforced Concrete Beams", Technical Report C-69-5, U.S. Army Engineer Waterways Experiment Station, March 1969.

10. Baker, A.L.L. and Amarakone, A.M.N., "Inelastic Hyperstatic Frames Analysis", Proceedings of the International Symposium on the Flexural Mechanics of Reinforced Concrete, ASCE-ACI, Miami, November 1964, pp. 85-142.

11. Blume, J.A., Newmark, N.M. and Corning, L.H., "Design of Multistory Reinforced Concrete Buildings for Earthquake Motions", Portland Cement Association, Chicago, 1961.

12. Burns, N.H. and Siess, C.P., "Load Deformation Characteristics of Beam-Column Connections in Reinforced Concrete", SRS (CE) No. 234, University of Illinois, January 1962. (Also Ph.D. Thesis by Burns, N.H.)

13. Norton, J.A., "Ductility of Rectangular Reinforced Concrete Columns", Master of Engineering Report, University of Canterbury, New Zealand, 1972.

14. Park, R. and Sampson, R.A., "Ductility of Reinforced Concrete Column Sections in Seismic Design", Journal ACl, Vol. 69, No. 9, September 1972, pp. 543-551.

15. Joint ASCE-ACl Task Committee 426, "The Shear Strength of Reinforced Concrete Members", Journal of the Structural Division, ASCE, Vol. 99, ST6, June 1973, pp. 1091-1187.

16. Fenwick, R.C. and Paulay, T., "Mechanisms of Shear Resistance of Concrete Beams", Journal of the Structural Division, ASCE, Vol. 94, ST10, October 1968, pp. 2235-2350.

17. Leonhardt, F. and Walther, R., "Contribution to the Treatment of Shear Problems in Reinforced Concrete" (in German), Beton - und Stahlbetonbau (Berlin), Vol. 56, No. 12, December 1961; Vol. 57, No. 2, February 1962; No. 3, March 1962; No. 6, June 1962; No. 7, July 1962; No. 8, August 1962.

18. Taylor, H.P.J., "Investigation of the Dowel Shear Forces Carried by the Tensile Steel in Reinforced Concrete Beams", Cement and Concrete Association, London, TRA 431, 1969.

19. Bauman, T. and Rüsch, H., "Versuche Zum Studium der Verdübelungswirkung der Biegezugbewehrung eines Stahlbetonbalken", Deutscher Ausschuss für Stahlbeton, Bulletin No. 210, Berlin 1970.

20. O'Leary, A.J., "Shear Flexure and Axial Tension in Reinforced Concrete Members", Ph.D. Thesis, University of Canterbury, Christchurch, New Zealand, 1970.

21. Taylor, H.P.J., "Investigation of the Forces Carried Across Cracks in Reinforced Concrete Beams in Shear by Interlock of Aggregate", Cement and Concrete Association, TRA 42.447, London 1970.

22. Kani, G.N.J., "Basic Facts Concerning Shear Failure", Journal ACl, Vol. 63, June 1966, pp. 675-692.

23. Zsutty, T.C., "Beam Shear Strength Prediction by Analysis of Existing Data", Journal ACl, Vol. 65, November 1968, pp. 943-951.

24. Kupfer, H. and Baumann, T., "Staffelung der Biegezugbewehrung bei Hohen Schubspannungen in Schlanken Stahlbetonträgern mit I-Querschnitt", Beton und Stahlbeton, Vol. 64, December 1969, pp. 278-283.

25. Mattock, A.N. and Hawkins, N.M., "Shear Transfer in Reinforced Concrete - Research Research", PCl Journal, March-April 1972, pp. 55-75.

26. Bresler, B. and Pister, K.S., "Strength of Concrete Under Combined Stresses", Journal ACl, Vol. 55, No. 3, September 1958, pp. 321-345.

27. Paulay, T. and Loeber, P.J., "Shear Transfer by Aggregate Interlock", Shear in Reinforced Concrete, ACl Special Publication 42, Vol. 1, Detroit, 1974, pp. 1-15.

28. Paulay, T., Park, R. and Phillips, M.H., "Horizontal Construction Joints in Cast in Place Reinforced Concrete", Shear in Reinforced Concrete, ACl Special Publication 42, Vol. 2, Detroit, 1974, pp. 599-616.

29. Leonhardt, F. and Walter, R., "Wandartiger Träger", Deutscher Ausschuss für Stahlbeton, Bulletin No. 178, Wilhelm Ernst und Sohn, Berlin, 1966.

30. Comité Européen du Béton - Federation International de la Précontrainte, (International Recommendations for the Design and Construction of Concrete Structures), Appendix 3, 1st ed. June 1970, Published by the Cement and Concrete Association, London.

31. de Paiva, H.A.R. and Siess, C.P., "Strength and Behavior of Deep Beams in Shear", Journal ASCE, ST5, October 1965, pp. 14-41.

32. Kani, G.N.J., "How Safe are Our Large Reinforced Concrete Beams?", ACl Journal, March 1967, pp. 128-141.

33. Ramakrishnan, V. and Anathanarayana, Y., "Ultimate Strength of Deep Beams in Shear", ACl Journal, February 1968, pp. 87-98.

34. Kong, F.K.K., Robins, P.J. and Cole, D.F., "Web Reinforcement Effect on Deep Beams", ACl Journal, December 1970, pp. 1010-1017.

35. Kong, F.K.K., and Robins, P.J., "Web Reinforcement Effect on Lightweight Concrete Deep Beams", ACl Journal, July 1971, pp. 514-520.

36. Crist, R., "Static and Dynamic Shear Behaviour of Uniformly Loaded Reinforced Concrete Deep Beams", Technical Report No. AFWL-TR-71-74, November 1971, Air Force Weapons Laboratory, Kirtland AFB, New Mexico.

37. ACl-ASCE Committee 326, "Shear and Diagonal Tension", Journal ACl, Vol. 59, January, February, March 1962, pp. 1-30, 277-334, 353-396.

38. Yamashiro, R. and Siess, C.P., "Moment Rotation Characteristics of Reinforced Concrete Members Subjected to Bending Shear, and Axial Load", University of Illinois, Department of Civil Engineering, SRS Report 260, December 1962. (Also Ph.D. Thesis by Yamashiro, R.)

39. Crist, R.A., "Shear Behavior of Deep Reinforced Concrete Beams", Vol. II: Static Tests, Technical Report. No. AFWL-TR-67-61, October 1967, Air Force Weapons Laboratory, Kirtland AFB, New Mexico.

40. Mayfield, B., Kong, F.K., Bennison, A. and Davis, J.C.D.T., "Corner Joint Details in Structural Lightweight Concrete", ACl Journal, Vol. 68, No. 5, May 1971, pp. 366-372.

41. Swann, R.A., "Flexural Strength of Corners of Reinforced Concrete Portal Frames", Technical Report TRA 434, Cement and Concrete Association, London, November 1969, 14 pp.

42. Nilsson, I.H.E., "Reinforced Concrete Corner Joints Subjected to Bending Moment", National Swedish Building Research, Document D7, 1973, 249 pp.

43. Conner, H.W. and Kaar, P.H., "Precast Rigid Frame Building-Component Tests", Bulletin D123, Development Department, Portland Cement Association, 1967.

44. Hanson, N.W., Discussion of the Paper by Beaufait, F. and Williams, R.R., "Experimental Study of Reinforced Concrete Frames Subjected to Alternating Sway Forces", ACl Journal, Vol. 66, No. 5, May 1969, pp. 442-443.

45. Balint, P.S. and Taylor, H.P.J., "Reinforcement Detailing of Frame Corner Joints with Particular Reference to Opening Corners", Cement and Concrete Association, Technical Report 46.462, London, February 1972, 16 pp.

46. ACl-ASCE Committee 352, "Recommendations for Design of Beam-Column Joints in Monolithic Reinforced Concrete Structures", ACl Journal, July 1976, pp. 375-393.

47. Criswell, M.E., "Strength and Behavior of Reinforced Concrete Slab-Column Connections Subjected to Static and Dynamic Loadings", Technical Report N-70-1, U.S. Army Engineer W.E.S., Vicksburg, Mississipp, December 1970, 388 pp.

48. Iten, R.M., "Behavior of Missile Silo Closures Designed to Resist High Overpressures", Ph.D. Thesis, Department of Civil Engineering, University of Illinois at Urbana-Champaign, 1968.

49. Gamble, W.L., Hendron, A.J., Jr., Rainer, J.H. and Schnobrich, W.C., "A Study of Launch Facility Closures", Department of Civil Engineering, University of Illinois at Urbana-Champaign, November 1967.

50. Ryan, M.O., Salem, M.H., Gamble, W.L. and Mohraz, B., "Thick Walled Multiple Opening Reinforced Concrete Conduits", Department of Civil Engineering, SRS 390, University of Illinois at Urbana-Champaign, December 1972.

51. Salem, M.H. and Mohraz, B., "Nonlinear Analysis of Planar Reinforced Concrete Structures", Department of Civil Engineering, SRS 410, University of Illinois at Urbana-Champaign, July 1974.

52. Ruzicka, G.C., Gamble, W.L. and Mohraz, B., "Strength and Behavior of Thick Walled Reinforced Concrete Conduits", Department of Civil Engineering, SRS 422, University of Illinois at Urbana-Champaign, May 1976.

53. Gamble, W.L., "Design of Thick-Walled Multiple Opening Conduits to Resist Large Distributed Loads", Department of Civil Engineering, SRS 440, University of Illinois at Urbana-Champaign, April 1977.

54. Crawford, E.R., Higgins, C.J. and Bultmann, E.H., "The Air Force Manual for Design and Analysis of Hardened Structures", AFWL-TR-74-102, October 1974.

55. Gut, J., "Waffenwirkungen und Schutzraumbau", Forschunginstitute für Militarische Bautechnik Zürich, Bericht Sammlung FMB 73-11, 1976.

56. Newmark, N.M., "An Engineering Approach to Blast Resistant Design", University of Illinois Bulletin , Reprint Series No. 56, June 1956.

57. Merritt, J.L. and Newmark, N.M., "Design of Underground Structures to Resist Nuclear Blast", Department of Civil Engineering, SRS 149, University of Illinois at Urbana-Champaign, April 1958.

58. Newmark, N.M., Hansen, R.J., Holley, M.J. and Biggs, J.M., "Protective Construction Review Guide", Vol. I, Department of Defense, June 1961.

59. Keenan, W.A., "Blast Loading of Concrete Beams Reinforced with High-Strength Deformed Bars", Technical Report R226, U.S. Naval Civil Engineering Laboratory, April 1963.

60. Newmark, N.M., "Design of Structures for Dynamic Loads Including the Effects of Vibration and Ground Shock", Symposium on Scientific Problems of Protective Construction, Zurich, July 1963.

61. Fuss, D.S., "Dynamic Compression Tests on Thin-Section Reinforced Concrete", Technical Report R 406, U.S. Naval Civil Engineering Laboratory, December 1965.

62. Cowell, W.L., "Dynamic Properties of Plain Portland Cement Concrete", Technical Report R447, U.S. Naval Civil Engineering Laboratory, June 1966.

63. Seabold, R.H., "Dynamic Shear Strength of Reinforced Concrete Beams", Part II, Technical Report R502, U.S. Naval Civil Engineering Laboratory, January 1967.

64. Fuss, D.S., "Dynamic Shear Resistance of Thin-Webbed Reinforced Concrete Beams", Technical Report R534, U.S. Naval Civil Engineering Laboratory, June 1967.

65. Furlong, R.W., Thompson, J.N., Burns, N.H. and Perry, E.S., "Shear and Bond Strength of High-Strength Reinforced Concrete Beams Under Impact Loads-First Phase", Technical Report AFWL-TR-67-113, Air Force Weapons Laboratory, May 1968.

66. Keenan, W.A., "Strength and Behavior of Restrained Reinforced Concrete Slabs Under Static and Dynamic Loadings", Technical Report R621, Naval Civil Engineering Laboratory, April 1969.

67. Seabold, R.H., "Dynamic Shear Strength of Reinforced Concrete Beams - Part III", Technical Report R695, Naval Civil Engineering Laboratory, September 1970.

68. Brown, W.M. and Black, M.S., "Dynamic Strength Study of Small Fixed-Edge, Longitudinally Restrained Two-Way Reinforced Concrete Slabs", Technical Report N-73-8, U.S. Army Engineer W.E.S., December 1973.

69. Watt, J.M., Jr., "Response of Two-Way Reinforced and Unreinforced Concrete Slabs to Static and Dynamic Loading", Technical Report N-69-2 (Report 8), U.S. Army Engineer W.E.S., June 1974.

70. Keenan, W.A., "Shear Stresses in One-Way Slabs Subjected to Blast Load", Seventeenth Explosives Safety Seminar - Denver, Colorado, September 1976.

71. Bundesamt Für Zivilschutz, "Technische Weisungen für die Schutzanlagen der Organisation und des Sanitatsdienstes", TWO 1977, Bern, 1977.

72. Bundesamt Für Zivilschutz, "Technische Weisungen für den Privaten Shutzraumbau", TWP 1966, Bern 1975.

73. Sheikh, S.A., "Effectiveness of Rectangular Ties as Confinement Steel in Reinforced Concrete Columns", Ph.D. Thesis, Department of Civil Engineering, University of Toronto, May 1978.

74. Balmer, G.G., "Shearing Strength of Concrete Under High Triaxial Stress-Computation of Mohr's Envelope as a Curve", Structural Research Report No. SP-23, U.S. Bureau of Reclamation, 1949.